1983

Turbulent Exchange of Carbon Dioxide, Water Vapor, Heat and Momentum Over Crop Surfaces

Dean E. Anderson
University of Nebraska-Lincoln

Progress Report 83-8
November 1983

TURBULENT EXCHANGE OF CARBON DIOXIDE, WATER VAPOR, HEAT AND MOMENTUM OVER CROP SURFACES

Dean E. Anderson

Under the Supervision of
Dr. Shashi B. Verma

Research Supported by
National Science Foundation
Grants ATM-7901017 and ATM-8205431

Center for Agricultural Meteorology and Climatology
Institute of Agriculture and Natural Resources
University of Nebraska-Lincoln

University of
Nebraska
Lincoln

TEACHING RESEARCH EXTENSION

Institute of Agriculture
and Natural Resources

TURBULENT EXCHANGE OF CARBON DIOXIDE,

WATER VAPOR, HEAT AND MOMENTUM OVER CROP SURFACES

by

Dean E. Anderson

A DISSERTATION

Presented to the Faculty of

The Graduate College in the University of Nebraska

In Partial Fulfillment of Requirements

For the Degree of Doctor of Philosophy

Major: Inderdepartmental Area of
Engineering
(Bio and Environmental Engineering)

Under the Supervision of
Dr. Shashi B. Verma

Lincoln, Nebraska

1983

TURBULENT EXCHANGE OF CARBON DIOXIDE, WATER VAPOR, HEAT AND MOMENTUM OVER CROP SURFACES

Dean E. Anderson, Ph.D.

University of Nebraska, 1983

Advisor: Dr. Shashi B. Verma

Turbulence was measured over soybean and sorghum crops at Mead, Nebraska. Measurements were made with a prototype, fast response CO_2 sensor employing infrared beam absorption techniques, a Lyman-alpha hygrometer, fine wire thermocouples,and with drag and one-dimensional vertical sonic anemometers. Calibration and operational procedures were developed for the use of the CO_2 sensor in the field.

Daytime and nocturnal CO_2 fluxes measured over soybeans and sorghum were found to be consistent with profile and chamber measurement results reported in the literature. On a clear day with moderate temperatures and wind speeds, peak CO_2 flux rates over well watered soybeans (leaf area index, LAI $\simeq$ 3.5) ranged around 1.0 mg m^{-2} (ground area) s^{-1} when flux density of photosynthetically active radiation (PAR) was about 1,750 μEi $m^{-2}s^{-1}$. Under similar environmental conditions with PAR = 1,350 μEi $m^{-2}s^{-1}$, peak CO_2 flux over sorghum (LAI $\simeq$ 4.0) ranged around 1.4 mg $m^{-2}s^{-1}$. Dark respiration rates (crop + soil + roots) for soybeans (LAI $\simeq$ 3.5) were between 0.1-0.2 mg $m^{-2}s^{-1}$. Respiration rates for sorghum (LAI $\simeq$ 4.5) were 0.12-0.25 mg $m^{-2}s^{-1}$.

Non-dimensional statistics were computed. The scaled standard deviation of CO_2 was found to be about 2.9. Statistics for water vapor temperature and wind velocity were also computed.

Normalized CO_2, humidity, and air temperature spectra had similar shapes and peak frequencies. The shapes of these spectra were found to be broader than the longitudinal velocity (U) or vertical velocity (W) spectra and their peak frequencies were found to lie between those of U and W spectra. Spectra shifted to higher frequencies and lower spectral density as thermal stability increased from neutral to stable regimes. The reverse situation occurred as stability decreased from neutral conditions.

CO_2, water vapor and heat cospectra were found to be similar while momentum cospectra were centered over lower frequencies. A strong similarity was found between CO_2 and water vapor cospectra.

Spectral correlation coefficients and Kolmogorov constants of CO_2, water vapor and momentum transport were calculated. Spectral correlation coefficients decreased with increasing non-dimensional frequency and with increasing thermal stability from neutral conditions. Kolmogorov constants compared well with values reported in the literature. The constant for CO_2 fluctuations was found to be 0.78 ± 0.11.

ACKNOWLEDGEMENTS

I gratefully acknowledge the support and cooperation of the following individuals without whom this project would not have been made possible; and, to those who have helped that I may have missed in this acknowledgement, I offer my humble apology.

I wish to extend to Dr. Shashi B. Verma my sincere appreciation and gratitude for his diligent guidance and encouragement during my study. I wish to thank Dr. Norman J. Rosenberg for his support and guidance and for serving on my reading committee. I wish to thank Dr. Luh Tao for serving on my reading committee as well as Drs. John Norman and Allen Edison, the other members of my graduate committee. I am grateful for Dr. Norman's assistance on certain matters concerning the drag anemometer and numerical high pass filter. I also wish to thank Dr. Edison for his help in electronic low pass filter selection and review of the data acquisition system.

It has been my fortune in the course of this study to have met and worked with Mr. Chen Jia-Yi of Beijing University. I sincerely appreciate his help, inspiration and friendship. I also wish to express my appreciation and thanks to Dr. Gail Bingham and Mr. Randall Kennedy of Lawrence Livermore National Laboratory in their earnest efforts enabling me to measure CO_2 fluctuations with the fast response sensor they designed and built. Messers. Dave Earl and Dale Sandin provided excellent technical support. They fabricated and maintained the Lyman-alpha hygrometer and drag anemometer electronics packages. I am also grateful to Mr. Ardan Buck of NCAR, Boulder, Colorado with whom I have consulted several times concerning the design and operation of the Lyman-alpha hygrometer. I am grateful to Mr. James Hines for his excellent technical assistance in systems operation of the data acquisition system and indispensible help in software development. I am grateful, too, for the technical assistance of Dr. Gordon Woodward of the Mathematics Department of UNL for his help concerning the numerical high pass filter and to Mr. Bert Tanner of Campbell Scientific in Logan, Utah for his assistance in the operation of the sonic anemometer. I also wish to thank Mr. Jake Schaffer of Precision Machine Co. of Lincoln for his help and patience in fabricating some of the rather unique hardware used in this project. I am grateful to Mr. T. Grayson Redford, Jr. for his instruction concerning operation and maintenance of the instrumentation used early in this study.

I am grateful for the technical assistance of Messers. Tom Keber and Gerald Lukens in the field, superb typing by Ms. Mary Coffey and Mrs. Nancy Brown, the drafting of many of the figures in this work by Ms. Sheila Smith and the technical assistance of Mrs. Terese Janovec in data reduction. I am grateful for the technical assistance and suport of my good friends and colleagues David Nielsen, Dennis Baldocchi, Kirk Clawson, Bronson Gardner, Wen Yuan Niu and Jose M. N. DaCosta. I also wish to thank Bonnie Jones, Randy Pryor, Brian Beer, Monte Swantek, Mike Harless, Cynthia Hobbs, Pedro DeAzevedo and Elizabeth Graser for their help.

This study was supported by the Atmospheric Sciences Division of the National Science Foundation under grants ATM-7901017 and ATM-8205431.

Finally, and certainly not least, I wish to thank my wife, Kathie, for her love, support and encouragement in helping me throughout this effort.

TABLE OF CONTENTS

Page

LIST OF FIGURES

LIST OF TABLES

CHAPTER 1

Introduction

The nature of the terrestrial environment and man's interactions with it have been the subject of intense study in recent times. As a result of an exponential growth of human population and the corresponding demand that this growth places upon the natural resources, a number of adverse anthropogenic impacts upon the terrestrial environment have already become apparent.

Among the anthropological activities of paramount concern is the extensive and accelerating use of fossil fuel combustion. One serious environmental impact that has already become obvious as a result of fossil fuel use is the rise in global atmospheric CO_2 concentration. The possible effects of the increase in CO_2 concentration have been considered by a large number of investigators who span a broad range of specialities. Most believe that the rise in atmospheric CO_2 concentration will result in an increase in the mean global surface temperature. There remains considerable controversy as to the magnitude of this warming.

If atmospheric models are used to predict further increases in CO_2 concentration and the resulting effects, an accurate assessment of sources and sinks of atmospheric CO_2 must be made. At present there are large gaps in our understanding of the sources and sinks of atmospheric CO_2 as was noted by Landsberg (1970). For instance, Machta (1972) and Keeling et al. (1976), among others, estimate that the global atmospheric CO_2 concentration should be rising by about 0.8-1.0 ppm per year as a result of anthropogenic activities. However, Keeling (1973) reported that the rise in CO_2 detected in the atmosphere is only 1/2 to 1/3 of the release due to fossil fuel combustion. As a result, considerable debate has emerged concerning the whereabouts of the 'missing' CO_2 (Baes et al. 1976; Broecker et al., 1979).

To date there have been only a few measurements of CO_2 fluxes over land or sea. Inoue (1957, 1965), Lemon (1960), Monteith and Szeicz (1960), Denmead (1966), Allen (1971) Brown and Rosenberg (1971), Biscoe et al. (1975), Verma and Rosenberg (1976), and Baldocchi (1982) are among those who have measured CO_2 fluxes over agricultural crops by flux-gradient methods. The flux-gradient methods (e.g. Bowen-ratio-energy balance method - see Chapter 2) are error prone over rough surfaces such as soybean and sorghum crops or forests because of the small gradients of CO_2 which are difficult to measure accurately with existing infrared gas analyzers (Kanemasu et al. 1979). With recent advances in integrated circuit technology and in optics, development of fast response CO_2 sensors have been made possible. With this sensor, investigators can measure CO_2 flux using the eddy correlation technique, a direct and theoretically superior measurement technique.

In view of the importance of accurate CO_2 flux measurements, a program was begun in the late 1970's at Lawrence Livermore National Laboratory in California under the direction of Dr. Gail Bingham to design and develop a fast response CO_2 sensor. The prototype instrument resulting from this effort was made available to the University of Nebraska Center for Agricultural Meteorology and Climatology for use in this study. Jones and Smith (1977) in Canada , Ohtaki (1980), and Ohtaki and Matsui (1982) in Japan measuring over an ocean and paddy fields, respectively are the only other investigators using fast response, tower mounted CO_2 sensors at this writing.

In recent years the eddy correlation technique has been used extensively for measurement of water vapor, heat, and momentum fluxes. However, very few detailed measurements have been made over agricultural crops. Information on turbulent exchange over actively transpiring crops is needed for a thorough understanding of atmosphere-crop interactions.

The following were the primary objectives of this study:

1. a. To employ a rapid response CO_2 sensor in an eddy correlation technique for direct measurement of the flux of CO_2 between the atmosphere and agricultural crops.

b. To obtain concurrent measurements of sensible and latent heat fluxes in order to evaluate the components of the energy budget over agricultural crops.

2. To evaluate the nature of turbulence over agricultural crops through the use of integral statistics of CO_2, humidity, temperature, and wind velocity fluctuations.

3. To examine the structure of turbulence in the frequency domain above agricultural crops through the use of spectral analyses.

In pursuit of these objectives, calibration and field operation procedures were devised for the prototype, fast response CO_2 sensor. This sensor and other rapid response instruments were used in measurements over a soybean canopy (Glycine max. L. Merrill) in 1980-1981 and over a sorghum canopy (Sorghum bicolor L.) in 1982.

CHAPTER 2

Theoretical and Experimental Background

Researchers in the field of turbulence have come to grips with some of the most difficult problems encountered in fluid mechanics, according to Liepmann (1979). Progress in this field is painfully difficult, fraught with a maze of interconnected facts and problems. Perhaps these words of Niels Bohr are appropriate in this context:

"Without paradox there is no hope of progress."

In the review that follows, the development of the basic principles and theories employed in the study of the turbulent transport of mass and energy in the atmospheric surface layer will be presented in brief. Pertinent literature is reviewed here as well as in Chapter 4 - the Results and Discussion. Instrumentation used in surface layer studies of turbulence and some important experimental findings will be covered in this chapter as well.

2.1 The Atmospheric Surface Layer and the Internal Boundary Layer

The atmosphere's planetary boundary layer is a layer of air lying between the surface and the zone of the quasi-geostrophic winds at some variable height, typically on the order of 100 to 1000 m (according to Plate (1971)). It is through this layer that momentum is carried from its quasi-geostrophic source to its sink at the surface. Through this mechanical mixing induced by surface shear from the ground as well as through the thermally induced mixing resulting from surface heating, mass and energy are transported through the planetary boundary layer.

The earth's surface can be thought of as being 'homogeneous' on a grand scale, comprised of a mixture of heterogeneous areas. The lower level of the planetary boundary layer, the surface layer, becomes characteristic of the surface. However, on smaller scales homogeneity exists within scaling limits and the lower portions of the surface layer become representative of the particular surface or area below it.

The scale of immediate interest to this study is that of a large agricultural field. In micrometeorological studies over a field, care is taken that the vegetative surface or crop canopy is as homogeneous as possible. Over this field an internal boundary layer within the surface layer develops downwind from the leading edge of the field as shown by Brakke (1977) and illustrated in Figure 2.1. (See Munroe and Oke, 1975).

The depth of the internal boundary layer gradually increases from the leading edge of the field as mixing of the surface and atmospheric constituents continues along it's length. The height of this internal boundary layer is given by Pasquill (1972) and by Munro and Oke (1975), among others. Pasquill's rule of thumb estimates that the thickness of the fully adjusted layer in which fluxes may be assumed to be constant with height increases at a rate of 1% in 100 m of fetch or a fetch to height ratio of 100:1. Munroe and Oke believe that this rule implies a smaller roughness value than that normally measured over most crops. For example, Baldocchi (1982) found typical roughness lengths (z_0) on the order of 0.07 to 0.08 over soybeans. Using a table produced by Munroe and Oke, one finds a fetch to height ratio of between 40:1 and 60:1.

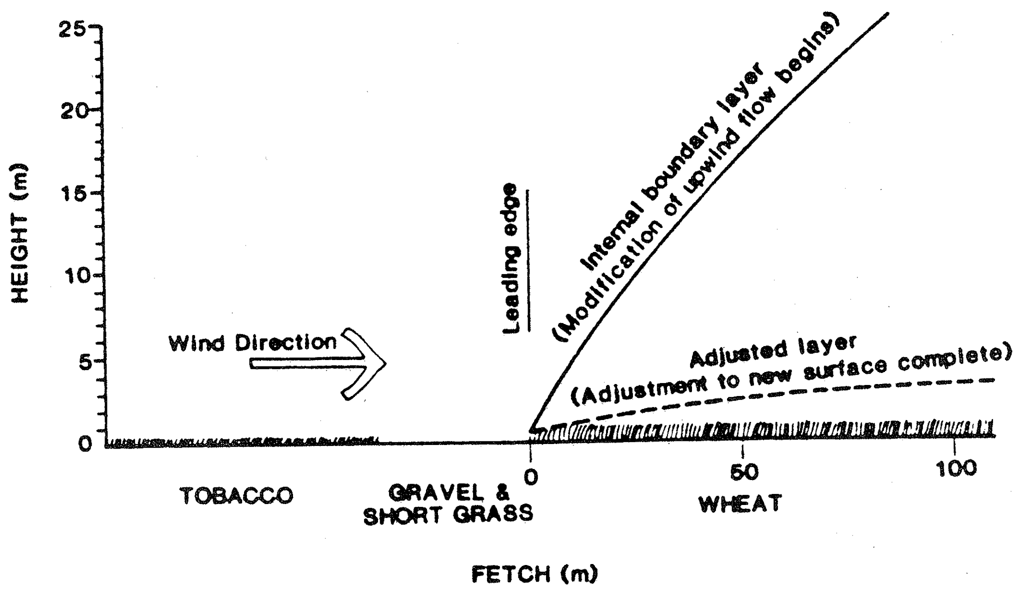

Fig. 2.1 Development of the internal boundary layer. (from Munroe and Oke, 1975).

The determination of the height of the internal boundary layer is very important to insure the best possible conditions for measuring surface layer turbulent transport. It is assumed that within this layer turbulent fluxes are constant with height. This assumption was criticized by Mordukhovich and Tsvang (1966), Dyer (1968) and by Tennekes (1973a) who pointed out that the vertical gradient of momentum flux is greater in the surface layer than in any other sublayer in the atmosphere. However, several more recent works have shown that vertical variation of fluxes is rather small. Dyer and Hicks (1972) for instance report that vertical variation in momentum and heat flux is on the order of 10% or less over heights of 4-14 m within the surface layer. Despite its limitations, the constant flux layer assumption is quite valuable in that it offers a means by which progress in further research in the surface layer may be pursued.

2.2 The Energy Budget

The major source of energy in the atmospheric surface layer region is solar radiation. The energy absorbed by the surface is primarily partitioned into sensible (H), latent (LE) heat, and soil (S) heat fluxes. Other energy terms to be considered include advection of sensible or latent heat, storage terms, and energy consumed in metabolic and photosynthetic processes. Tanner (1960) considered these terms in his study of a complete energy balance of a crop volume which is shown in Figure 2.2. The energy balance may be written:

$$R_n + H_A + LE_A + S + H + LE + H_{SC} + H_{SA} + LE_{SC} + P + M = 0 \qquad (2.1)$$

where R_n is net radiation, H_A is the advected sensible heat, LE_A is

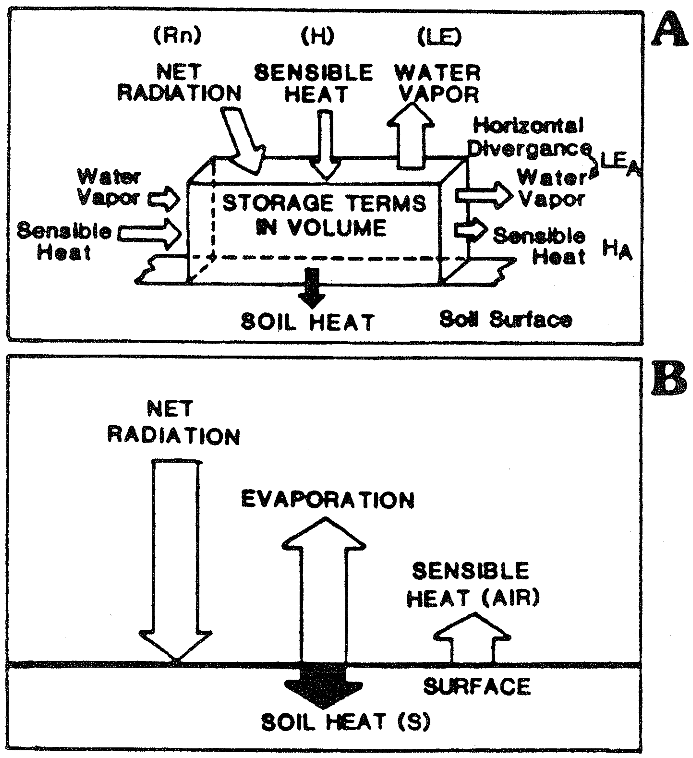

Fig. 2.2 Total energy budget of: (a) a crop volume and (b) a crop surface (from Tanner, 1960).

the advected latent heat, H_{SC} is the heat stored in the crop, H_{SA} is the heat stored in the crop volume by the air and LE_{SC} is the latent heat stored in the crop volume. P is the energy consumed by photosynthesis; M is the energy consumed by miscellaneous metabolic activities also considered very small. It is common to neglect the terms P and M with little error. Tanner estimates P to be 1 to 2% of the total energy. The storage terms may be significant, especially during transition times, i.e. early morning or late afternoon when radiation and temperature levels change rapidly. Hicks et al. (1975) found the storage terms in a forest to be about 60 ± 20 Wm^{-2} for a $1^{o}C$ per hour canopy temperature change.

The advection terms, H_A and LE_A may be quite substantial at times but can be minimized if a sufficiently large field is considered (i.e. large fetch). However, some divergence can be expected even within prescribed fetch to height ratios if a substantial surface discontinuity in water vapor or heat content exists upwind. Thom (1975) has found H_A to be 100 Wm^{-2} on occasion when the upwind temperature gradient was $1^{o}C$ per 100 m. Despite the significance of horizontal advection of sensible or latent heat, these terms too are often neglected; primarily because of the difficulty in measuring them accurately. It is very important, therefore, that fetch to height ratios are adequate.

Considering the simplifications mentioned above, the energy budget may be re-written simply as:

$$R_n + S + H + LE = 0 \qquad (2.2)$$

Methods of measuring R_n and S are relatively well established while means of accurately measuring H and LE are not as solid. Reviews of the various means of measuring H and LE are contained in Kanemasu et al.

(1979) and in Rosenberg et al. (1983). The eddy correlation and flux gradient methods will be discussed later in the chapter.

2.3. Theoretical Description of Turbulence

2.3.1. Descriptive Equations

Scientific research in turbulence began roughly a hundred years ago with the pioneering works of Osborne Reynolds (1883, 1895) describing laminar and turbulent flows. By this time, the Navier-Stokes equations governing fluid motion were already founded. A system of six equations, including the three Navier-Stokes equations of motion (in Cartesian coordinates), an equation for conservation of mass, the equation of state, and the thermodynamic energy equation describe fluid (or gaseous) flow governing transport of energy and mass in the atmosphere. A development of these equations can be found in Lumley and Panofsky (1964), Monin and Yaglom (1971), Plate (1971) or Tennekes and Lumley (1972).

The present study will be concerned with the transport of momentum, heat, water vapor and CO_2 above a vegetated surface. The governing equations of importance to this study are the momentum equation:

$$\frac{\partial u_i}{\partial t} + u_j \frac{\partial u_i}{\partial x_j} = -1/\rho_o \frac{\partial P}{\partial x_i} + g \frac{T_1}{T_o} \delta_{3i} + \nu \frac{\partial^2 u_i}{\partial x_i \partial x_i} - 2\Omega\varepsilon_{ijk}\eta_j u_k \; ; \qquad (2.3)$$

and the diffusion equation for heat:

$$\frac{\partial T_1}{\partial t} + u_j \frac{\partial T_1}{\partial x_j} = D_T \frac{\partial^2 T_1}{\partial x_j \partial x_j} - \frac{1}{\rho_o C_p} \frac{\partial R_i}{\partial x_j} \qquad (2.4)$$

water vapor;

$$\frac{\partial \rho_v}{\partial t} + u_j \frac{\partial \rho_v}{\partial x_j} = D_v \frac{\partial^2 \rho_v}{\partial x_j \partial x_j} ; \tag{2.5}$$

and for CO_2;

$$\frac{\partial \rho_c}{\partial t} + u_j \frac{\partial \rho_c}{\partial x_j} = D_c \frac{\partial^2 \rho_c}{\partial x_j \partial x_j} . \tag{2.6}$$

In the above equation, u, ρ_v, and ρ_c are wind velocity, absolute humidity and absolute CO_2 concentration, respectively; P is atmospheric pressure; ρ and T are air density and temperature where subscripts (o) indicate reference state and (1) the departure from reference; R is radiative flux; D is the diffusivity constant of temperature, water vapor and CO_2, indicated by the subscripts T, v and c, respectively; ν is the kinetic viscosity; Ω is Coriolis acceleration as applied by the unity tensor ε; η is a unit vector parallel to the earth's axis of rotation; g and C_p are the constants of gravitational acceleration and specific heat of air, respectively; δ is the Kronecker Delta, and the subscripts i, j, and k = 1, 2, or 3 for the longitudinal, latitudinal and vertical directions, respectively. (A list of all symbols can be found in Appendix 1). In surface layer studies, the last term in equation 2.3, the Coriolis acceleration, is often neglected since it is quite small compared with the other terms. The last term in equation 2.4 is the temperature change due to radiative flux divergence. In micrometeorological studies this term is also often neglected for reasons of simplification, with the notion that its contribution to the total equation is negligible. According to Munn (1966) and, Monin and Yaglom (1971) citing the work of Funk (1960, 1964) radiative flux divergence can be significant, particularly within a few meters of the earth's surface. Apparently radiative flux divergence is largest in the lower few meters of the surface layer, just above the earth's surface, where atmospheric transmissivity in the radiative transfer equation is most affected by water vapor concentration. Thus, the vertical gradient of radiative flux as influenced by water vapor gradients can be significant in the energy balance of turbulent air parcels.

The equations of motion, 2.3 - 2.6, are written in terms of instantaneous parameters: u_j, T_1, ρ_v and ρ_c. These values can be Reynolds decomposed into mean and fluctuating components. For example:

$$u_j = \overline{U}_j + u_j'$$
$$T_1 = \overline{T}_1 + T' \qquad (2.7)$$

where $(\overline{\ })$ indicates a mean quantity and a $(')$, time deviation from the mean. The other variables are handled in like manner. By decomposing equations 2.3 - 2.6,employing Reynolds rules of decomposition and averaging term by term the mean flow equations are found for momentum:

$$\frac{\partial \overline{U}_i}{\partial t} + u_j \frac{\partial \overline{U}_i}{\partial x_j} = \frac{-1}{\rho_o} \frac{\partial \overline{P}}{\partial x_j} \delta_{ij} + \frac{\partial}{\partial x_j} \left(\nu\left(\frac{\partial \overline{U}_i}{\partial x_j} + \frac{\partial \overline{U}_j}{\partial x_i}\right) - \right.$$

$$\left. \overline{u_i' u_j'}\right) + \frac{g T_1}{T_o} \delta_{i3}; \qquad (2.8)$$

for heat:

$$\rho_o C_p \left(\frac{\partial \overline{T}_1}{\partial t} + u_j \frac{\partial \overline{T}_1}{\partial x_j}\right) = \rho_o C_p \frac{\partial}{\partial x_j} \left(D_T \frac{\partial \overline{T}_1}{\partial x_j} - \overline{u'_j T'}\right); \qquad (2.9)$$

for water vapor:

$$\frac{\partial \overline{\rho}_v}{\partial t} + u_j \frac{\partial \overline{\rho}_v}{\partial x_j} = \partial/\partial x_j \left(D_v \frac{\partial \overline{\rho}_v}{\partial x_j} - \overline{u'_j \rho'_v}\right); \tag{2.10}$$

and for CO_2:

$$\frac{\partial \overline{\rho}_c}{\partial t} + u_j \frac{\partial \overline{\rho}_c}{\partial x_j} = \partial/\partial x_j \left(D_c \frac{\partial \overline{\rho}_c}{\partial x_j} - \overline{u'_j \rho'_c}\right) \tag{2.11}$$

Further manipulations of these equations lead to very useful expressions of energy and variance budgets of the parameters u_i, T_1, ρ_v and ρ_c. However, simplifications of equations 2.8 to 2.11 lead to relations of immediate importance to this study and will be discussed below.

2.3.2. Equations of Horizontally Homogeneous Flows

A method of simplifying equations 2.8 - 2.11 described in Busch (1973), Munn (1966) and Monin and Yaglom (1971) is outlined here. Considering quasi-steady state, horizontally homogeneous conditions and neglecting the molecular flux contributions, the turbulent fluxes are given as:

momentum flux: $$\tau = -\rho_o \overline{u'w'} \tag{2.12}$$

heat flux: $$H = -\rho_o C_p \overline{w'T'} \tag{2.13}$$

vapor flux: $$E = -\overline{w'\rho_v'} \tag{2.14}$$

CO_2 flux: $$F_c = -\overline{w'\rho_c'} \tag{2.15}$$

where $w' = u_3'$. The practical application of these equations in surface layer experiments will be discussed later.

2.3.3. Semi-Empirical Theories

In an effort to solve the Navier-Stokes equations, expressions for the momentum flux (or Reynolds stress) in terms of mean flow parameters were obtained by Boussinesq (1877, 1897). These were subsequently documented by Taylor (1915), Prandtl (1925) and von Kármán (1930). Boussinesq approximated Reynolds stress in this way:

$$\rho\ \overline{u'w'} = \rho\ \overline{l'w'}\ \frac{d\overline{U}}{dz}\ . \tag{2.16}$$

The length scale, l' can be thought of in analogous terms to the molecular free path of Brownian motion, in this case for eddies instead of molecules. It is useful to define an eddy diffusivity:

$$K = \overline{l'w'} \tag{2.17}$$

and apply it to (2.16). It follows that:

$$\rho\ \overline{u'w'} = \rho K_M \frac{\partial \overline{U}}{\partial z} = \tau \tag{2.18}$$

and similarly for heat, water vapor and CO_2 fluxes:

$$H = \rho K_H \left(C_p \frac{\partial \overline{T}}{\partial z}\right), \tag{2.19}$$

$$E = K_W \frac{\partial \rho_v}{\partial z} \tag{2.20}$$

and $$F_c = K_c \frac{\partial \rho_c}{\partial z}\ , \tag{2.21}$$

where K_m, K_H, K_W and K_c are the eddy diffusivities of momentum heat, water vapor, CO_2, fluxes, respectively. While these equations are of considerable practical importance they do not have the sound theoretical basis that equations 2.12 - 2.15 have as a result of the assumptions made in their derivation.

2.4. Similarity Theory

From the constant flux layer assumption discussed earlier, it follows that momentum flux must be constant with height:

$$\tau_o = -\rho_o\ \overline{u'w'} = -\rho_o u_*^{\,2}, \tag{2.22}$$

where u_* is the characteristic velocity scale, also called the friction velocity. Heat, water vapor and CO_2 fluxes have similar scaling arguments:

$$\text{(heat)} \qquad H = \rho_o C_p \overline{w'T'} = -\rho_o C_p u_* T_* \ , \tag{2.23}$$

$$\text{(water vapor)} \quad E = \overline{w'\rho'_v} = -u_* \rho_{v_*} \ , \tag{2.24}$$

$$(CO_2) \qquad F_c = \overline{w'\rho'_c} = -u_* \rho_{c_*} \ . \tag{2.25}$$

From these equations, values for the characteristic scales of surface layer turbulence: u_*, T_*, ρ_{v*} and ρ_{c*} may be easily found. Recently Berkowicz and Prahm (1981) have proposed another scaling velocity (in place of u_*) which is related to certain terms in the turbulent kinetic energy balance of the surface layer.

Under the constraints of the constant flux layer assumption, the characteristic logarithmic wind speed profile, may be developed (Tennekes and Lumley, 1972):

$$\frac{\partial \overline{U}}{\partial z} = \frac{u_*}{kz} \tag{2.26}$$

where k is the von Kármán constant. The bounds of this relationship were discussed by Tennekes (1973b). Integration of 2.26 yields:

$$\frac{\overline{U}}{u_*} = \frac{1}{k} \ln (z/z_o) \tag{2.27}$$

where z_o, the roughness length, is related to the aerodynamic roughness of the surface objects (see Thom, 1975). For tall objects or vegetation, for example, z in equation (2.27) is replaced by (z - d). Similar arguments to (2.26) exist for heat, water vapor, and CO_2 profiles. Further discussion of this subject may be found in Thom (1975), Brutsaert (1975), Hicks (1977), and Shaw and Pereira (1982).

Another important scaling parameter is the characteristic length scale, L, first determined by Monin and Obukhov (1954) and named after them. The ratio of the height above the surface, z, to the Monin-Obukhov scaling length, L, yields a non-dimensional stability parameter. This value is related to the flux Richardson number, R_f. As discussed in Tennekes and Lumley (1972), R_f is the ratio of the buoyancy and mechanical-shear production terms in the balanced kinetic energy equation. It is written as:

$$R_f = \frac{g}{T_o} \frac{\overline{w'T'}}{\overline{u'w'}\,\partial U/\partial z} \tag{2.28}$$

Substituting 2.22, 2.23 and 2.26 into 2.28 one finds:

$$R_f = z/L. \tag{2.29}$$

where:
$$L = \frac{u_*^3 T_o}{kgH} \tag{2.30}$$

Equation 2.30 may be corrected for density variations due to water vapor content. This may be done by replacing T by the virtual temperature, T_v

where:
$$T_v \simeq T\,(1 + 0.61q) \tag{2.31}$$

Using equation 2.31, 2.30 becomes:

$$L = \frac{u_*^2 T_v}{gkT_*} + \frac{u_*^2 T_v \rho}{0.61gk\rho_{v*}T} \tag{2.32}$$

$$= L_T + L\rho_v \tag{2.33}$$

as developed by Busch (1973) and McBean (1971). Note that 2.30 is actually a special case of 2.33 for $\rho_v = 0$.

2.5 Statistical Description of Turbulence

Turbulence consists of a complex array of atmospheric motions that occur over a continuous range of scales. Turbulent motion is deterministic by nature but due to its complexity it is not yet possible to describe motions at all points. A convenient method of analyzing turbulence is to consider it to be of random nature. Some other simplifying concepts enumerated in Munn (1966), Monnin (1965), and Hinze (1959) include stationarity and homogeneity, in which case probability distributions of turbulent fluctuations are considered independent of time and space (horizontal), respectively. Also considered are isotropic conditions in which turbulent fluctuations have no preferred direction of motion; and similarity, claiming that the characteristic length and velocities scales are all that is needed to determine the structure of turbulence. Munn cites criticism of the isotropy concept in its application to the surface layer which is generally dominated by shear flow. However, the concept of local isotropy, pertaining to high frequency fluctuations, is valid (Munn, 1966).

2.5.1. Integral Statistics

There are several important statistics which can be used to characterize turbulent motions over the entire frequency domain of fluctuations. These include (using w and T for example):

$$\text{variances:} \quad \sigma_T^2 = \overline{T'^2} \tag{2.34}$$

covariances: $\overline{w'T'}$ (2.35)

correlation coefficients: $r_{wT} = \dfrac{\overline{w'T'}}{(\overline{w'^2}\,\overline{T'^2})^{\frac{1}{2}}} = -\dfrac{u_* T_*}{\sigma_w \sigma_T}$ (2.36)

and turbulent intensities (or scaled standard deviations):

$$\frac{\sigma_T{}^2}{T_*} = \frac{\overline{T'^2}}{T_*} \tag{2.37}$$

The correlation coefficients and turbulent intensities are non-dimensional and provide the investigator a means by which turbulent fields in different space or time may be compared. The correlation coefficient enables one to examine the efficiency of turbulent transport of various quantities such as momentum, sensible and latent heats, and CO_2 (McBean, 1972). In many studies, it is popular to examine relationships between the correlation coefficients, turbulent intensities, and surface layer stability. Quite often in these studies the stability parameter chosen is z/L.

2.5.2. Turbulence Spectra

Principles set forth in the 1930's established the means by which kinetic energy of atmospheric motions or eddies may be expressed as a function of frequency. In quasi-steady state, homogeneous, isotropic turbulence, the correlation tensor between velocity vectors ($\vec{x}$) spacially separated by a distance vector ($\vec{r}$) in time (t) is defined (after Hinze, 1959) as:

$$R_{ij}\,(\vec{r}) = \overline{u_i'(\vec{x},t)\;u_j'(\vec{x} + \vec{r},\, t)} \tag{2.38}$$

For one dimension, 2.38 reduces to:

$$R_1(r) = \overline{u_i'(x)u_i'(x + r)} \tag{2.39}$$

Taylor (1938) noted that the Fourier transform of the correlation tensor yielded spectral energy:

$$S_{ij}(\vec{\kappa}) = \frac{1}{(2\pi)^3} \iiint_{-\infty}^{\infty} e^{i\vec{\kappa}\vec{r}} R_{ij}(\vec{r})\, d\vec{r} \tag{2.40}$$

or in one dimension for the longitudinal velocity:

$$S_1(\kappa_1) = \frac{1}{2\pi} \int_{-\infty}^{\infty} e^{-i\kappa_1 r_1} R_1(r)\, dr \tag{2.41}$$

Unlike the energy spectrum of light in which electromagnetic waves preserve their wavelength, turbulent waves or eddies undergo a continuous erosion process in which large eddies decompose into succesively smaller eddies until dissipated by viscosity. Kolmogorov (1941) hypothesized this occurrence in isotropic turbulence. His rules of similarity are summarized in Munn (1966). The Kolmogorov hypothesis stems from the energy equation (after Long, 1982):

$$\frac{\partial S}{\partial t} = -\frac{\partial E}{\partial k} - 2\nu\kappa^2 S \tag{2.42}$$

where κ is wave number (related to frequency by Taylor's frozen turbulence hypothesis i.e. $\kappa = 2\pi n/\overline{U}$), S is total energy, and E is the energy transfer function. Energy (S) is contained in large eddies. It is transferred to consistently smaller eddies until finally transformed from the smallest eddy sizes into heat energy by viscosity at a rate denoted by $2\nu\kappa^2 S$. Energy lost to dissipation in the transfer of energy to smaller eddies is small and is given by $\partial E/\partial\kappa$.

Kolmogorov also hypothesized that turbulence in the region of local isotropy was governed by viscosity, ν, and dissipation, ε.

Employing some dimensional analysis Kolmogorov developed a relationship between the spectral energy and wave space (or length):

$$S = \alpha \varepsilon^{2/3} \kappa^{-5/3} \tag{2.43}$$

where α is the Kolmogorov constant. This universal relationship describes eddies of the inertial sub-range - those that transport energy from the large, energy containing eddies to the eddies of the viscous dissipation range. An idealized plot of spectral energy over the range of surface layer eddy sizes is given in Figure 2.3.

Subsequent work by Kolmogorov (1962) and others (see Long, 1982, for a review) have modified the original argument in 2.43 in an effort to properly match the inertial sublayer to the viscous dissipation region. Recently, Long and Chen (1981) and Long (1982) have re-described the problem and have suggested the existence of a "meso layer" between the inertial sub-range and the viscous dissipation range. Support for this hypothesis has not been assembled at this time.

The inverse Fourier transform of 2.41 in terms of frequency (n) is:

$$\overline{u'^2} = \int_0^\infty S_{uu}(n)dn \tag{2.44}$$

This is in accordance with the frozen hypothesis assumption where

$$n = \frac{k\overline{U}}{2\pi} \tag{2.45}$$

Replacing $\overline{u_i'u_i'}$ with $\overline{u'w'}$ in equation (2.39) , the inverse Fourier transform of (2.41) in terms of n becomes:

$$\overline{u'w'} = \int_0^\infty S_{uw}(n)dn \tag{2.46}$$

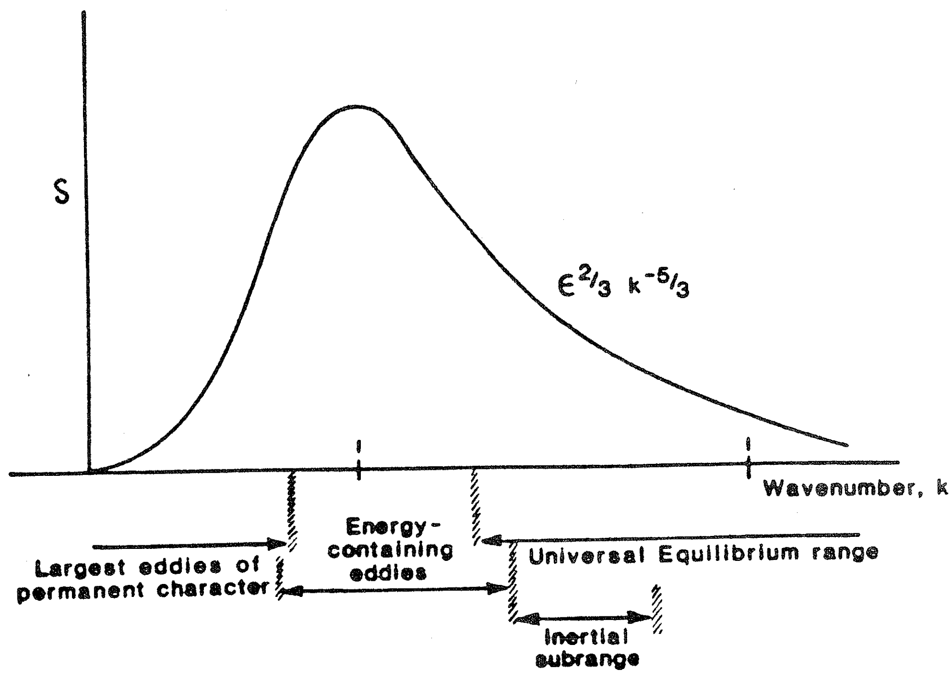

Fig. 2.3 The energy spectrum of eddies in the surface layer (from Hinze, 1959).

and likewise for other covariances in time.

Using similar forms of equations (2.44 and 2.46) spectral correlation coefficients may be found as McBean (1970) has done:

$$R_{uw} = \frac{C_{uw}(n)}{[S_{uw}(n)S_{uw}(n)]^{\frac{1}{2}}} \tag{2.47}$$

and likewise for other pairs. The spectral correlation coefficient is valuable in the comparison of turbulent transport efficiencies of, for instance, heat, water vapor, or CO_2 by eddies of various sizes.

Generally, spectra and cospectra are normalized by the respective variances and covariances. By use of the non-dimensional frequency, f the spectra or cospectra become, approximately, independent of height (Munn, 1966):

$$f = \frac{nz}{\overline{U}} \tag{2.48}$$

The interpretation of spectra and cospectra in terms of the evaluation of tendencies and peak frequencies is typically done from analyses of logarithmically transformed spectra i.e. log-log plots of the data. Possible errors associated with interpretation of the characteristics of spectra from linear plot presentations were discussed by Zangvil (1981).

2.6 Measurement Techniques

2.6.1. The Eddy Correlation Method

2.6.1.1. Theoretical Considerations

The theoretical development of the eddy correlation method follows directly from equation 2.12 - 2.15 in section 2.3.2. Swinbank (1951) formalized the technique stating that the flux of any entity (s) may be written as:

$$F = \overline{\rho ws} \tag{2.49}$$

Decomposing (2.49) and applying Reynold's averaging rules, (2.49) becomes:

$$F = \rho\overline{ws} + \rho\overline{w's'} \tag{2.50}$$

Equation (2.50) consists of a mean flux $\rho\overline{ws}$ and an eddy flux, $\rho\overline{w's'}$. Over a sufficiently long period of time $\bar{w} = 0$ and 2.50 reduces to:

$$F = \rho\overline{w's'} \tag{2.51}$$

Recent work by Webb and Pearman (1977), Jones and Smith (1978), Bakan (1978), Smith and Jones (1979) and Webb et al. (1980) have shown that some difficulty exists with the assumption that $\bar{w} = 0$ when the net flux of ρ_a, i.e. $\overline{w\rho_a}$ is also assumed to be zero. Warm and moist parcels of air rising from the surface will have less density than displaced cool and dry parcels descending in accord with conservation of mass principles. Thus, if net mass flux is assumed to be zero, some mean wind speed, $\bar{w} \neq 0$, must exist. Webb et al. (1980) found that a flux equation of the form of (2.50) must be employed to account for $\bar{w} \neq 0$, which incorporates the effects of sensible heat and water vapor fluxes on air density. As $\bar{w}$ is generally too small to measure, a means by which $\bar{w}$ may be calculated was derived by Webb et al. (1980). This correction becomes especially significant for the measurement of constituents in low concentration. Further discussion on this correction will be found in Chapter 3.

2.6.1.2. Instrumentation

While the theoretical expressions for flux measurements appear rather simple, the instrumentation in many cases is quite complicated because of the need for sufficient accuracy and resolution in the sensing of U, V, W, T, ρ_v, and ρ_c fluctuations. The required accuracy, resolution, response and reliability of the instruments must be considered if experimentation is to be productive. These requirements are discussed by Kaimal (1975),McBean (1972) and Dyer and Hicks (1972). In addition to sensor requirements, data logging devices must be capable of handling large amounts of data at sufficiently high rates. Sampling rate and signal resolution requirements are equally important as sensor requirements.

A review of some of the more widely used turbulence sensors of wind speed, temperature, humidity and CO_2 follows.

Wind Speed Sensors

Propellor anemometers have been used extensively in surface layer turbulence research and details of the performance of certain models may be found in Hicks (1972), Gill (1975) and Motha (1978). While propellers are simple to use and maintain, their response characteristics at high frequencies are not as good as that of the drag anemometer (Redford et al. 1981).

The drag anemometer works by measuring the drag force exerted by the wind on a uniform aerodynamic body. It has good response characteristics in the high frequency range and has a resonant frequency near 20 HZ. Details of this instrument may be found in Perry (1977) and Norman et al. (1976). Also having good response and resolution characteristics is a one dimensional sonic anemometer (Campbell and Unsworth, 1979). This instrument measures the difference in the speed of sound, between two fixed points, due to wind speed. It has the potential for higher frequency response and greater sensitivity than the drag anemometer. Maintenance requirements are normally very minimal since it has no moving parts. However, the electrical design is quite sophisticated. A discussion of the use and calibration of the one dimensional sonic anemometer will be given in Chapter 3. Discussions of 3-dimensional sonic anemometers are given in Kaimal and Businger (1963) and Mitsuta (1966).

Other wind speed sensors used, though much less frequently than the above three anemometer types in field studies, are the pressure-sphere anemometer (Thurtell et al. (1970), the hot film anemometer (Ling and Hubbard, 1956; Champagne et al., 1967 and Lang and Leuning, 1981) and the hot wire anemometer (Gjessing et al. 1969 and, Olin and Kiland, 1970).

Temperature Sensors

Temperature is probably the easiest atmospheric variable to measure. Two major groups of sensors exist: the thermocouple type in which a current or voltage varies with temperature and the resistance type in which the resistance of a material varies with temperature. A comparison of fine wire thermocouple and microbead thermistor measurements was made by Verma et al. (1979).

Humidity Sensors

Fast response atmospheric humidity measurements have been made with fine wire thermocouple - psychrometers, Lyman-alpha hygrometers and infrared beam hygrometers. The thermocouple-psychrometer consists of side-by-side thermocouples, one dry and one wrapped in wetted thread (the "wet bulb"). The psychrometer's response is slowed by the thermal mass of the thermocouple junction, lead wire, and its wick.

The Lyman-alpha hygrometer described in Tillman (1965) and Buck (1976) measures the absorption of ultra-violet radiation by water vapor over an open air sensing path. It has a very fast response and was shown by Redford et al. (1980), using humidity spectra, to have superior frequency response to that of the psychrometer. Further discussion of the Lyman-alpha hygrometer is continued in Chapter 3.

The infrared hygrometer functions similarly to the Lyman-alpha hygrometer but uses infrared radiation rather than UV to sense water vapor. Hyson and Hicks (1975), Takeuchi et al. (1980), and Ohtaki and Matsui (1982) have reported the use of infrared hygrometers in their experiments. Takeuchi et al. (1980) showed that the infrared hygrometer exhibited superior response to that of the thermocouple-psychrometer.

Another humidity sensor, the refractometer, has been developed to measure humidity fluctuations. This sensor detects the change of the dielectric constant of air as affected by humidity. Martin (1971) found the refractometer to compare rather well with the Lyman-alpha hygrometer.

CO_2 Sensors

Fast response CO_2 sensors are a rare find. Some attempts have been made (Desjardins and Lemon, 1974) to modify slow response infrared gas analyzers for eddy correlation measurements but no effort has succeeded in matching the requirements necessary for accurate measurements within a few meters of the surface.

Ohtaki and Matsui (1982), Brach et al. (1981), Ohtaki (1980), and Jones et al. (1978) report fast reponse CO_2 measurements made by infrared radiation absorption methods using an open cell path, similar in principle to the Lyman-alpha and infrared hygrometers. Ohtaki (1980) and Ohtaki and Matsui (1982) report favorable sensitivity and response characteristics with their sensor placed 1-2 meters above a crop.

A fast response CO_2 sensor similar in principle to that of Ohtaki (1980) was designed and built by Bingham et al. (1978). A prototype was made available to this study in the 1981 growing season and a refined version was used during the 1982 growing season. Details of this sensor including response, sensitivity, repeatability, and reliability characteristics; accuracy; and calibration methods are presented in Chapter 3.

2.6.2. The Flux-Gradient Theory

2.6.2.1. Theoretical Considerations

The theory employed in flux gradient measurement is based upon the semi-empirical relationships presented in section 2.3.2 that lead to equations 2.18 to 2.21. Time or spatially averaged responses to atmospheric parameters measured at two or more heights are used in computing the necessary gradients. Two methods for obtaining the eddy diffusivity coefficients, K_M, K_H, K_W, and K_C have been used extensively.

The aerodynamic method involves the use of the flux gradient equations 2.18 - 2.21, e.g.:

$$\tau = \rho K_M \frac{\partial U}{\partial z} \qquad (2.52)$$

the surface flux equations 2.22 - 2.25, e.g.:

$$\tau = -\rho u_*^{\,2} \tag{2.53}$$

and the gradient:

$$\frac{\partial U}{\partial z} = \frac{u_*}{kz}\,\phi_m \tag{2.54}$$

where ϕ_m is the stability adjustment parameter proposed by Monin and Obukhov (1954). The eddy diffusivity (K_M) can be solved using equation 2.52 and substituting $\partial U/\partial z$ from 2.54 and $-\tau/\rho$ from equation 2.53. Similar methods are used in solving for K_H, K_W and K_C. The values of ϕ_m, Φ_H, Φ_W and Φ_C must be assumed from prior experiments such as those of Pruitt et al. (1973), Dyer and Hicks (1970), Webb (1970) and Businger et al. (1971). Pioneering work using the aerodynamic method over crops was done by Inoue (1957), Lemon (1960) and Monteith and Szeicz (1960).

Another method of solving for eddy diffusivity is known as the Bowen ratio energy balance method and is based on equation 1.2. By assuming that the eddy diffusivities for heat, water vapor and CO_2 are equal, the eddy diffusivity coefficient may be factored out of the fluxes resulting in:

$$K = \frac{(R_n + S)}{(\rho C_p \frac{\partial \overline{T}}{\partial z} + \frac{\partial \overline{\rho}_v}{\partial z})} \tag{2.55}$$

2.6.2.2. Instrumentation

The instrumentation requirements for use with the flux-gradient method are considerably less stringent than those for the eddy correlation method since, in the former case, time averaging becomes a desirable characteristic. The primary requirements are for accuracy, resolution and durability. Typically cup anemometers are used to measure wind speed and thermocouple psychrometers measure dry and wet bulb temperatures. Mean CO_2 concentrations are measured by infrared gas analyzers. Rosenberg et al. (1983) describe the kinds of sensors used in conjunction with aerodynamic methods.

CHAPTER 3

Materials and Methods

The ability to characterize the nature of turbulence over a vegetative surface is dependent upon the accuracy, sensitivity, response time and spatial resolution of the instrumentation as pointed out by Gill and Hexter (1972) and Kaimal (1975). The physical placement of the instruments relative to one another determines the accuracy of measured turbulent fluxes. Proper data recording and processing procedures reduce the errors resulting from electronic noise, signal aliasing and sensor output drift (for details, see Kaimal, 1975).

This chapter includes a description of the experimental site, the instrumentation, data acquisition system, data logging and data processing procedures used in this study.

3.1 The Experimental Site

Studies reported here were conducted at the University of Nebraska's Agricultural Meteorology Laboratory (41° 09' N, 96° 30' W, altitude of 354 m above mean sea level), approximately 10 kilometers south of Mead, Nebraska. Mead is situated on the eastern edge of the northern Great Plains in eastern Nebraska. The land is gently rolling over most of eastern Nebraska although the immediate area about Mead is an ancient Platte River bed and is therefore much flatter. The soil in the experimental field is a Typic Argiudoll (Sharpsburg silty clay loam) and its physical characteristics are reported by Garay (1981).

In 1980 a densely pubescent isoline of (Glycine max. L. Merrill, Harosoy cv.) was planted in 0.75 m rows oriented north-south at the site. An adjacent field to the east was planted with a normally pubescent

Harosoy isoline (see Baldocchi, 1982 for description of the microclimate of the cultivars and isolines). The experimental field was approximately 210 m north to south and 85 m east to west. The adjacent field of normally pubescent soybeans was 210 m N-S and 65m E-W. Surrounding fields were planted with normally pubescent Harosoy soybeans.

In 1981 the experimental field, 210 m N-S by 73 m E-W was planted with soybeans (Clark cv.) having normal leaf width while the adjacent field to the east, 210 m N-S by 85 m E-W was planted with a narrow leaf isoline. Row spacing was again 0.75 m and rows were oriented N-S. Bordering fields were planted with Colland cv. soybeans. Grain sorghum (Sorghum bicolor L. Moench cv. Dk-57) was planted on the experimental field, 210 m N-S by 150 m E-W, for the 1982 study. Row spacing was again 0.75 m.

3.2 Instrumentation

3.2.1 General Consideration

Location of turbulent sensors (height, proximity with one another) is determined by the typical nature of turbulence. In general, the closer measurements are made to the surface, the more sensitive the instruments must be to higher frequencies in order to accurately measure turbulence fluctuations. This is easily shown in the non-dimensional spectrum plot presented in Figure 2.3. Guidelines for the height of instrument placement and required response time and spatial resolution given in McBean (1972), Garratt (1975) and Kaimal (1975) were used in this study.

Considering the requirements of fetch, spatial resolution and the response time of the instruments and data acquisition system, an optimal height of 2.25 m was chosen. Distance between instruments was optimized in consideration of desirable spatial resolution, the number and physical size of the instruments. It was also necessary to consider the effects of flow distortion caused by supporting structures as well as the instruments themselves. This has been discussed by Wieringa (1980), Dyer (1981, 1982), Hogstrom (1982) and Wyngaard (1982). Sensor arrangements at the 2.25 m height for the studies in 1980, 1981 and 1982 are illustrated in photographs given in figures 3.1, 3.2 and 3.3 respectively. Note that the fast response CO_2 sensor was absent in 1980, and that the open cell structure of the CO_2 sensor was different in 1981 and 1982. In addition, sensor designs of the sonic anemometer and Lyman-alpha hygrometer were slightly different in 1982 than in 1981.

The instruments were mounted on masts of steel pipe, steadied against vibration and swaying by a triangular array of guy wires. Various types of horizontal brackets fixed to the masts enabled daily installation and removal of the instruments to be done easily. Vertical alignment of the drag anemometer to with ½° was made possible with the aid of a bubble level mounted on the anemometer itself. Adjustment was made by altering the length of the guy wires through the use of turnbuckles.

The sonic anemometer was mounted on a ball joint for adjustment. A bubble level mounted on it was used for vertical reference check. Levelling is not as critical in the case of the Lyman-Alpha hygrometer and fast response CO_2 sensor. A visual check that the open cells or path lengths were perpendicular to the mean wind direction was all that was needed.

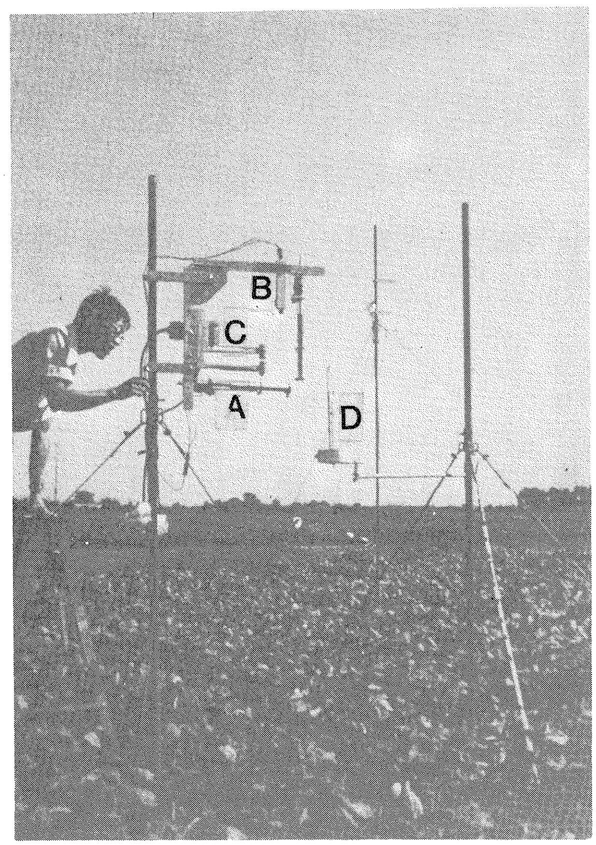

Figure 3.1 Turbulence Sensors Employed in 1980. A. Drag Anemometer, B. Fine wire thermocouple, C. Lyman-alpha hygrometer and D. Sonic Anemometer

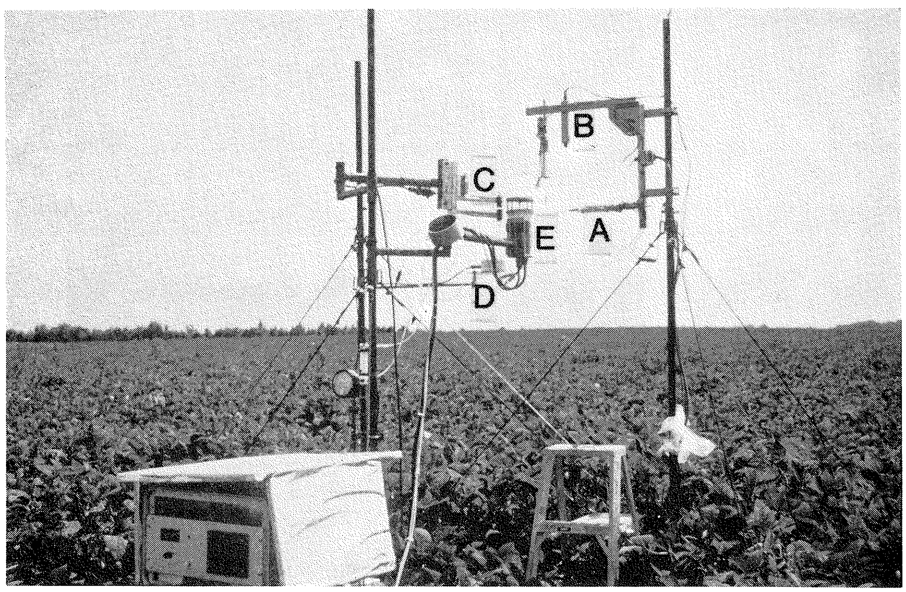

Figure 3.2 Turbulence Sensors Employed in 1981. A. Drag Anemometer, B. Fine wire thermocouple, C. Lyman-alpha hygrometer, D. Sonic Anemometer and E. Fast response CO_2 sensor.

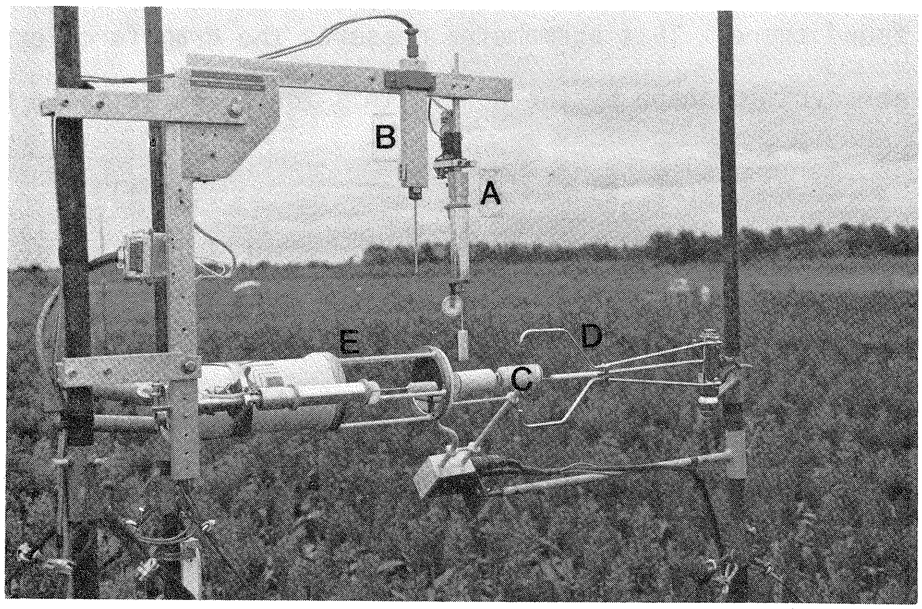

Figure 3.3 Turbulence Sensors Employed in 1982. A. Drag Anemometer, B. Fine wire thermocouple, C. Lyman-alpha hygrometer, D. Sonic anemometer and E. Fast response CO_2 sensor.

3.2.2 Wind Sensing - Fast Response

Drag Anemometer

The drag anemometer used in this study was designed and developed by Dr. J. M. Norman* at Pennsylvania State University. The anemometer has been used in several studies (Norman et al., 1976; Perry, 1977; Redford et al., 1981) and details of its hardware and operation may be found there. This anemometer measures the drag force exerted upon an aerodynamic shape by the wind. This force, F, is given by:

$$F = f\ (Re,\ S)\ \rho A U^2/2 \qquad (3.1)$$

where the coefficient of friction (f) is a function of the Reynolds number (Re) and the shape factor (S) of the element of cross-sectional area (A) perpendicular to the wind direction. The air density is given by ρ and wind speed by U. The drag elements (styrofoam cylinders 15 mm diameter, and 45mm long) are fixed onto thin, hollow, ceramic rods. The rods are mounted onto stainless stæl cantilevers attached to vertical or horizontal supporting arms. The flexing of the thin (0.3 mm) cantilevers is sensed by strain gauges, fixed to the metal, which undergo a change in electrical resistance in response to the deformation of the cantilever.

*Present address: Department of Agronomy, University of Nebraska-Lincoln.

The strain gauge may be placed in a branch of a Wheatstone Bridge circuit to modify the voltage of a stable source. This voltage (V) may be related to wind speed (U) using:

$$V = kf\rho\frac{AU^2}{2} \qquad (3.2)$$

where k is a constant. Voltage may be cosine corrected for winds perpendicular to the element by:

$$V = kf\rho\frac{AU^2}{2} \cos\theta \qquad (3.3)$$

where θ is the angle between the wind vector and the normal to the sensing element. With little error, k, A, and ρ may be considered constant, and f is virtually constant with windspeeds of 0.40 m s^{-1} or larger (Bird et al., 1960). The relationship between wind speed (U) and voltage (V_u-u component voltage) may now be expressed as:

$$U = c_1 + c_2 \, |V_u|^{\frac{1}{2}} \left(\frac{|V_u|}{V_u} \right) \qquad (3.4)$$

where c_1 and c_2 are constants and $\frac{|V_u|}{V_u}$ preserves the sign of the voltage. The intercept (c_1) is a manifestation of the behavior of f (Re, S). With little error the calibration equation (3.4) may be used for wind speeds > 0.20 m s^{-1}. The calculation of component winds (u, v and w) involves the interaction between wind components. According to Dr. Norman (personal communication) this interaction causes each of the voltages to be proportional to the product of the total wind speed and its respective component. The working equation for the u component becomes:

$$u = (U)^2 \,/\, [U^4 + V^4 + W^4]^{\frac{1}{4}} \qquad (3.5)$$

where

$$U = c_1 + c_2 \; |V_u|^{\frac{1}{2}} \; \frac{|V_u|}{V_u} \tag{3.4}$$

$$V = c_3 + c_4 \; |V_v|^{\frac{1}{2}} \; \frac{|V_v|}{V_v} \tag{3.6}$$

and

$$W = c_5 + c_6 \; |V_w|^{\frac{1}{2}} \; \frac{|V_w|}{V_w} \tag{3.7}$$

Equations similar to 3.5 are used to calculate the v and w components. Calculations of u, v and w wind components need to be corrected for the imperfect vertical or horizontal alignment of the anemometer to the wind flow (through coordinate rotation) and for non-cosine response of the individual sensors.

According to Perry (1977), for winds approaching the vertically oriented U-V drag element at elevation angles smaller than 10°, the error in uncorrected response can be greater than 2%. For winds with yaw angles less than 20° the error in the horizontally oriented w sensor measurement may be more than 4%. A first order correction is made with equations of the form (e.g. u component):

$$u = \frac{u_R}{C_u} \tag{3.8}$$

where u_R is the raw velocity and u is the corrected velocity. The correction factor C_u as well as similar factors for v and w components were experimentally determined by Perry (1977) and Norman (personal communication). The elevation and yaw angles with respect to the orthogonal sensor array are calculated from the drag anemometer signals and used to select the proper correction factors. Coordinate rotation needed to obtain $\overline{v}$ and $\overline{w}$ = 0 is performed following a transformation developed by Tanner and Thurtell (1969).

As mentioned above, equation 3.4 may be used for wind speeds in the neighborhood of 0.20 m s^{-1}. Due to the nature of the friction factor (f) and difficulty in measuring very low wind velocities during calibration a non-zero intercept is normally found. This intercept presents difficulty in finding low velocities accurately from the calibration equation in the region of about zero volts. With little measurement error (less than 0.04 to 0.05 m s^{-1} in most cases), the non-zero intercept problem may be avoided. This is done by substituting the calibration equation with a related equation over the range of 0 to 0.2 m s^{-1}. This related equation matches a zero intercept at one end and the calibration equation at the high end (0.20 m s^{-1}). The related equation is given by:

$$U = c_2 (V_u)^{\frac{1}{2}}/(1-5c_1) \qquad (3.9)$$

where c_1 and c_2 are the calibration constants. The sequence of execution of these corrections and other calculations in the wind speed calibration from the drag anemometer voltage output are discussed in Perry (1977) and Redford et al. (1981).

Zero drift arises from electrical components and the hysteresis of the strain gauge, among other factors. For this reason, shrouds are used each hour to shield the sensor from the wind and record a 'zero wind speed' or offset voltage. The drag anemometer has a natural resonant frequency of about 20 Hz and for this reason the drag elements are dampened by a mechanism using a viscous silcon oil (20,000 centipoise).

Drag Anemometer Calibration

The drag anemometer was calibrated in a pusher type wind tunnel. This type of tunnel provided more reliable calibration than did enclosed tunnels. It was found that flow was accelerated around the drag sensors due to the size of the anemometer's supporting structure with respect to the confinement of the enclosed wind tunnel.

Calibration is performed at various wind speeds with the strain gauges oriented perpendicular to the flow. To do this, the W sensor had to be rotated 90° from its normal sensing position. This involved the removal of a viscous oil damper used to dampen sensor vibration. The damper is also used in the U-V sensor arrangement but it does not have to be removed since sensor rotations for calibration occur in the horizontal plane. A pitot tube - pressure transducer combination is used for winds speeds greater than 1.5 m sec^{-1}. A low velocity anemometer (Disa Electroncs, Inc., Franklin Lakes, NJ) was used to calibrate the drag anemometer from 0.30 to 1.5 m s^{-1}. A typical calibration appears in figure 3.4 (a, b and c). Velocity calculated from the standard sensors is plotted against the drag anemometer output voltage corrected for gain and offset.

Another calibration involving the dynamic temperature compensation of the strain gauge is performed at the time of strain gauge installation. Dynamic temperature compensation is achieved by an iteration method in which temperature is varied between hot and cold. Resistors of proper value are found which reduce the change in voltage output of the strain gauges with temperature change (Perry, 1977).

One Dimensional Sonic Anemometer

The sonic anemometer used in this study is described by Campbell and Unsworth (1979) who used a prototype version manufactured by Campbell

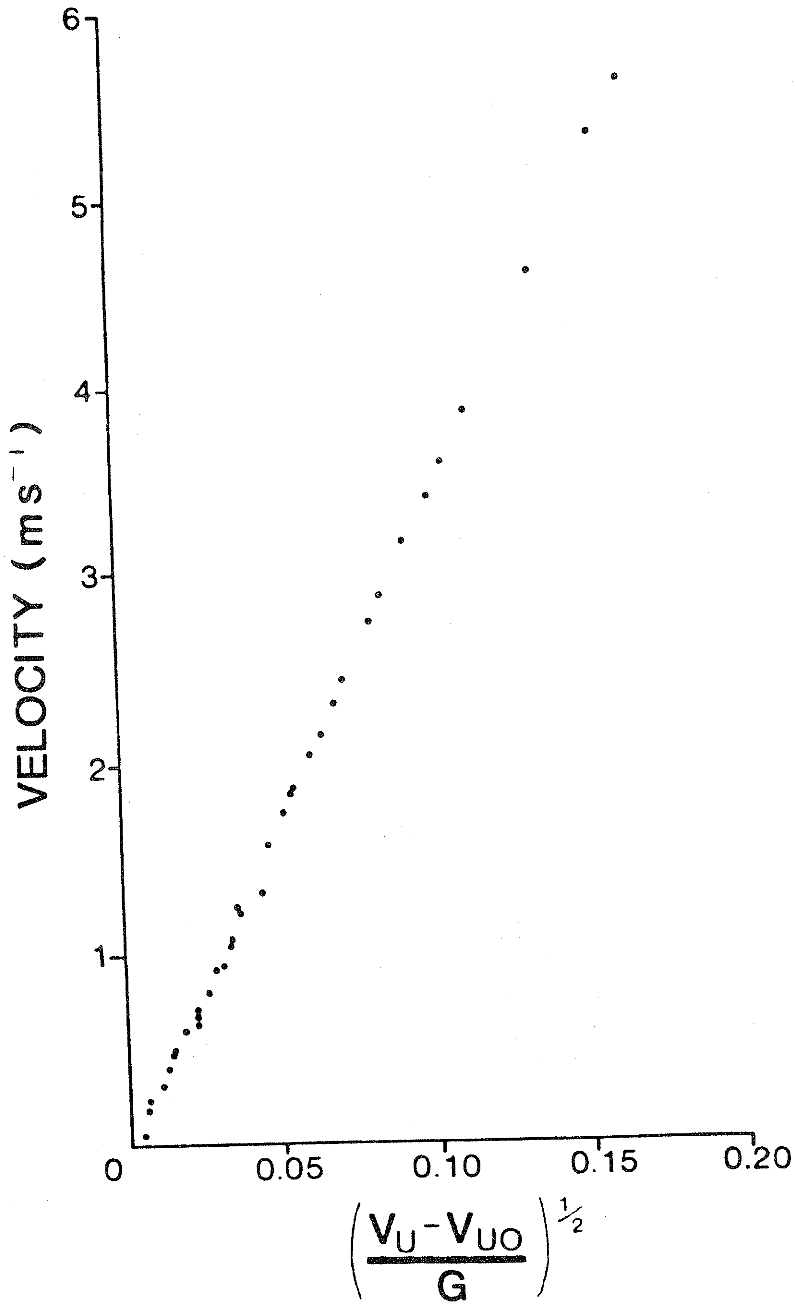

Fig. 3.4 (a) Typical drag anemometer calibration: u component

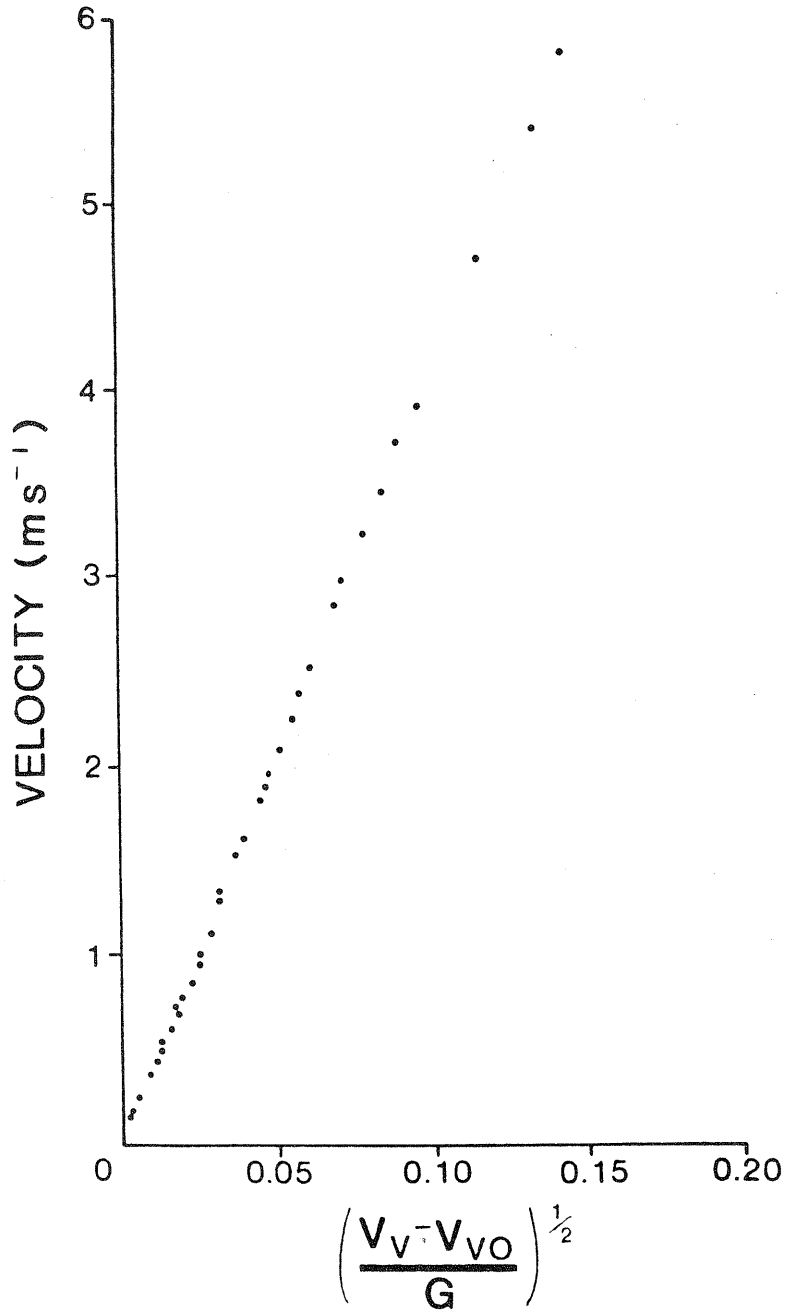

Fig. 3.4 (b) Typical drag anemometer calibration: v component

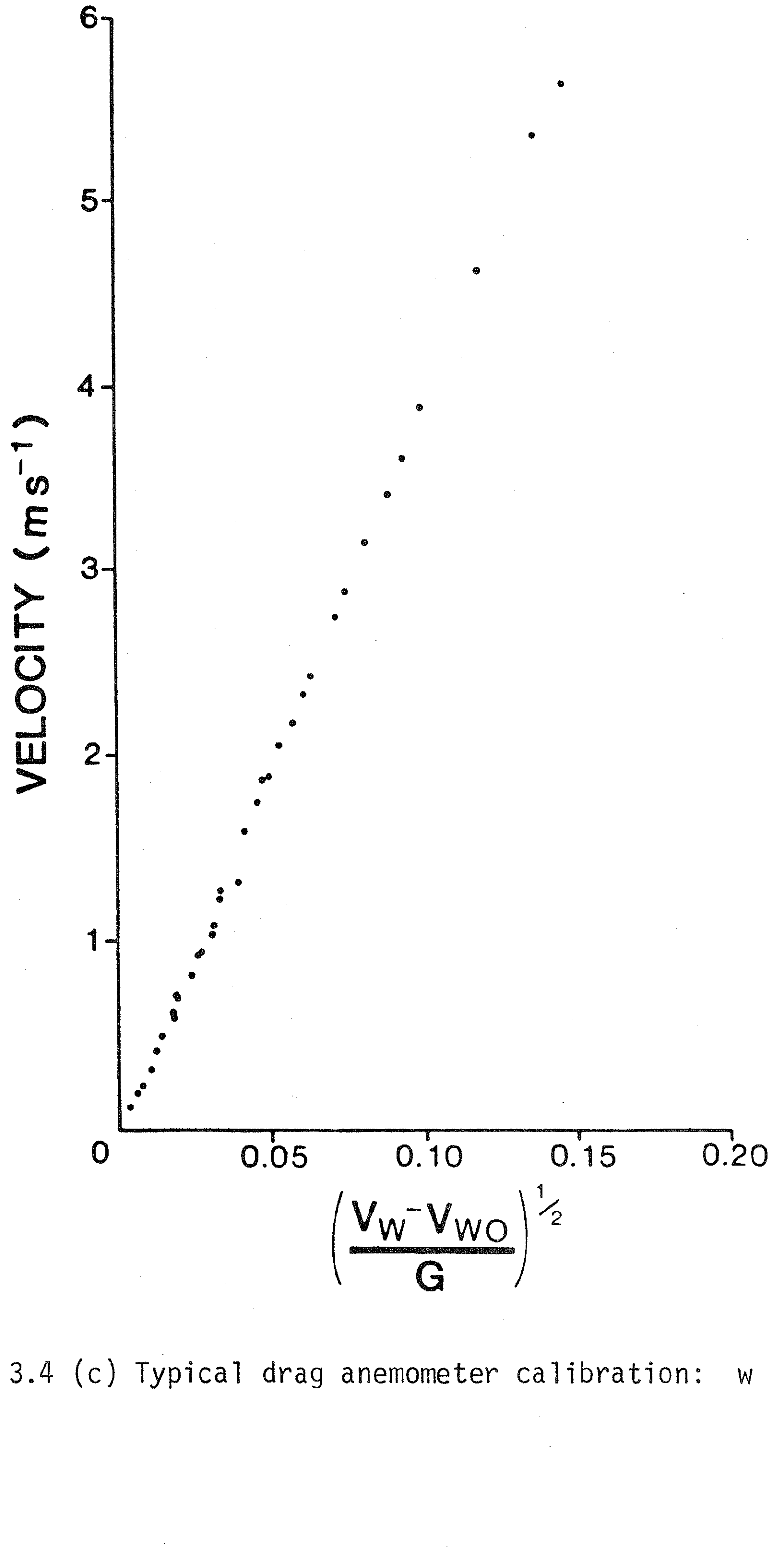

Fig. 3.4 (c) Typical drag anemometer calibration: w component

Scientific, Logan, Utah. It is shown in Figure 3.5. Wind speed is measured between two ultrasonic transducers spaced 0.1m apart and operating at about 40 kHz. The phase shift difference in sound waves sent in the downward direction and the upward direction is measured through the use of phase-locked loop integrated circuitry. According to Campbell and Unsworth, an average is computed from the phase shifts in the down and up direction and used to adjust the frequency for temperature and humidity variations. Wind speed is then related to phase difference by:

$$w \approx c^2 \Delta n / 2d\nu \qquad (3.10$$

where c is the speed of sound and ν is frequency; d is the spacing between the transducers (path length) and Δn is the phase difference in sound waves travelling in the down versus up directions. The variation in c with temperature is about 0.2% C^{-1} (Campbell and Unsworth, 1979).

Sonic Anemometer Calibration

Calibration is performed using a pitot-tube pressure transducer combination and the Disa Low Velocity anemometer in a pusher type wind tunnel, a similar method to the drag anemometer calibration. The sonic anemometer was calibrated with its path length parallel to the flow or a position of 0°.

3.2.3 Slow Response Wind Instruments

Low inertia three cup anemometers (Model WP-1 Cayuga, Cayuga Development, Ithaca, NY) were used at 1.25, 1.50, 1.75, 2.00, 2.25, 2.50 and 2.75 m heights above ground level. In all years, the anemometers were calibrated in a wind tunnel.

Wind direction measurements were made with a wind vane (Model 413,

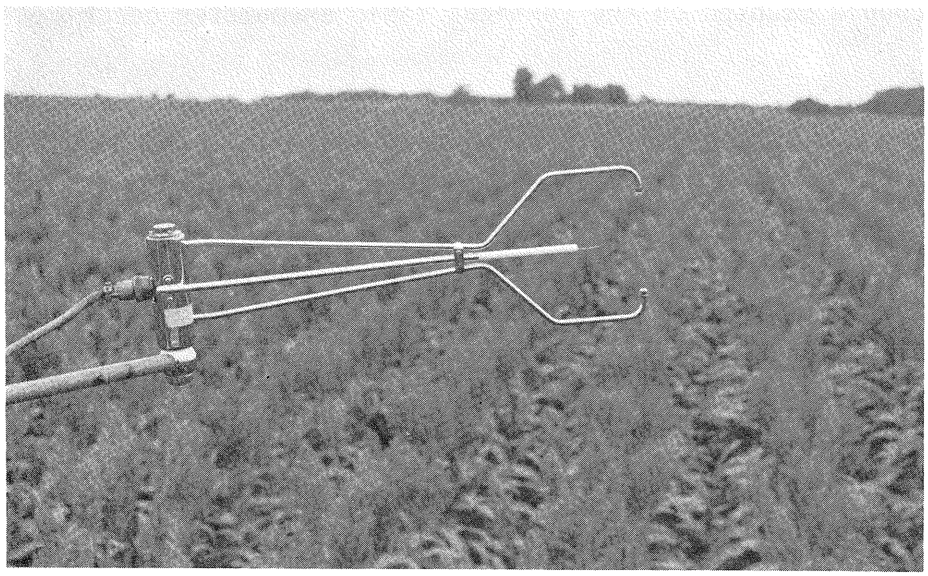

Figure 3.5 Sonic Anemometer Used in 1982.

Science Associates, Princeton, NJ) employing a full turn potentiometer.

3.2.4 Temperature Sensing

Air temperature was measured with a fine wire 0.025mm thickness, 0.050mm junction , constantan-chromel thermocouple described in Verma et al. (1979). First stage amplification is accomplished with circuitry developed by Mr. Fred Weller of the University of Washington. Air temperature was also measured with a fine wire 0.025mm, constantan-chromel thermocouple mounted on the vertical sonic anemometer described previously.

Mean air temperature profiles were made with self-checking psychrometers described in Rosenberg and Brown (1974). The psychrometers were installed at the same heights as the cup anemometers.

3.2.5 Humidity Sensing

Lyman Alpha Hygrometer

Theory and Development

Humidity measurements are difficult to make and the instrumentation tends to be relatively complicated. The Lyman-alpha hygrometer has been widely used for measuring humidity fluctuations in the atmospheric surface layer. It has a fast response time (12 ms) and it does not display hysteresis.

The principles and development of Lyman-alpha hygrometry are covered in Tillman (1965), Randall et al. (1965), Buck (1975, 1976) and Redford et al. (1980). The measurement principle is based upon Beer's law of radiation extinction:

$$I = I_o e^{-k(\rho/\rho_o)x} \qquad (3.11)$$

where I is the portion of radiative flux density received some distance (path length, x) from the source emitting a flux density (I_o), k is the absorption coefficient for gases (ambient air), ρ is the ambient air density, and ρ_o is the air density at STP conditions. Other than water vapor, only oxygen is a significant absorber of Lyman-alpha radiation in ambient conditions. Means of correcting for oxygen absorption are discussed in Buck (1975).

The source of Lyman-alpha radiation is a small tube filled with hydrogen gas. Atomic hydrogen is excited when electrodes within the tube are activated with a potential of about 300 volts. Electrons returning to ground state in the hydrogen atoms emit Lyman-alpha radiation which passes through magnesium fluoride windows. Radiation in the path from source to detector is absorbed in proportion to the concentration of water vapor molecules (absolute humidity) in the path length. A detector chamber, also outfitted with magnesium flouride windows and filled with nitric oxide gas, receives the unabsorbed Lyman-alpha radiation. Nitric oxide is photo-ionized by the Lyman-alpha radiation allowing a current to flow between the electrodes in the chamber. The magnitude of this current is related to the water vapor content of air in the path of radiation and is assumed to be linearly proportional to the number of photons received (Randall et al., 1965; Buck, 1976).

The primary difficulties in the practical application of the hygrometer lie in its non-linear response and exponentially decaying output. Non-linear, decaying output may be described by:

$$V = V_o e^{-\alpha t} \tag{3.12}$$

where V_o is the initial output voltage, V is the voltage level at some time (t) and α is the decay rate. From detailed laboratory tests the decay rate was determined to be time dependent, although error in assuming it to be constant is rather small. Decay rate also appears to change over the lifetime of the source. This was also observed by Buck (personal communication). After the initial few hours of use, source output assumes its characteristic exponential decay. The process appears to be rather steady and occurs over most of the source's lifetime. An accelerated rate of decay is apparent in the last few hours of source life. Source and detector lifetimes and decay rates vary. Buck (1975) reports a typical lifetime for a "conventional" (Hydrogen) source to be about 200 hours and that for a detector to be about 500 hours. With regular periodic monitoring of the decay rate, accurate and reliable data may be obtained.

Calibration

A calibration equation for Lyman-alpha hygrometers in terms of absolute humidity was developed by Buck (1975):

$$\rho_v x = f_v \, (V_p) \tag{3.13}$$

where V_p is given by:

$$V_p = \ln V - f_{21} \left(\frac{Px}{T}\right) - f_c(x) \tag{3.14}$$

V is the sensor output voltage, P is atmospheric pressure, T is air temperature (°K), x is path length, and f_v, f_{21} and f_c are empirically derived polynomials for water vapor calibration, oxygen correction and collimation correction, respectively. For a fixed path length hygrometer such as that used in this study (7.5 mm path length), f_c is constant. Details of the oxygen and collimation corrections may be found in Buck (1975). The term f_v, given by equation 3.13 may be written as:

$$\rho_v x = a_0 + a_1 V_p + a_2 V_p^2 + a_3 V_p^3 \qquad (3.15)$$

where a_0, a_1, a_2 and a_3 are regression constants.

The constants a_o, a_1, a_2 and a_3 of equation 3.15 are obtained through polynomial regression of sensor output V_p on $\rho_v x$ using equation 3.14.

Calibrations were performed in a thermal static chamber. The hygrometer was inserted in a closed system humidity generator which included a resistance thermometer and dew point hygrometer for absolute humidity measurement. A decay rate for the calibration was determined by a method described in Chen et al.(1983a) using data recorded at repeated humidity levels. This value was used to adjust output voltage of the hygrometer. After correction for oxygen absorption a relationship between lnV and ρ_v was calculated. Typical results are shown in Figure 3.6.

Since decay occurs throughout the lifetime of the source, it is necessary to regularly determine the decay rate. This is done by referencing or "baselining" the hygrometer's output to a reliable sensor with a stable output such as the self-checking psychrometer. A method of performing this adjustment is described in Chen et al. (1983a).

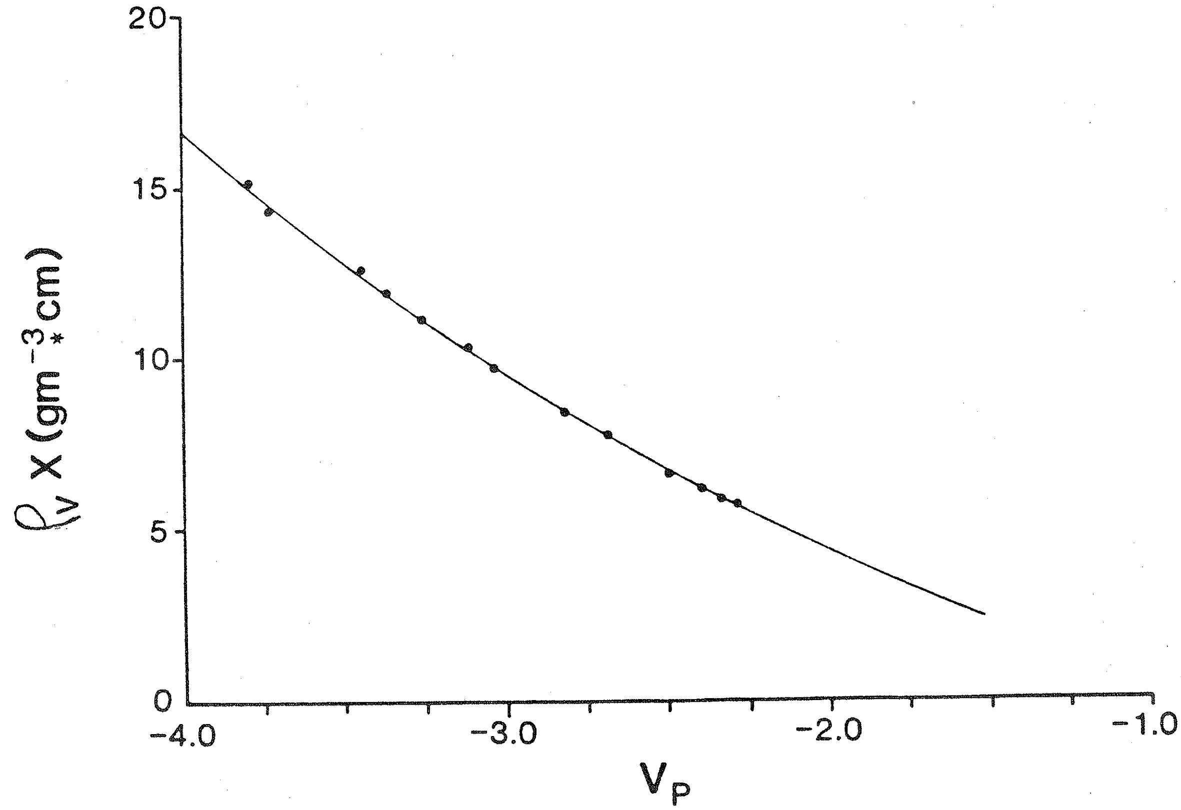

Fig. 3.6 Typical Lyman-Alpha calibration curve. ρ_v is the absolute humidity (g m^{-3}), x is path length (cm) and V_p is defined in the text.

3.2.6 CO_2 Sensing

Fast Response CO_2 Sensor

Theory and Development

The rapid response CO_2 sensor used in this study was designed and built at Lawrence Livermore National Laboratory, Livermore, California, under the direction of Dr. Gail Bingham. Details of its mechanical and electronic features are given by Bingham et al. (1978).

The sensor is known, technically, as a dual wavelength differential infrared absorption spectrometer. It makes use of a strong CO_2 absorption band at 4.27 μm $\pm$ 0.05 μm and a 'reference' band at 3.85 μm in which absorption is minimal. The reference band is used to adjust for system instabilities arising from electronic drift, optical system degradation resulting from mirror contamination, or variations in source emission. The difference in sensor output between the absorbed band and the reference band is directly proportional to the CO_2 concentration.

The instrument is shown in Figure 3.7. The open portion is the volume absorption cell in which CO_2 is "sensed." The enclosed portion contains the small blackbody source, lead-selenium detector and some supporting electronics.

There are a number of unique and sophisticated hardware items that are of critical importance to the success of the sensor. The source voltage and detector temperature are precisely controlled affording the sensor with high accuracy and low drift. Temperature control is a critical element in operation of the sensor. Detector temperature is maintained at -30° C in order to assure high sensitivity and low drift. The temperature is regulated through the use of Peltier cooling blocks. Heat

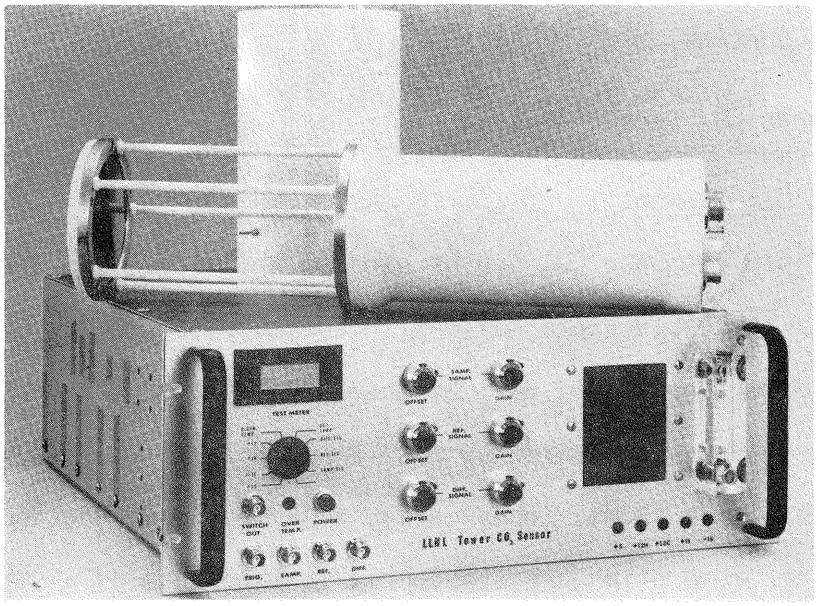

(a)

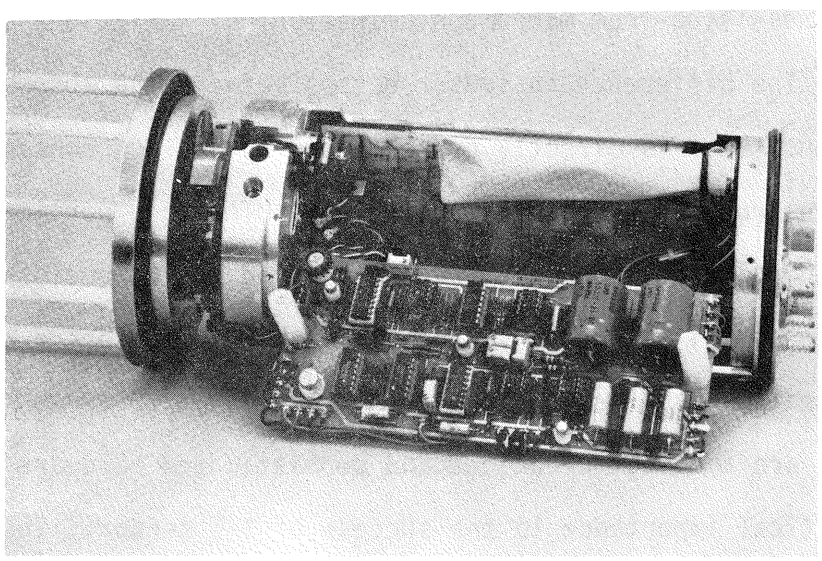

(b)

Figure 3.7 Fast Response CO_2 Sensor. (a) Sensor Head and Ground Based Electronics Package, (b) Internal View of Sensor Head Electronics.

generated by the source and electronics within the sensor enclosure is carried away by an enclosed water cooling system, maintained by the ground support package.

The unique design and use of exotic materials in the sensor's optics are fundamental to its success. The cylindrical source and detector lenses are made of anti-reflection coated germanium having a 95% transmission of source radiation. To increase sensitivity to CO_2 while maintaining the sensor's size, it was necessary to fold the sensor's path length. Folding is made possible through multiple reflections between two mirrors spaced 0.20 m* apart, yielding an effective path length of about 2.50 m. The mirrors made of fused silica are coated with a chrome-gold, vapor deposited, surface affording very high reflectivity and durability.

Another element critical to the sensor's success is the chopper motor. Its speed must be precisely controlled since it rotates a filter wheel synchronized with regular sampling intervals of detector output. The filter wheel is divided into segments containing the 4.27 μm, 3.85 μm and opaque filters.

Also enclosed in the sensor package is the preamplifier which is positioned in close proximity to the detector. In this way, the relatively low impedance detector output may be sufficiently amplified with minimal interference from noise.

---

*In 1981 a 0.1 m spacing was used.

The primary function of the ground based support package is to house some of the supporting electronics, power supplies and the cooling system pump and radiator.

Calibration

Calibration for sensor response to CO_2 concentration was normally done hourly or in bi-hourly intervals. A hood (hollow cylinder) was placed over the sensor's open cell and purged with a dry gas mixture of known CO_2 concentration. The pressure within the hood was typically about 0.25 mb above ambient when sensor output was read. Pressure and temperature within the hood were recorded during calibration. Absolute CO_2 concentration was calculated from the following equation:

$$\rho_c \ (\mathrm{mgm}^{-3}) = (C_{ppm} \times 10^{-6}) \ m_c \left(\frac{P-e}{R\,T}\right) \qquad (3.16)$$

where C_{ppm} is the parts per million CO_2 concentration, m_c is the molecular weight of CO_2, R is the universal gas constant for dry air, P is atmospheric pressure and e is the vapor pressure (equal to zero during CO_2 calibration). A calibration curve was developed using at least three standard gases of known concentration extending beyond the range of expected CO_2 concentrations. The curves were quite linear as is shown in Figure 3.8. From this data, calibration equations of the following form were generated:

$$\rho_c = a_0 + a_1 V_c + a_2 V_c^2 \qquad (3.17)$$

where a_0, a_1 and a_2 are regression constants and V_c is sensor output.

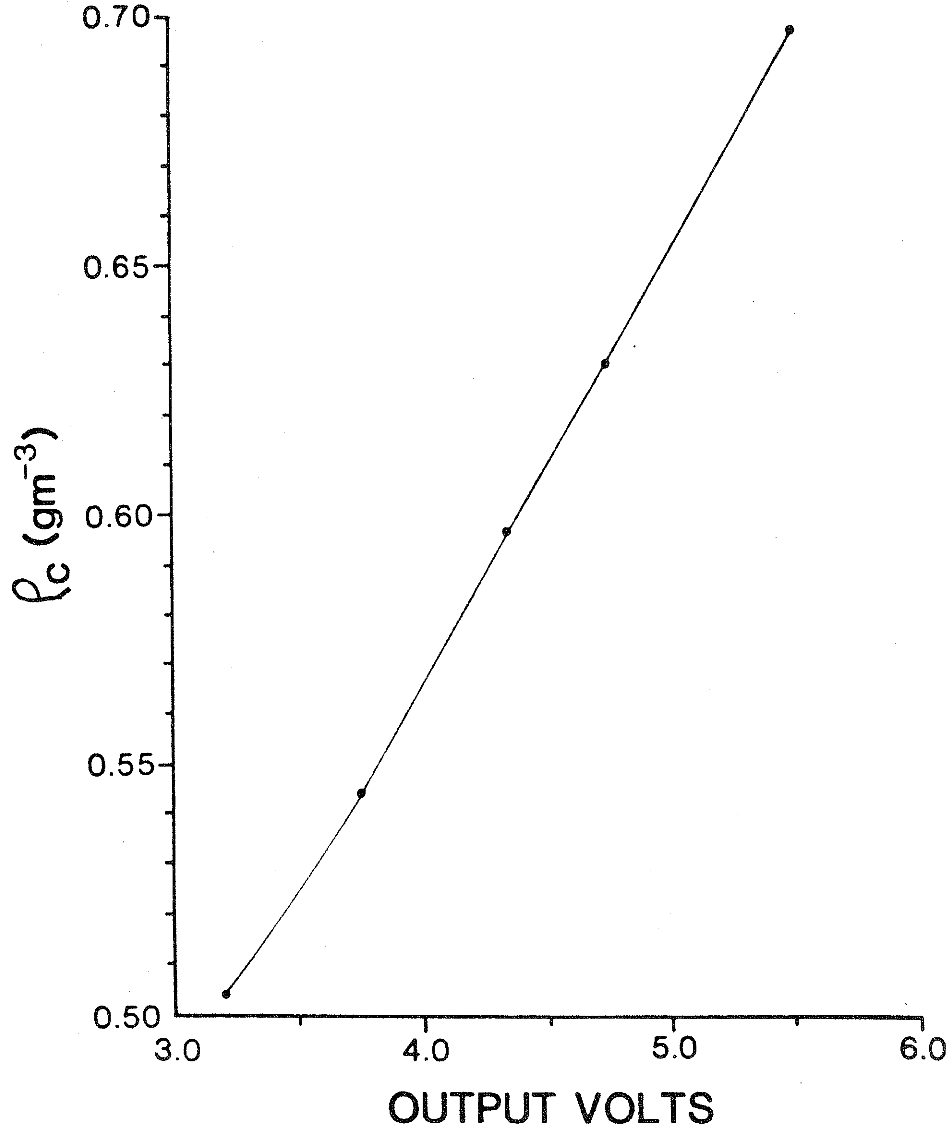

Fig. 3.8 Typical calibration of fast response CO_2 sensor.

Due to the sensor's increased sensitivity to CO_2 in 1982, it became necessary to calibrate the sensor for H_2O concentration as well. Voltage output during data collection could be represented by:

$$V = V_c + V_{H_2O} \tag{3.18}$$

where V is the total voltage output made up of voltage due to the presence of CO_2 (V_c) and that due to the presence of water vapor (V_{H_2O}). Thus, to calculate ρ_c through the use of Equation (3.17), it became necessary to find V_{H_2O} and subtract it from V.

To calculate a relationship between sensor response (V) and absolute concentrations of ρ_c and ρ_v the calibration procedure diagrammed in Figure 3.9 was employed. In the top branch of the system the calibration gas flows directly from its tank to the ADC infrared gas analyzer and serves as a reference. The calibration gas flowing through the bottom branch is humidified by the saturator, filled with water and glass beads (to aid aeration of the water). Various levels of humidification may be reached by adjusting flow through the saturator. Flow meters make it possible to reproduce humidity levels for succeeding measurements. The humidified air now passes into the hooded open cell of the CO_2 sensor where air temperature and pressure is measured. The humidified air leaving the CO_2 sensor's hood is measured for water vapor concentration by dew point hygrometer #1. The air stream is dried by anhydrous magnesium perchlorate, a very effective drying agent which does not absorb or release CO_2. The drying process is monitored by dew point hygrometer #2. Any difference in concentration of air streams through the top and bottom branches is attributed to absorption or release of CO_2 by the saturator. This difference is measured by the

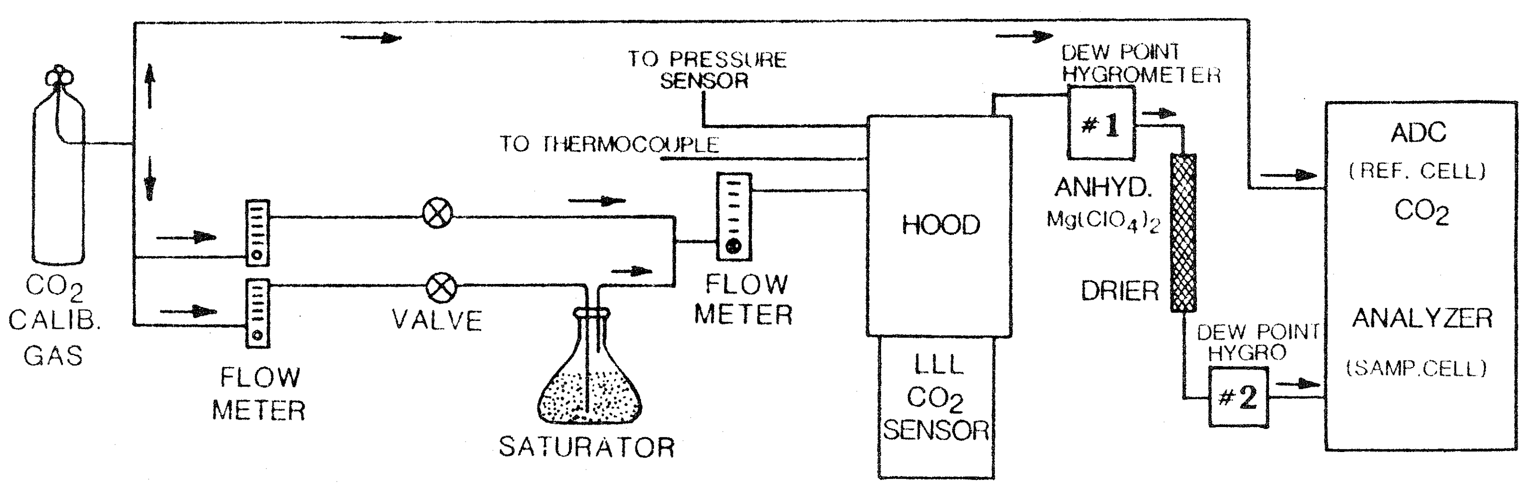

Fig. 3.9 Calibration set-up for water vapor sensitivity of fast response CO_2 sensor.

ADC analyzer. Measurements were taken after the entire calibration system was allowed to thermally stabilize.

An inverse relationship to that of equation 3.17 was calculated to aid in finding V_{H_2O} through the use of equation 3.18:

$$V_c = a_o' + a_1' \rho_c + a_2' \rho_c^2 \text{ for } \rho_v = o \qquad (3.19)$$

Sensor output (V) was recorded at various levels of ρ_v for each value of ρ_c.

Some results of the water vapor sensitivity test indicating the relationship between V_{H_2O} and ρ_v are shown in Figure 3.10. A linear regression fit was used to describe the data. Note, however, that the ρ_v-V_{H_2O} relationship depends on the value of ρ_c. These data suggest the need of an interaction term. Therefore, a multiple linear regression of the type:

$$V_{H_2O} = b_o + b_1 \rho_c + b_2 \rho_v + b_3 \rho_c \rho_v \qquad (3.20)$$

was used. In this equation $b_o = b_1 = 0$ since the intercept and sensor response to ρ_c are already accounted for in equation 3.17. Therefore, equation 3.20 reduces to:

$$V_{H_2O} = b_2 \rho_v + b_3 \rho_v \rho_c \qquad (3.21)$$

V_{H_2O} so obtained can be adjusted to account for changes in instrument's sensitivity through the use of a system gain factor (G).

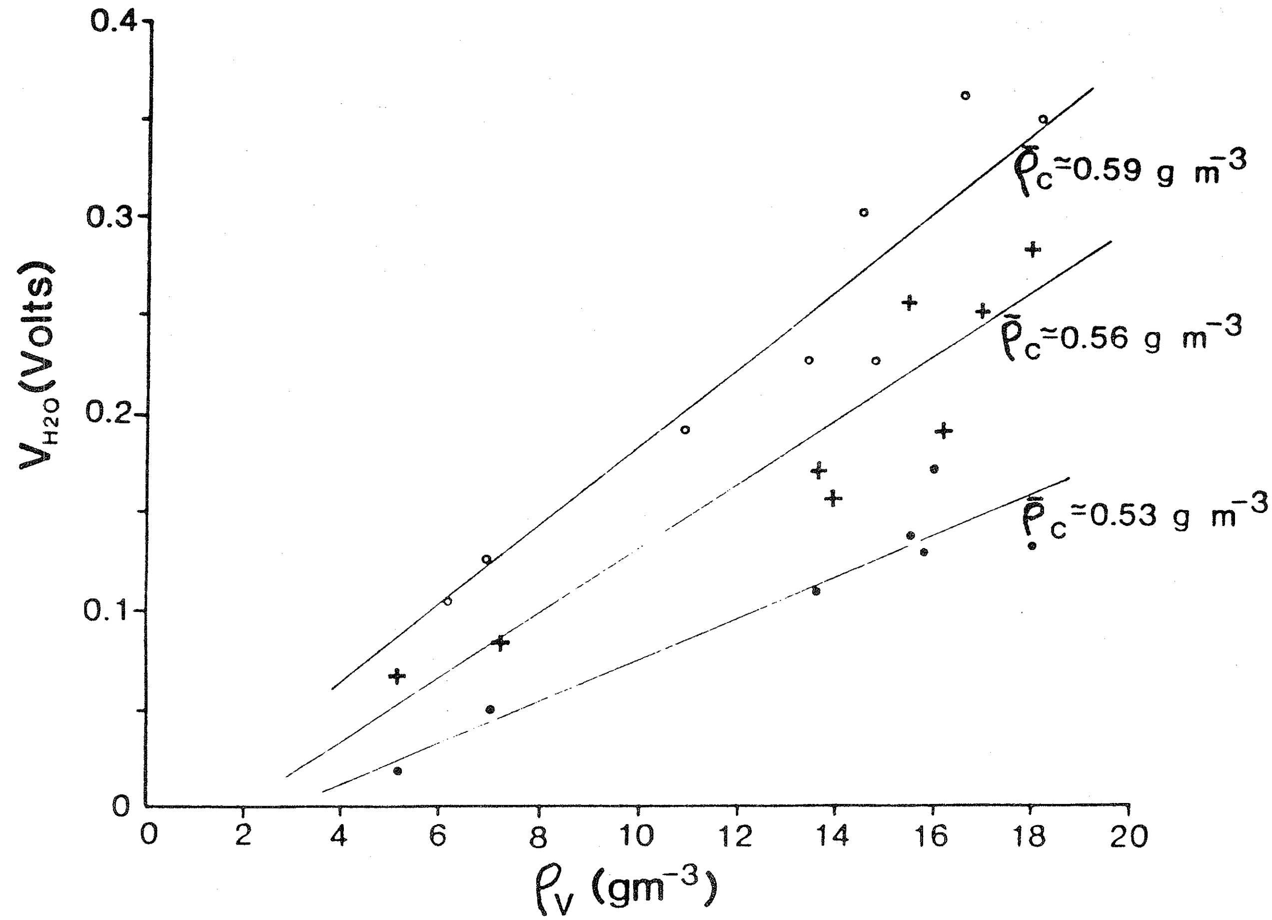

Fig. 3.10 Sensitivity of fast response CO_2 sensor to presence of water vapor in the sample at three densities of CO_2.

This factor may be calculated in terms of the CO_2 sensitivity measured during the water vapor calibration and that during the hourly field calibrations:

$$G = \left(\frac{\partial \rho_c}{\partial V_c}\right)_V \Big/ \left(\frac{\partial \rho_c}{\partial V_c}\right)_H = \frac{(a_1+2a_2V_c)_V}{(a_1+2a_2V_c)_H} \tag{3.22}$$

(The subscripts V and H refer to the water vapor calibration and hourly CO_2 calibrations, respectively). Values for V_c were normally on the order of -1 volt. This value for V_c was used in Eq. (3.22) to calculate G. Note that G is not very sensitive to the value of V_c since a_1 and a_2 are of the order 10^{-1} and 10^{-4}, respectively. V_{H_2O} can now be solved from a working form of equation (3.21):

$$V_{H_2O \text{ Adjusted}} = G\,(b_2\rho_v + b_3\rho_c\rho_v) \tag{3.23}$$

Data analysis followed the following steps: a) Calculate ρ_v from the Lyman-alpha hygrometer, b) compute ρ_c using equation (3.17), c) compute G using equation (3.22), d) compute V_{H_2O} using equation (3.23), e) compute V_c using equation (3.18) and f) compute ρ_c using equation (3.17).

Based on CO_2 flux measurements made in 1982, the water vapor sensitivity correction is on the order of 3%.

3.2.7 Supporting Measurements

Net radiation (Rn) was measured with a net radiometer (Type S-1, Swissteco Pty. Ltd., Melbourne, Australia) and photosynthetically active radiation (PAR) was measured with a quantum sensor (Model LI-190S, Lambda Instr., Inc., Lincoln, NE).

Crop height (h) was measured bi-weekly at 20 randomly selected locations within the experimental plot. Leaf area index (LAI) was measured weekly with an automatic area meter (Type AAM-5 Hayaski-Denco, Japan). Randomly selected crop samples of 0.75 m^2 were taken in two locations for LAI measurement.

Stomatal resistance measurements were made with a steady-state porometer (Model LI-1600, Lambda Instr. Co., Lincoln, NE). Measurements were made on both sides of six randomly selected leaves in the upper portion of the canopies. A resistance for each leaf was computed assuming that the resistance of both sides of the leaf work in parallel. Details on these measurements may be found in Baldocchi (1982).

3.3 Data Acquisition System

A computer-controlled data acquisition system was used to record meteorological data. A block diagram of this system is shown in Figure 3.11. Signals from the fast response instruments are pre-amplified in the field before being sent over individually shielded, twisted pair cable to the laboratory, approximately 100 m away. In the laboratory, the signals pass through a bank of differential amplifiers (Dencor Corp., Inc.) serving as buffers; through 8 pole Butterworth low pass active filters; and finally, through a 12 bit analog to digital converter and multiplexer module where signals are read and recorded on to magnetic tape by a Data General, Nova 210 minicomputer.

The 8 pole Butterworth filters have a very sharp roll off between pass and stop band frequencies. Pass band frequencies are very smooth. The cut-off frequency selected for these filters was a function of the sampling frequency of the data acquisition system. According to

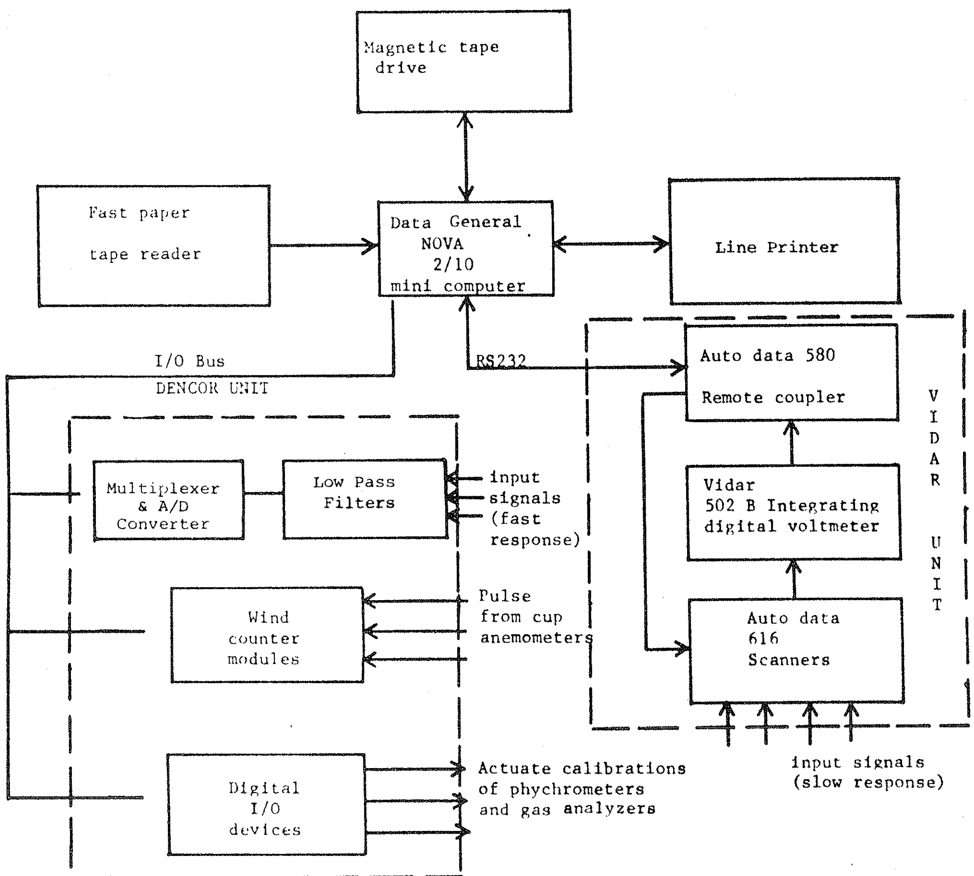

Figure 3.11. Block diagram of the computer controlled micrometeorological data acquisition system.

sampling theory, the sampling frequency should be at least twice the frequency of interest. A sampling frequency roughly two or three times the estimated minimum is needed to minimize aliasing effects (Kaimal, 1975). In 1980 the sampling frequency was 12.8 Hz and Butterworth filters having a 6.25 Hz cut-off were used. Sampling frequency was increased in 1981 to 15 Hz. In 1982 sampling frequency was increased to 25 Hz and 8 pole Butterworth filters with a 12.5 Hz cut-off were used.

The Nova 210 minicomputer also recorded signals from slow response sensors at a rate of approximately 2 samples per minute. Data were digitized and multiplexed by a VIDAR 200 channel scanner.

Each hour, the minicomputer recorded data for 45 minutes. In the final 15 minutes of the hour, offset and gain checks were made on the bank of differential amplifiers; shrouds were closed on the drag anemometer for offset checks at zero wind speed; self-checking psychrometers were set into a horizontal position for offset checks; and, analytical calculations on various data were performed. All data were recorded on the basis of solar time (approximately 1.5 hours behind Central Daylight Savings Time).

3.4 Computational Procedures

Turbulence data recorded at the field were analyzed with the aid of a turbulent flux and statistics program and a spectral analysis program described below. All data on magnetic tape were analyzed on an IBM 370 computer at the University of Nebraska-Lincoln.

Turbulence Flux and Integral Statistics Computations

The turbulent flux and statistics program consists of five subroutines: RFT, PAB, FILTIN, FILTOU, and DFLUX. Subroutine RFT calculates voltages from digital information and adjusts the data for system gain and offset.

Subroutine PAB has several functions. It contains all the calibration equations for the calculation of fluctuating variables from instrument voltages. Computation of temperature (T) and vertical wind speed (w) for the Weller Thermocouple and sonic anemometer-thermocouple combination requires only a voltage and a calibration equation of the type:

$$Y = a + bV \qquad (3.24)$$

where V is voltage, a and b are constants, and Y is the variable of interest (w or T). Computations for other instruments are more complex.

To compute velocities from drag anemometer data it is necessary to compute raw velocities from voltages using the calibration constants and voltages from the u, v, and w components in equations similar to equation 3.5. The velocities are then cosine corrected and the average component velocities (u, v, w) are used to perform a coordinate transform. Fluctuations u', v' and w' may now be computed.

Computation of Lyman-alpha hygrometer data are done as follows. An average logarithmic voltage is computed for each 15 minute period during which psychrometer data provide an average absolute humidity (ρ_{vs}). Fluctuation statistics of Lyman-alpha voltage are computed in terms of first, second and third order moments. These values together with ρ_{sv} are used to determine the decay rate constant (Δ) using an iteration method discussed in Chen et al. (1983a). Once Δ is found, ρ_v may be calculated directly from the calibration equation in terms of lnV.

CO_2 concentration calculations described in Sec. 3.2.6 have also been programmed for the IBM 370 computer.

At this stage, data on u, v, w, t, ρ_v and ρ_c are input to a digital high pass filter in subroutine FILTIN. The symmetric, exponentially weighted filter used is described in detail in Chen et al. (1983b). This filter removes data in the low frequencies that are of little significance to turbulence flux measurements and which are often contaminated by electronic noise and drifts in the electronics or mechanics of the instruments. The half power cut-off frequency was approximately 0.0012 Hz and response of the filter was similar to that of a double stage RC filter.

In the FILTIN subroutine, filter weights (W_i) are constructed from the exponential function:

$$W_i = e^{-tF} \tag{3.25}$$

where t is time and F is the time constant of the filter. To reduce computantional time, the data input to the subroutine are block averaged (4 data points were averaged in a block). The weights constructed in the use of equation (3.25) are multiplied by the blocked averaged time series. The products of weights and blocks are summed. The series of sums constitute a smoothed time series. This series and the raw data from the PAB subroutine are input into the FILTOU subroutine. By subtracting the smoothed time series from the raw data a high pass filtered data set is found. This scheme may be followed in Figure 3.12.

The filtered data from the FILTOU subroutine is input to the DFLUX program where integral turbulence statistics are calculated. Means and statistics of fluctuating components of the instantaneous parameters: u, v, w, T, ρ_v, and ρ_c are computed.

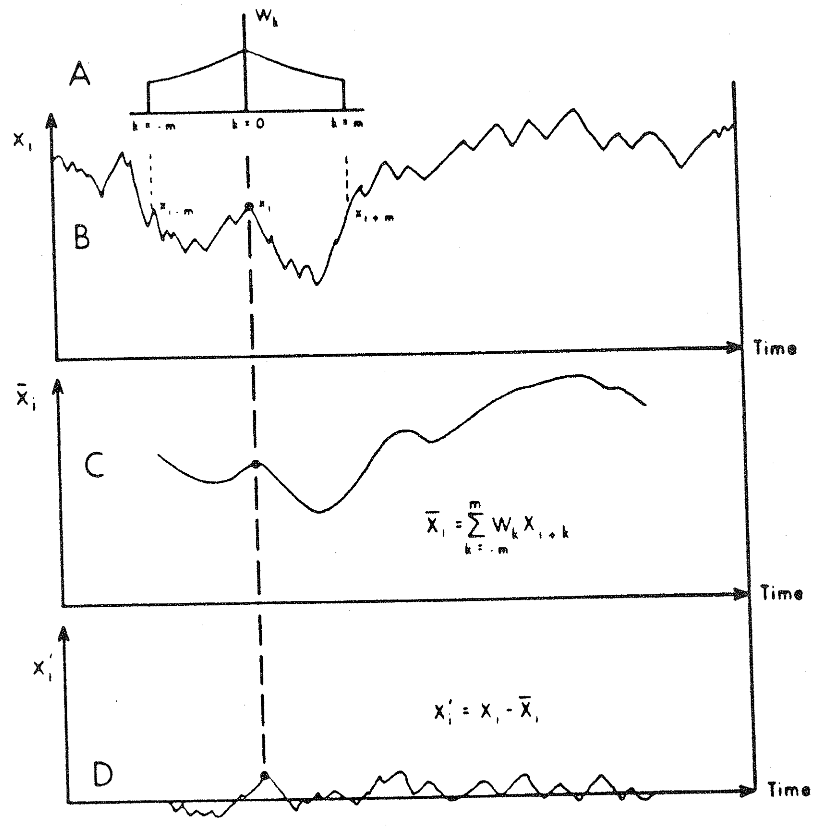

Fig. 3.12 Schematic representation of the filtering technique used in these studies.

(A) Weighting function, (B) Original time series,

(C) Smoothed (low pass filtered) time series,

(D) Resultant (high pass filtered) time series

Spectral Analysis Program

The spectral analysis program used in these studies is a version of a program originally obtained from IBM and modified and supported by further work at Pennsylvania State University by Parhami (1971). It utilizes a Fast-Fourier Transform algorithm devised by Cooley and Tukey (1965). Details on this program may be found in Parhami (1971).

CHAPTER 4

Results and Discussion

Turbulent transport of CO_2, water vapor, sensible heat and momentum was measured over soybeans in 1980 and 1981, and over sorghum in 1982. Results of the investigation are reported in three parts: 1) an analysis of the exchange of mass and energy between the atmosphere and the crops; 2) an analysis of the characteristics of turbulence over these crops employing integral statistics of fluctuations of wind velocity, air temperature, humidity and CO_2 concentration; and 3) an analysis of the structure of turbulence in the frequency domain using spectral techniques. The effects of atmospheric thermal stability are considered in parts 2 and 3.

4.1. Mass and Energy Fluxes over Crops

In this section the diurnal patterns of mass and energy fluxes above soybean and sorghum canopies as well as certain interactions between micrometeorological and crop physiological variables will be examined.

4.1.1. Diurnal Patterns of Mass and Energy Fluxes over Soybeans

4.1.1.1. Components of the Energy Budget

Typical diurnal patterns of the energy budget over a well-watered soybean crop (LAI = 3.5) are presented in Figure 4.1. Plotted in this figure are sensible (H) and latent heat fluxes (LE) measured by the eddy correlation method and, net radiation (Rn) and soil heat flux (S) measured with a net radiometer and soil heat flux plates, respectively

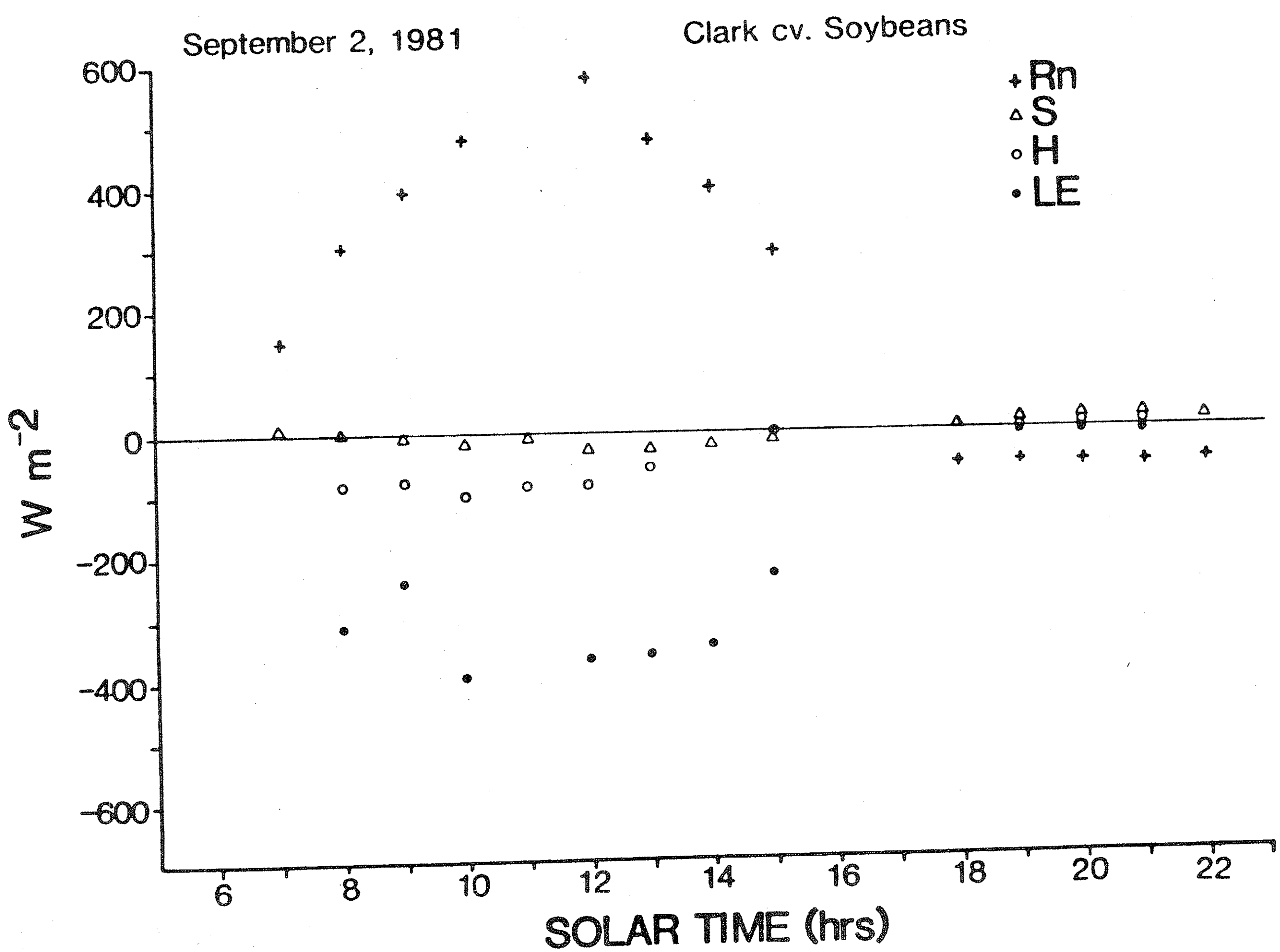

Fig. 4.1 Diurnal patterns of energy budget components over a soybean crop. Mead, Nebraska September 2, 1981.

(fluxes to the crop are considered positive). Ideally, the fluxes (Rn + S) should be balanced by -(LE + H) measured, independently, by the eddy correlation technique. This balance is indicated in Figure 4.2.

The early morning hours on September 2, 1981 were characterized by fog and light southerly winds. Clearing occurred in the late morning with moderate winds. The sky remained clear in the afternoon and during that night. A plot of mean wind speed, mean air temperature and thermal stability parameter (z/L) is given in Figure 4.3. As the fog cleared and wind speeds increased, the flux density of solar radiation increased as did the mean air temperature, and the fluxes of Rn, S, LE and H. Rn reached its peak value of about 575 W m^{-2} at midday. The maximum downward soil heat flux (-30 W m^{-2}) lagged Rn flux by about one hour, possibly because of the large thermal inertia of the wet soil. Sensible and latent heat flux from the crop increased sharply with the sharp rise in net radiation in the morning hours. By 1000 solar time, H and LE had reached their maximum value of 104 W m^{-2}, 393 W m^{-2}, respectively. In the late afternoon the crop surface began to cool. Thermal stability in the air above changed from unstable to stable.

The nocturnal energy balance is dominated by a net upward radiative flux which causes the earth's surface to cool and increases the thermal stability of the surface layer. As wind speed became light, surface cooling rapidly progressed. The leaves of the soybean canopy cooled to the dew point of the ambient air. Dew fall was visually determined at about 2000 hrs. This observation supports the measurement of downward latent heat flux (to the crop) beginning at about 1900 hrs. During this time, soil heat flux was directed into the canopy.

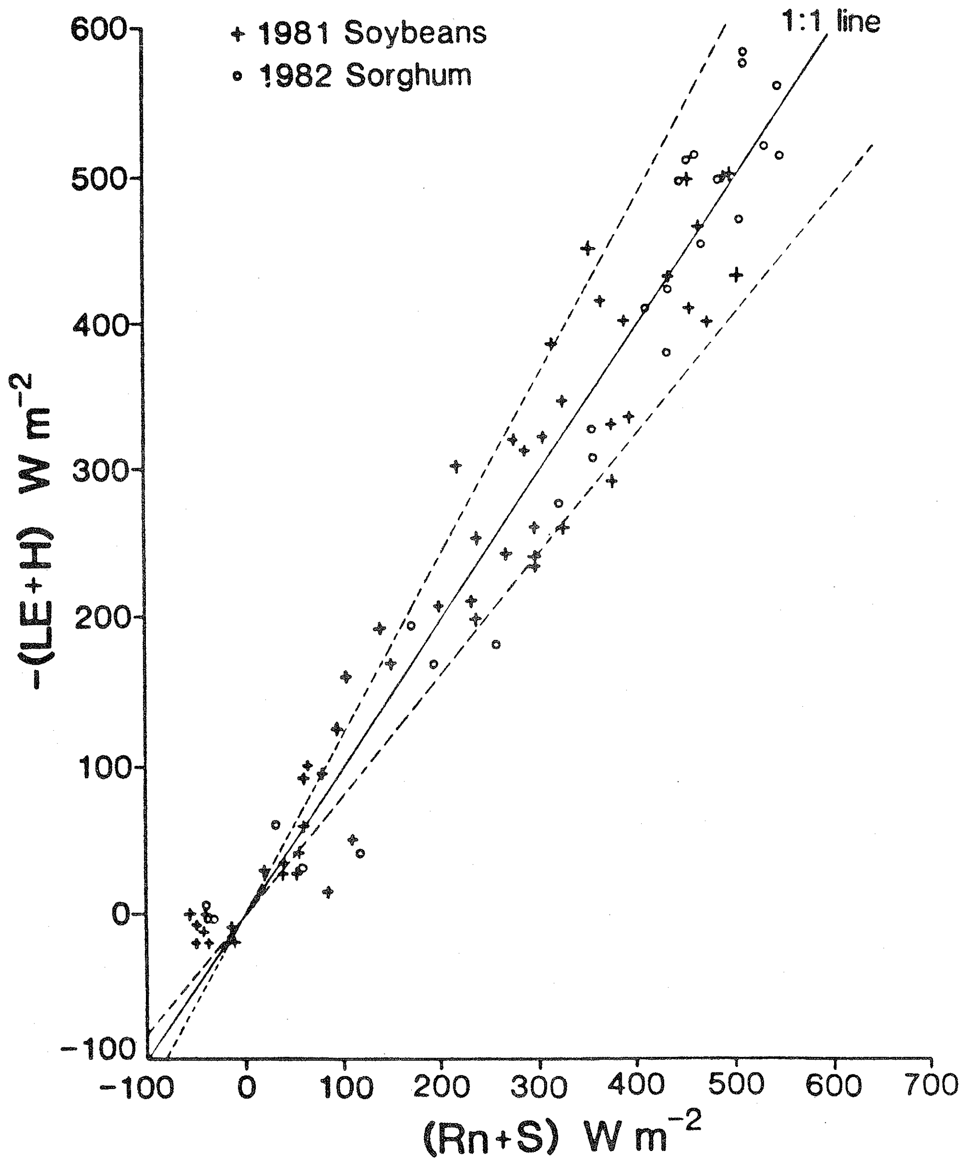

Fig. 4.2 Balance of energy budget flux terms. Rn and S measured with net radiometer and soil heat flux plate; LE and H measured by eddy correlation. Dotted lines indicate $\pm$ 20% deviation from 1:1 line.

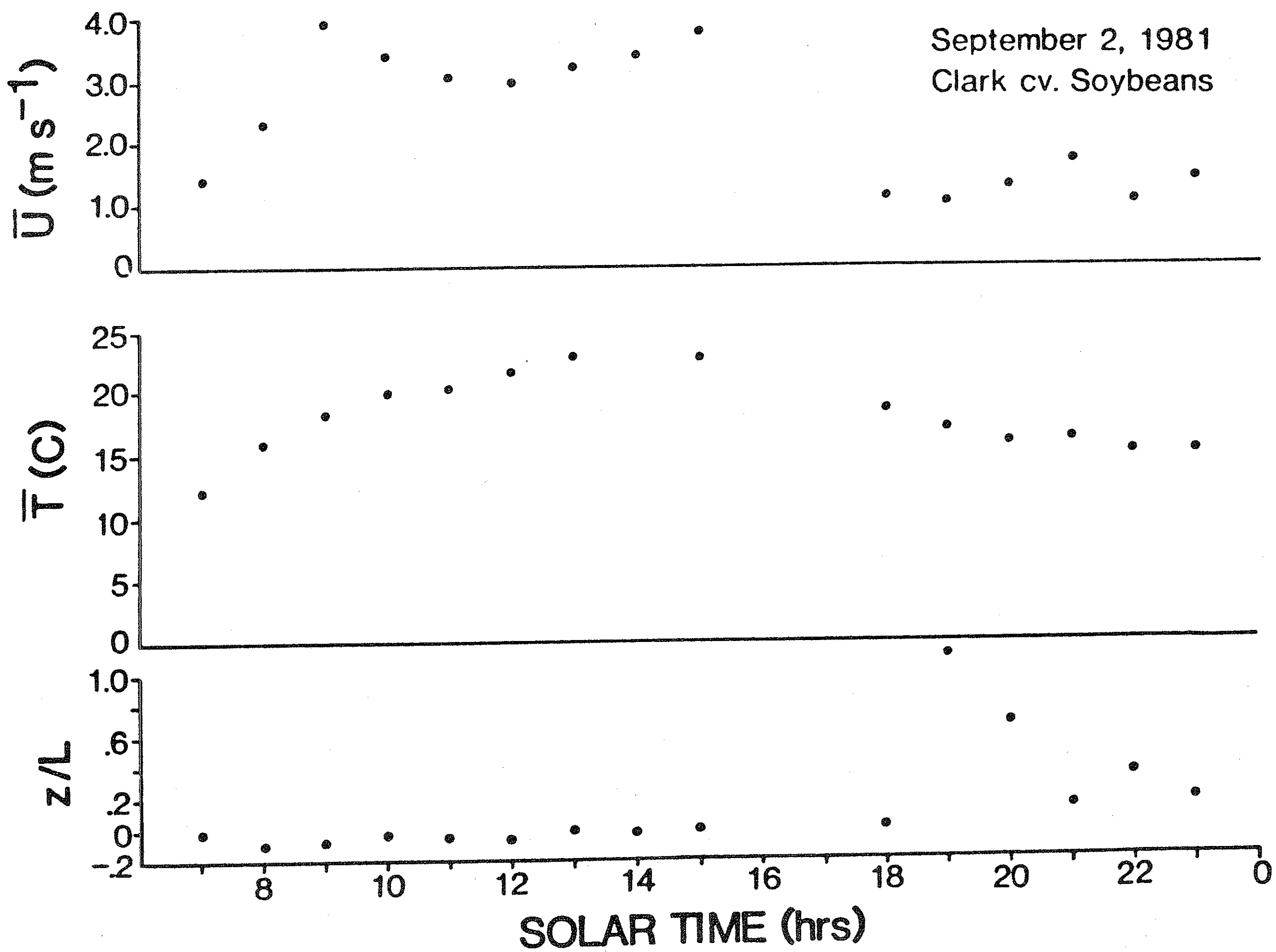

Fig. 4.3 Mean wind speed, air temperature and thermal stability over a soybean crop. Mead, Nebraska September 2, 1981.

4.1.1.2. CO_2 Fluxes

Diurnal trends in CO_2 flux (Fc) and photosynthetically active radiation (PAR) measured over soybeans are shown in Figure 4.4. The leaf area index[1] was 3-3.5 at this time. With the clearing of the fog in mid-morning, Fc and PAR increased sharply since the sun was already at a high elevation angle. Fc reached a maximum value[2] of about 1.0 mg m^{-2} s^{-1}. This value is in general agreement with the results of chamber studies reported by Sinclair (1980) and Larson et al. (1981) and flux-gradient measurements by Baldocchi (1982). It is interesting to note that, on this clear day, the maximum value of Fc occurred at 1000 hrs (solar time) well ahead of the maximum in PAR. A similar observation was made by Baldocchi (1982) over soybeans he studied at Mead in 1979, and by Rawson et al. (1978) in the Colorado plains. There are many possible causes for this late morning decrease in Fc. High air temperatures are known to inhibit photosynthesis. In addition, water stress, increased stomatal resistance and, possibly, starch accumulation in the leaves can influence the magnitude of Fc. The starch accumulation hypothesis of photosynthesis inhibition in soybeans has been invoked by Thorne and Koller (1974), Nafzinger and Koller (1976), Peet and Kramer (1980) and Clough et al. (1981). Turner et al. (1978), Mauney et al. (1979) and Potter and Breen (1980) also working with soybeans have produced contrary arguments to this hypothesis. Unfortunately,

---

[1]The leaf area index is the ratio of leaf surface area (one side) to ground area.

[2]All values of Fc reported here will be a ground area basis unless stated otherwise.

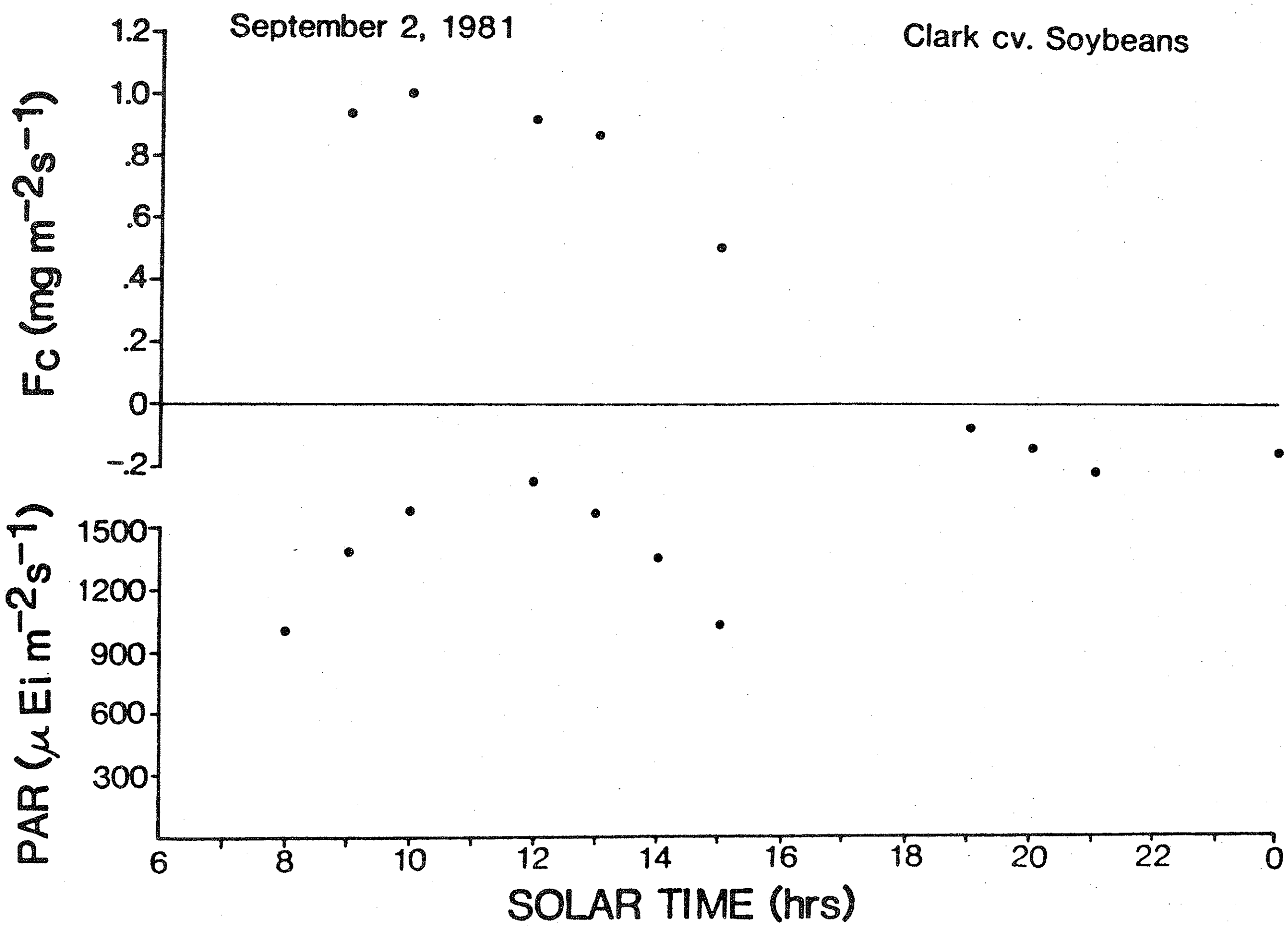

Fig. 4.4 Diurnal trends of CO_2 flux (F_c) and photosynthetically active radiation (PAR) over a soybean crop at Mead, Nebraska September 2, 1981.

no measurements of starch content were made in this study. It is doubtful that high temperature and water stress were factors in the late morning decrease in Fc. Temperatures fell within the optimum range for soybean photosynthesis (25 - 30 C) reported by Jeffers and Shibles (1969) while stomatal resistance was low ranging between 50 and 150 s m^{-1}.

Some nocturnal measurements of CO_2 flux (Fc) are also included in Figure 4.4. There are very few accurate field measurements of nocturnal Fc over crops. The Bowen-ratio energy balance method is unreliable at night due to the magnitude (small) of Rn. Chamber measurements are suspect because of the disturbance of the natural environment of the plant community. Dark respiration is known to be largely dependent upon temperature and soil moisture status. As shown in the Figure 4.4 eddy correlation measurements of nocturnal CO_2 flux (plant + roots + soil respiration rate), reached a maximum of 0.23 mg $m^{-2}s^{-1}$. DaCosta et al. (1981) using an open flow chamber technique over soybeans at Mead reported respiration rates ranging from about 0.09 to 0.25 mg $m^{-2}s^{-1}$

4.1.1.3. The Carbon-Water Flux Ratio

The efficiency with which a crop uses water in conducting photosynthesis is often described by a water use efficiency, or alternately by the carbon-water flux ratio (CWFR) defined below:

$$CWFR = \frac{Fc}{E} \quad [mg\ g^{-1}] \tag{4.1}$$

CWFR measured on September 2, 1981 is shown in Figure 4.5. With the exception of early morning data, the values decrease monotonically from a maximum of 12 mg g^{-1} at 0900 hrs. throughout the day, reaching a

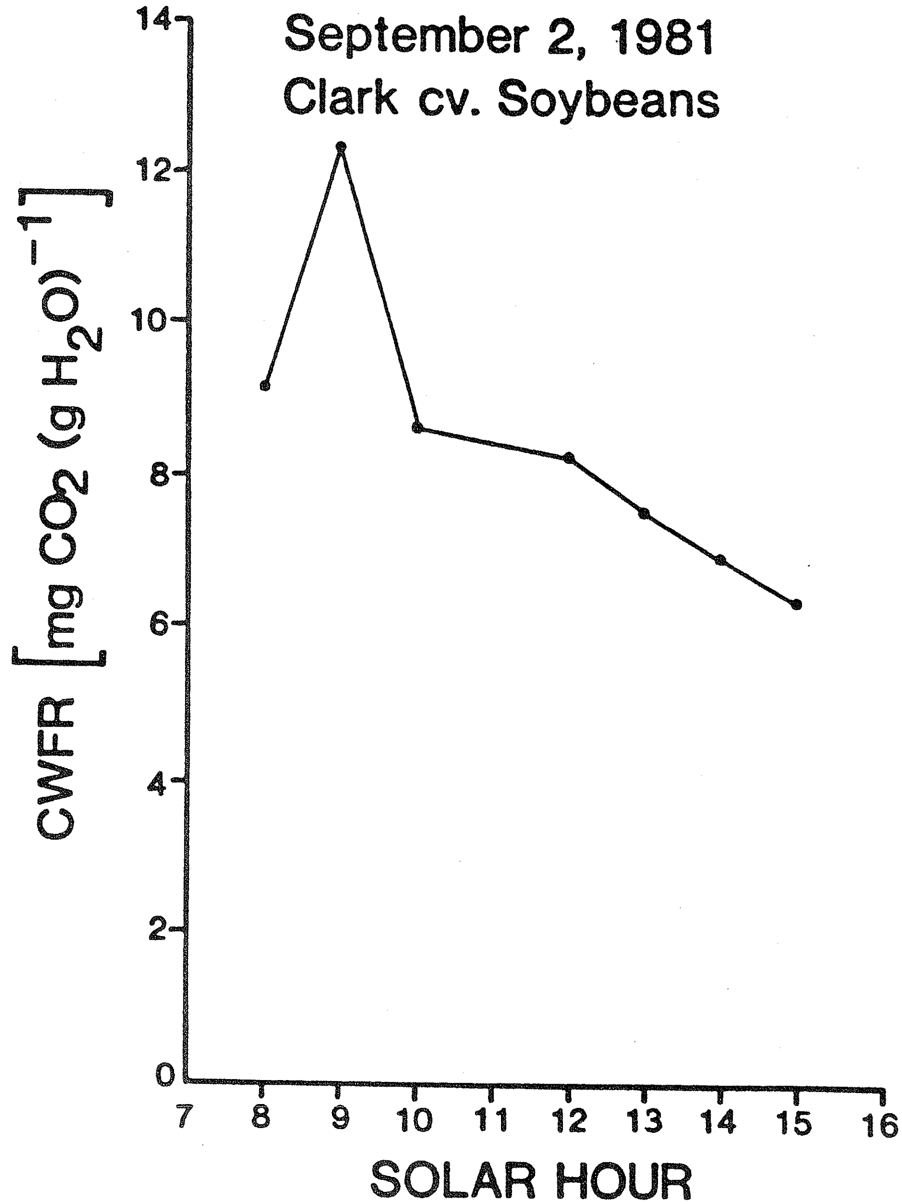

Fig. 4.5 Diurnal trend of the carbon water flux ratio (CWFR) over a soybean crop on September 2, 1981 Mead, Nebraska.

minimum of 4 mg g^{-1} late in the afternoon. Under apparently similar environmental conditions over soybeans, Rawson et al. (1978) observed a range in CWFR between 11.7 to 6.4 mg g^{-1}. Baldocchi (1982) found a diurnal range of 8 to 3 mg g^{-1}. CWFR is relatively greater in the morning, probably because plants are better hydrated at this time.

4.1.2. Diurnal Patterns of Mass and Energy Fluxes over Sorghum

4.1.2.1. Components of the Energy Budget

Diurnal measurements of Rn, S, LE, and H over a sorghum canopy on September 10, 1982, a clear day with moderate winds, are shown in Figure 4.6. Mean wind speed, mean temperature, and the thermal stability parameter (z/L) are plotted in Figure 4.7. The net radiation (Rn) and soil heat flux (S) follow expected symmetrical patterns for a clear day. Maximum fluxes of 568 W m^{-2} and 41 W m^{-2} for Rn and S respectively, occurred at midday. Sensible and latent heat fluxes are negative during most of the day, indicating that lapse conditions prevailed. Sensible heat flux reached a maximum of 128 W m^{-2} at 1000 hrs. and latent heat flux reached a midday maximum of 402 W m^{-2}. Sensible heat flux (H) trended towards positive values during the day. H became positive (flux to the crop) by 1600 hrs. Under the influence of the cooling crop, the thermal stability parameter (z/L) became positive late in the day.

4.1.2.2. CO_2 Fluxes

A diurnal pattern of Fc over sorghum for September 10, 1982 appears in Figure 4.8. At this time, sorghum plants (LAI = 3-3.5) were generally

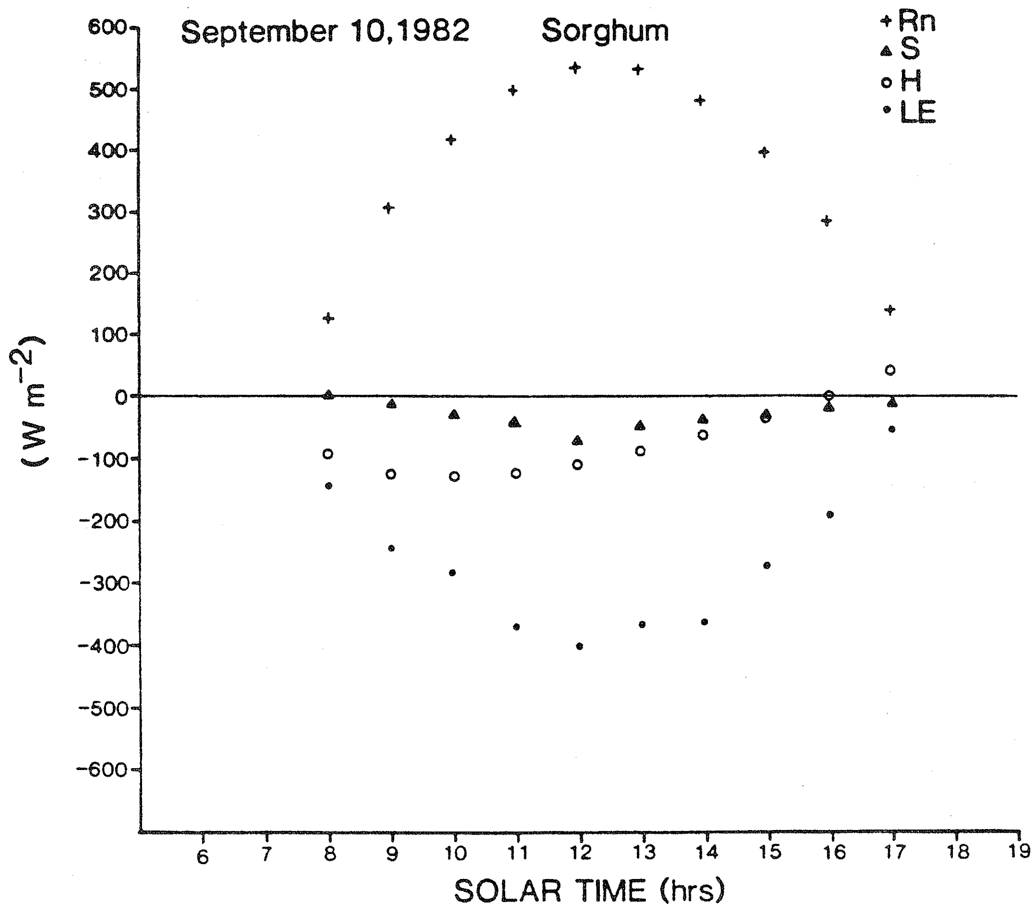

Fig. 4.6 Diurnal trends of energy budget components over a sorghum crop. Mead, Nebraska September 10, 1982.

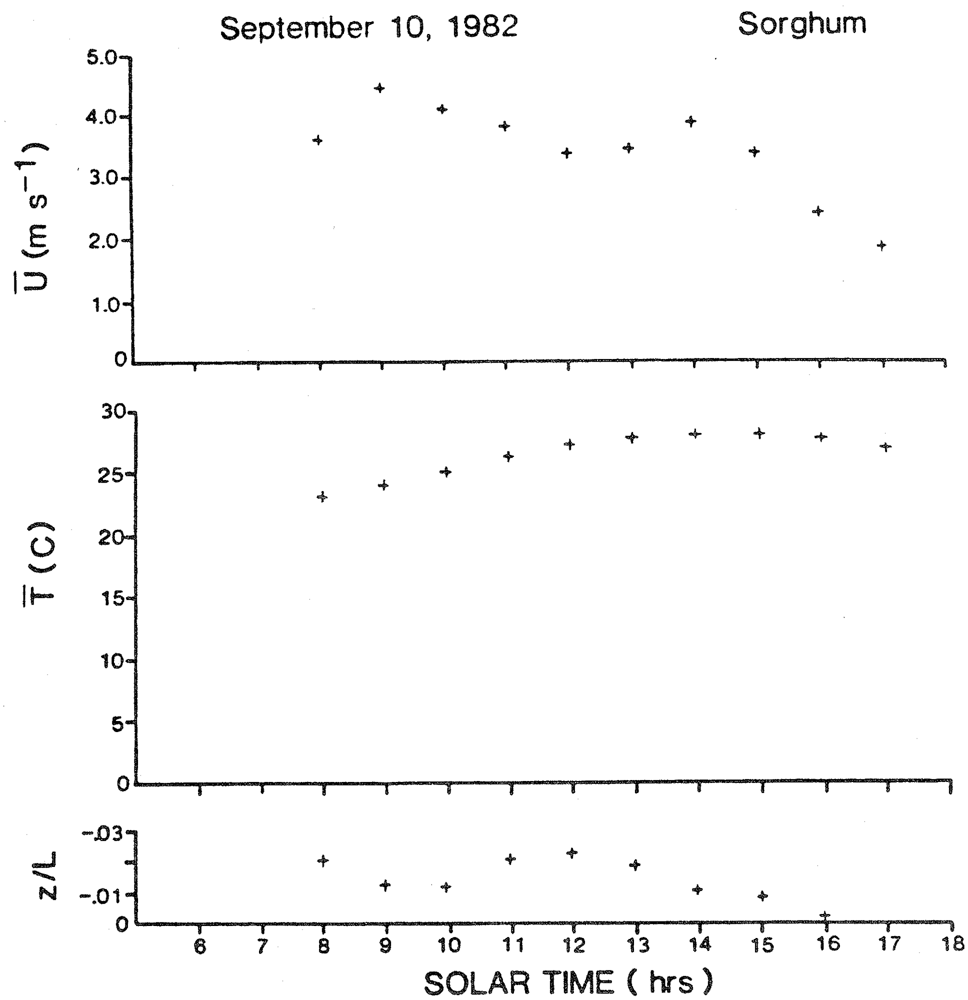

Fig. 4.7 Mean wind speed, air temperature and thermal stability over a sorghum crop. Mead, Nebraska September 10, 1982.

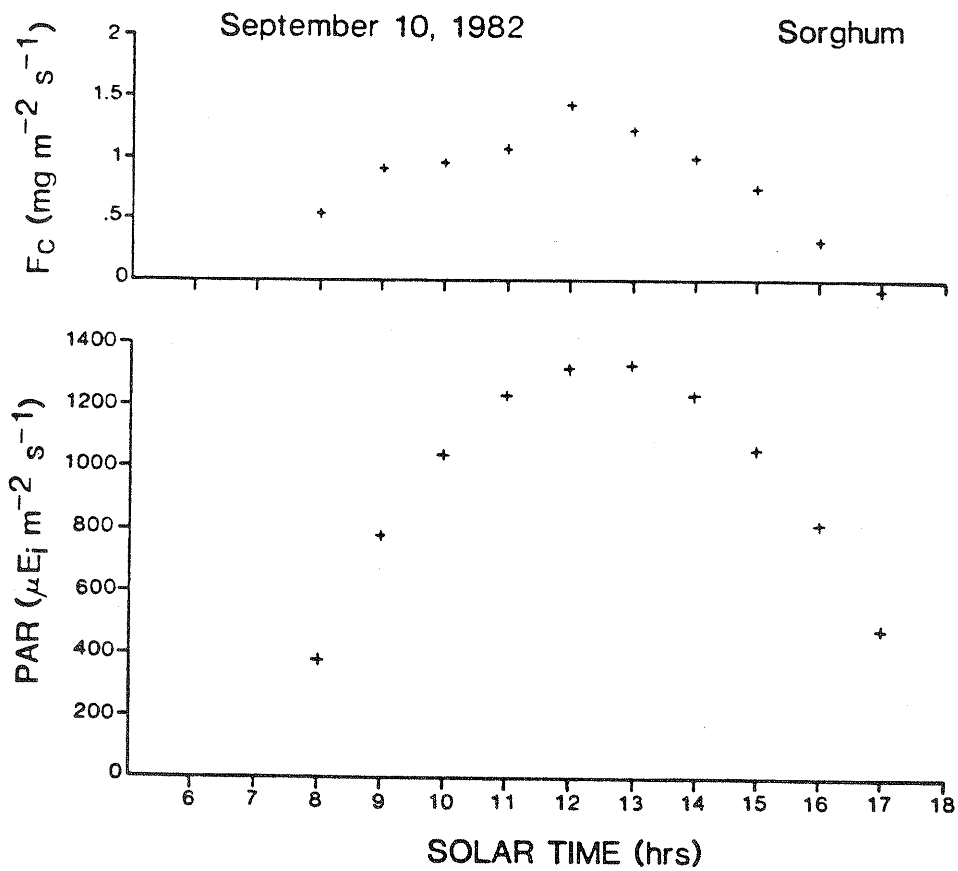

Fig. 4.8 Diurnal trends of CO_2 flux (F_c) and photosynthetically active radiation (PAR) over a sorghum crop. Mead, Nebraska September 10, 1982.

between the half-bloom and soft-dough stages of development.[1] Fc followed a parabolic course, corresponding with a similar trend in PAR. Unlike the response of soybeans to PAR shown earlier, Fc over sorghum reached a maximum at midday. This midday value was 1.4 mg $m^{-2}s^{-1}$. Allen et al. (1974) found peak values of about 1 mg $m^{-2}s^{-1}$ over sorghum.

The pattern of nocturnal respiration rates over sorghum on August 25, 1982 is shown in Figure 4.9, as part of the diurnal trend for that day. The corresponding energy budget components, the mean temperature and wind speed, and the thermal stability index (Ri) are plotted in Figures 4.10 (a, b). The sorghum crop was at the half bloom stage of development (LAI = 4.5). Respiration ranged between 0.16 - 0.24 mg m^{-2} s^{-1} (ground area) for most of the night. Allen et al. (1974) extrapolated a photosynthesis light response curve for field grown sorghum and estimated a nocturnal respiration rate of 0.09 mg $m^{-2}s^{-1}$ on a leaf area basis. A median nocturnal respiration rate calculated per leaf area from the data shown in Figure 4.9 is about 0.04 mg $m^{-2}s^{-1}$. Respiration rates measured on other nights ranged between 0.02 and 0.08 mg m^{-2} (leaf area) s^{-1}.

4.1.2.3. The Carbon Water Flux Ratio

The diurnal trend of CWFR over a sorghum crop on September 10, 1982 is shown in Figure 4.11. CWFR values decreased on an irregular basis from early morning and midday peaks near 10 mg CO_2 (g $H_2O)^{-1}$ to a low value of 2.7 mg CO_2 (g $H_2O)^{-1}$ by the end of the day. Similar

---

[1] See Vanderlip and Reeves (1972) for growth stage description.

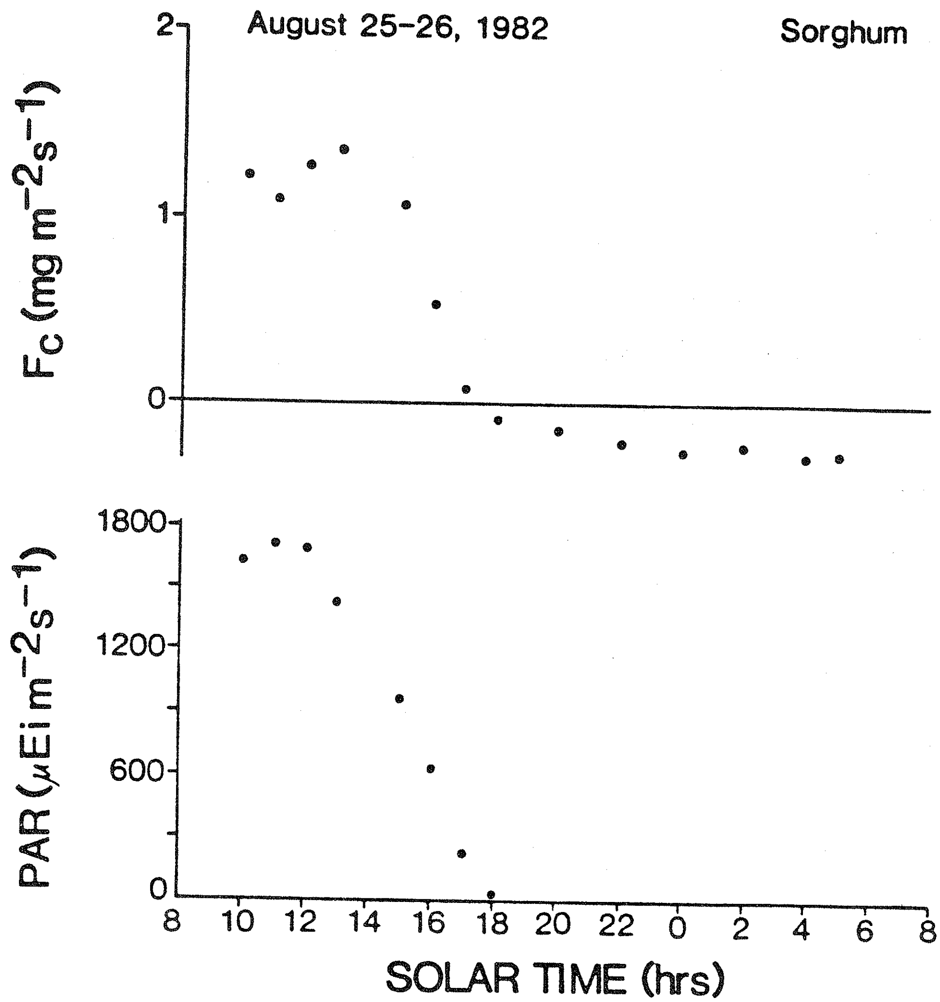

Fig. 4.9 Diurnal trend of CO_2 flux (F_c) and photosynthetically active radiation (PAR) over a sorghum crop. Mead, Nebraska August 25 and 26, 1982.

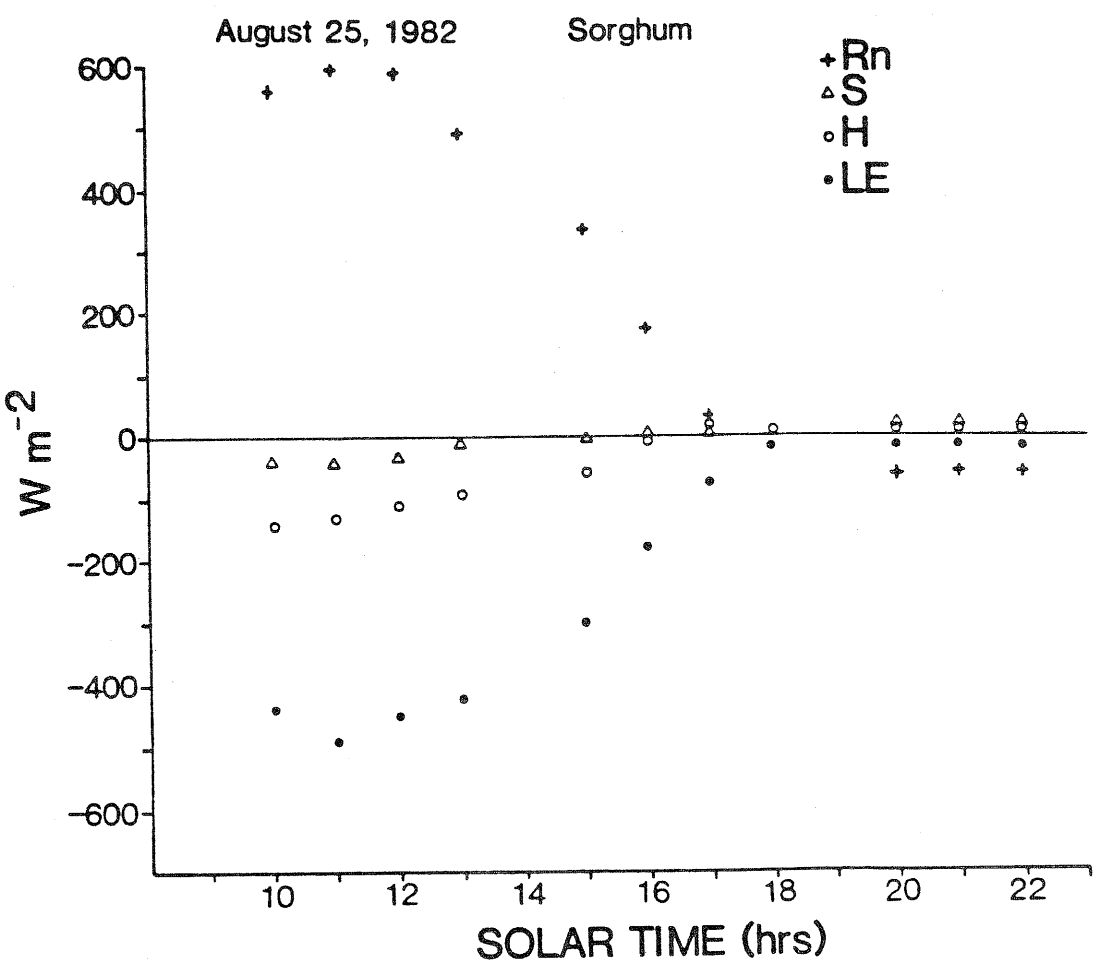

Fig. 4.10 (a) Diurnal trends of energy budget components over a sorghum crop. Mead, Nebraska August 25, 1982.

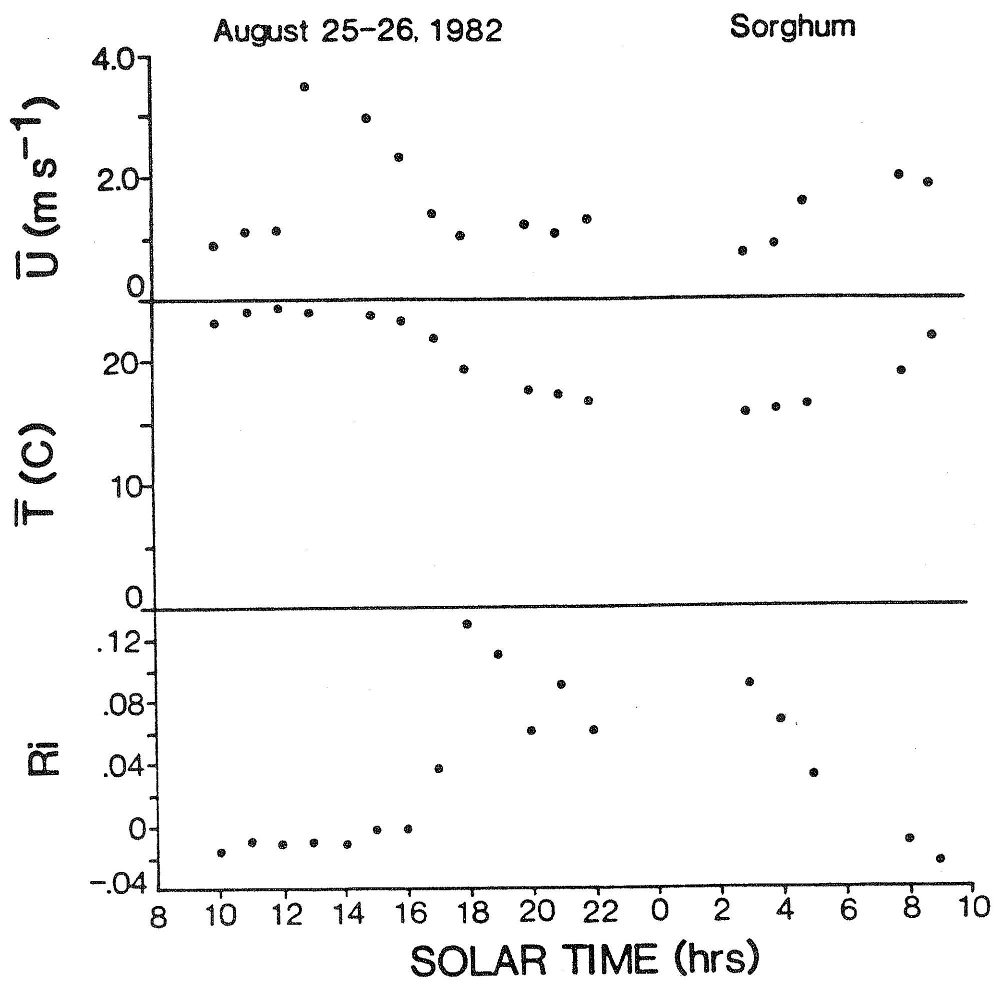

Fig. 4.10 (b) Mean wind speed, air temperature and thermal stability over a sorghum crop. Mead, Nebraska August 25 and 26, 1982.

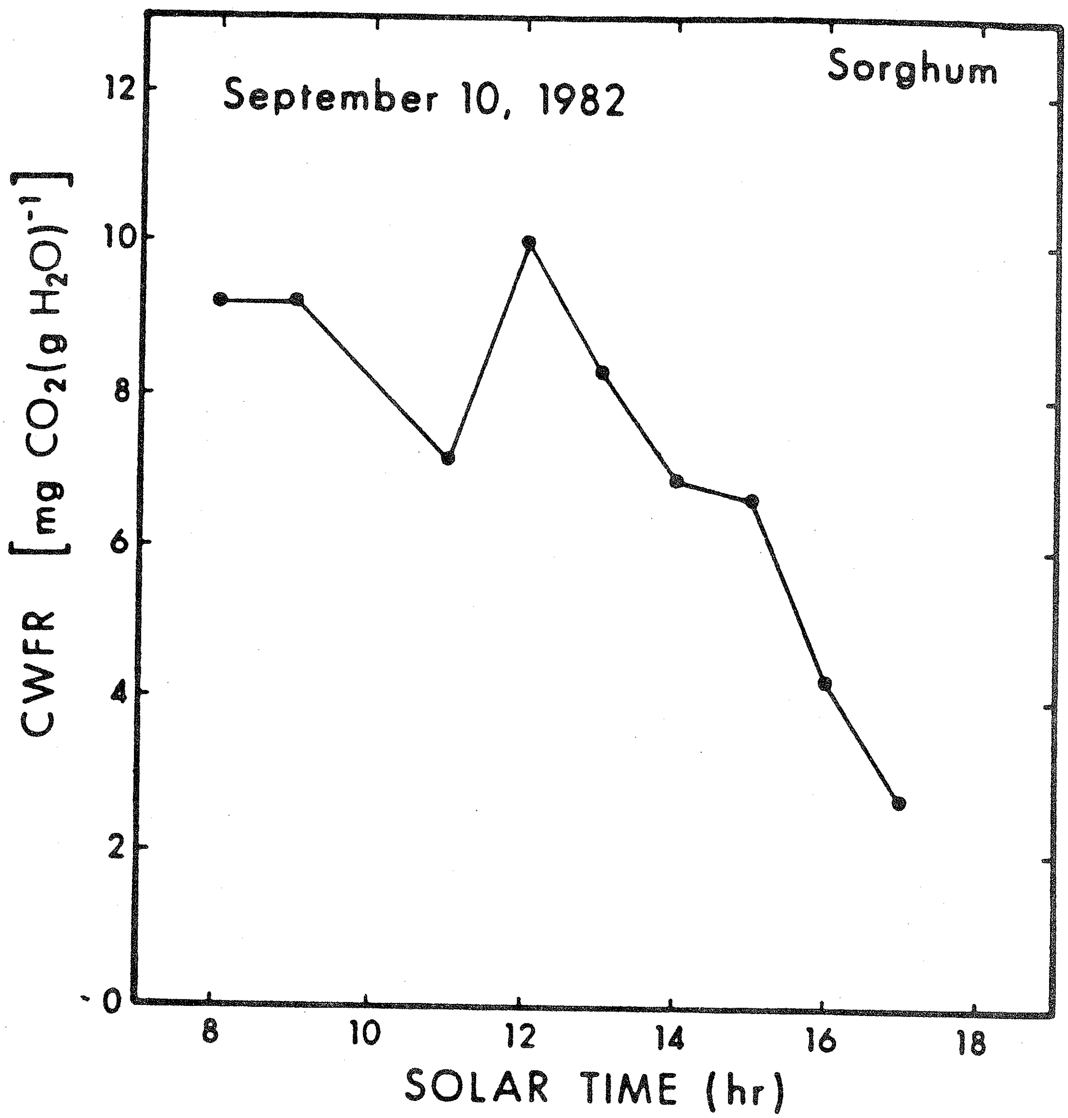

Fig. 4.11 Diurnal trend of the carbon water flux ratio (CWFR) over sorghum on September 10, 1982. Mead, Nebraska.

arguments to those mentioned earlier for soybeans may explain the sorghum CWFR behavior.

4.1.3. Micrometeorological and Physiological Interactions

The photosynthetic activity of plants may be affected by micrometeorological variables such as irradiance, air temperature, humidity, (or vapor pressure deficit), and CO_2 concentration. Physiological variables such as water potential, stomatal resistance, nutrient availability and leaf age may also affect photosynthetic rates (Salisburg and Ross, 1978).

There have been several studies of the response of a soybean canopy to light. Photosynthesis-irradiance relationships were obtained by Jeffers and Shibles (1969), Sakamoto and Shaw (1967), Egli et al. (1970), Larson et al. (1981) and Baldocchi (1982). Measurements over mature soybeans (LAI $\gtrsim$ 4.0) in 1981 from the present study depicting the dependency of CO_2 flux (Fc) on photosynthetically active radiation (PAR) appear in Figure 4.12. At the time these data were collected, there was no evidence of water stress and air temperature ranged between 15 and 30 C.

As with studies by Egli et al. (1970), Larson et al. (1981) and Baldocchi (1982), the response shown in Figure 4.12 does not indicate light saturation of the canopy at PAR levels of 1800 μEi $m^{-2}s^{-1}$. Sakomoto and Shaw (1967), however, have found evidence of light saturation near 1250 μEi $m^{-2}s^{-1}$. A light compensation point (the level of PAR at which Fc is zero) found from a parabolic fit to the data in Figure 4.12 was approximately 160 μEi $m^{-2}s^{-1}$. Baldocchi and, Sakamoto and Shaw have found light compensation points near 40 W m^{-2} or about

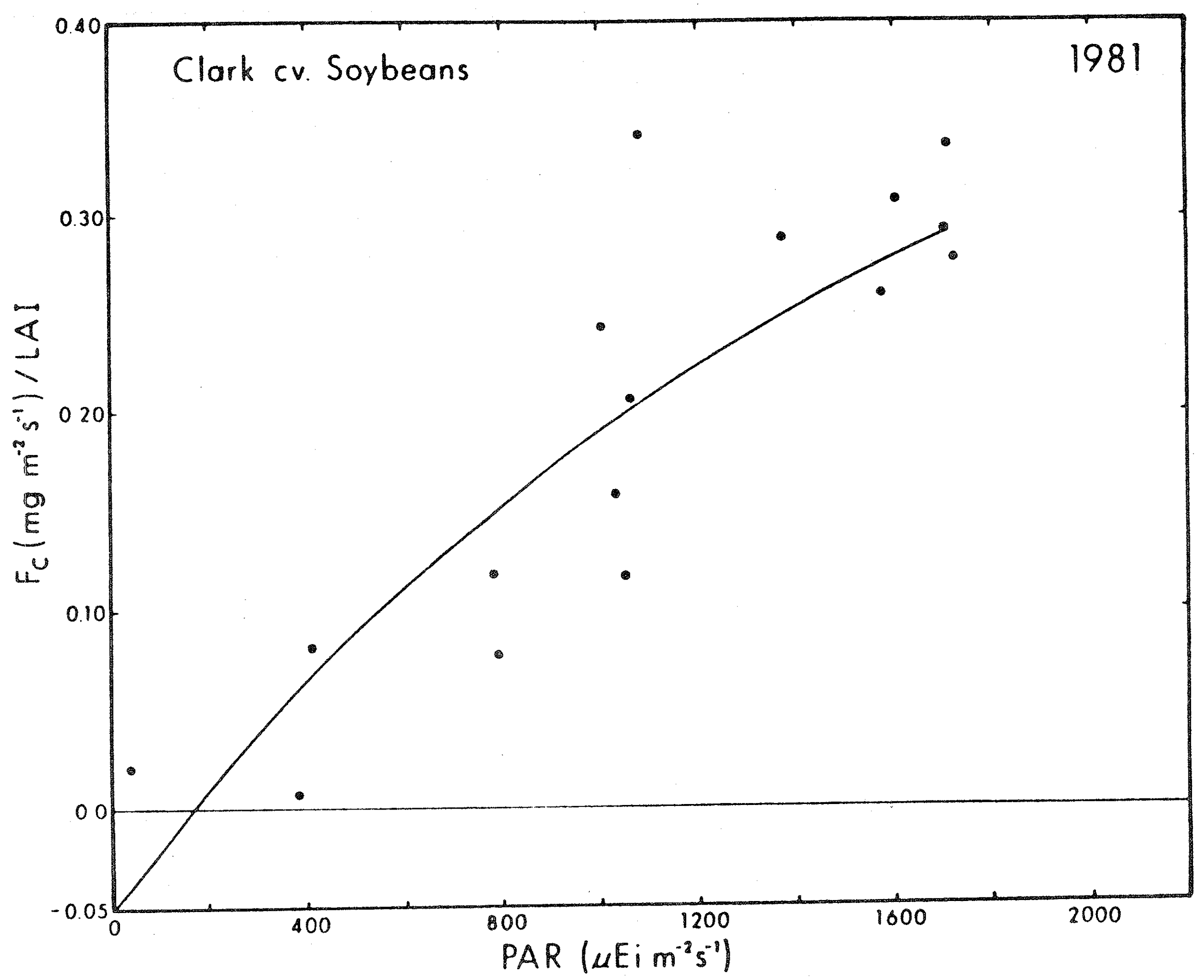

Fig. 4.12 Soybean CO_2 flux (per unit leaf area) as a function of photosynthetically active radiation (PAR). LAI $\geq$ 4.0.

190 μEi $m^{-2}s^{-1}$ PAR.

A light response relationship for the sorghum canopy (LAI $\geq$ 4.0) is shown in Figure 4.13. Maximum Fc rates are near 1.3 mg $m^{-2}s^{-1}$ although maximum PAR values were only 1600 μEi $m^{-2}s^{-1}$. Allen et al. (1974) working in the high plains of Colorado found a peak value of about 1 mg $m^{-2}s^{-1}$ at 700 W m^{-2} (or about 3290 μEi $m^{-2}s^{-1}$). With high illuminance, Allen found that Fc decreased slightly. Chamber studies by Rawson et al. (1978) indicate an Fc of 2.4 mg $m^{-2}s^{-1}$ at 2000 μEi $m^{-2}s^{-1}$ while Turner and Incoll (1971) report 1.1 mg $m^{-2}s^{-1}$ at 872 W m^{-2} irradiance and Beadle et al. (1973) found 1.5 mg $m^{-2}s^{-1}$ flux at 2600 μEi $m^{-2}s^{-1}$ in their chamber study. A light compensation point for sorghum based upon a parabolic fit of the observations in Figure 4.13 is found to be 150 μEi $m^{-2}s^{-1}$ (about 40 W m^{-2}). Allen found a compensation point of 70 W m^{-2} in his study.

The effects of air temperature upon crop apparent photosynthesis were studied by Jeffers and Shibles (1969), Larson et al. (1981) and Baldocchi (1982) over soybeans. The range of conditions encountered during this study did not permit an investigation of the effects of air temperature on Fc. In both growing seasons (1981, 1982), temperature fell within the 15 to 30 C range. Optimal temperature for soybean photosynthesis range between 25-30 C according to Jeffers and Shibles (1969). Baldocchi (1982) showed a decrease in soybean Fc at air temperatures beyond 36 C.

The relationship between Fc and stomatal resistance (r_s) was studied by Turner et al. (1978), Silvius (1977), Vignes and Planchon (1979) and Baldocchi (1982) for soybeans. These studies indicated a decrease in Fc as stomatal resistance (r_s) increased. Due to lack of sufficient

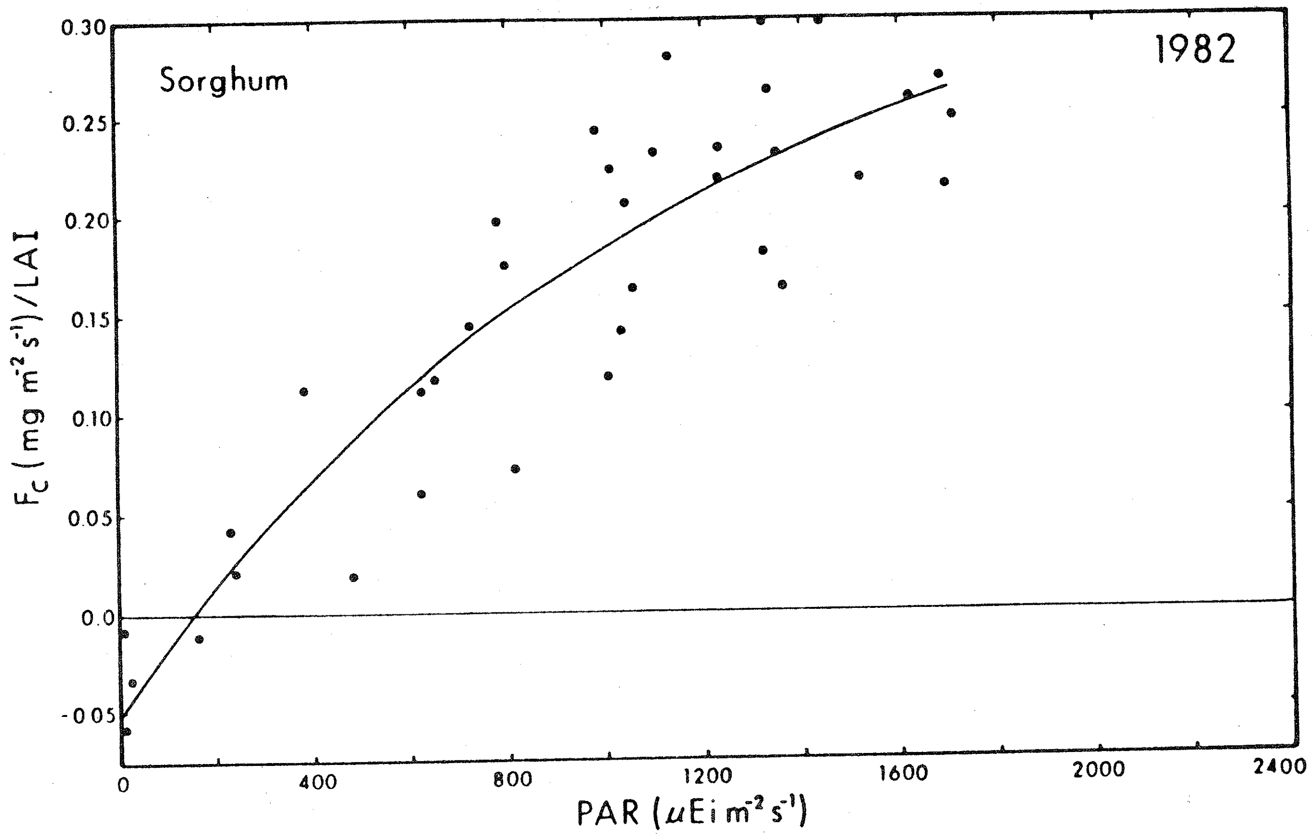

Fig. 4.13 Sorghum CO_2 flux (per unit leaf area) as a function of photosynthetically active radiation. August 25-September 10, 1982. Mead, Nebraska.

stomatal resistance data during the period in which eddy correlation measurements were made in 1981, the Fc - r_s relationship was not studied. F_c and r_s measured over the sorghum crop in 1982 are shown in Figure 4.14 (PAR $\geq$ 1400 μEi $m^{-2}s^{-1}$). Due to sufficient soil moisture conditions in 1982, only a narrow span of stomatal resistance was observed. Stomatal resistance averaged about 100 s m^{-1}, and no trend in Fc is observed over the range.

4.2. Turbulence Integral Statistics

The nature of turbulence above a surface may be described in terms of integral statistics (means, standard deviations and correlation coefficients) of the pertinent meteorological variables over the entire frequency domain. In this section integral statistics of wind velocity, air temperature, humidity and CO_2 concentration measured over both soybean and sorghum canopies are examined. Results are compared with information available in the literature.

4.2.1. Diurnal Trends in Mean and Standard Deviations

Typical diurnal trends in the mean and standard deviations of wind speed, temperature, absolute humitidy and absolute CO_2 concentration over a soybean crop appear in Figures 4.15 and 4.16. As the morning of September 2 progressed the fog cleared and clear skies prevailed for the remainder of the day. Surface heating led to increases in mean air temperature ($\bar{T}$) and the temperature standard deviation (σ_T). Wind speed increased and turbulent mixing increased standard deviations in all quantities under neutral thermal stability (as defined by the stability parameter z/L in Figure 4.16). Near midday mean CO_2 density

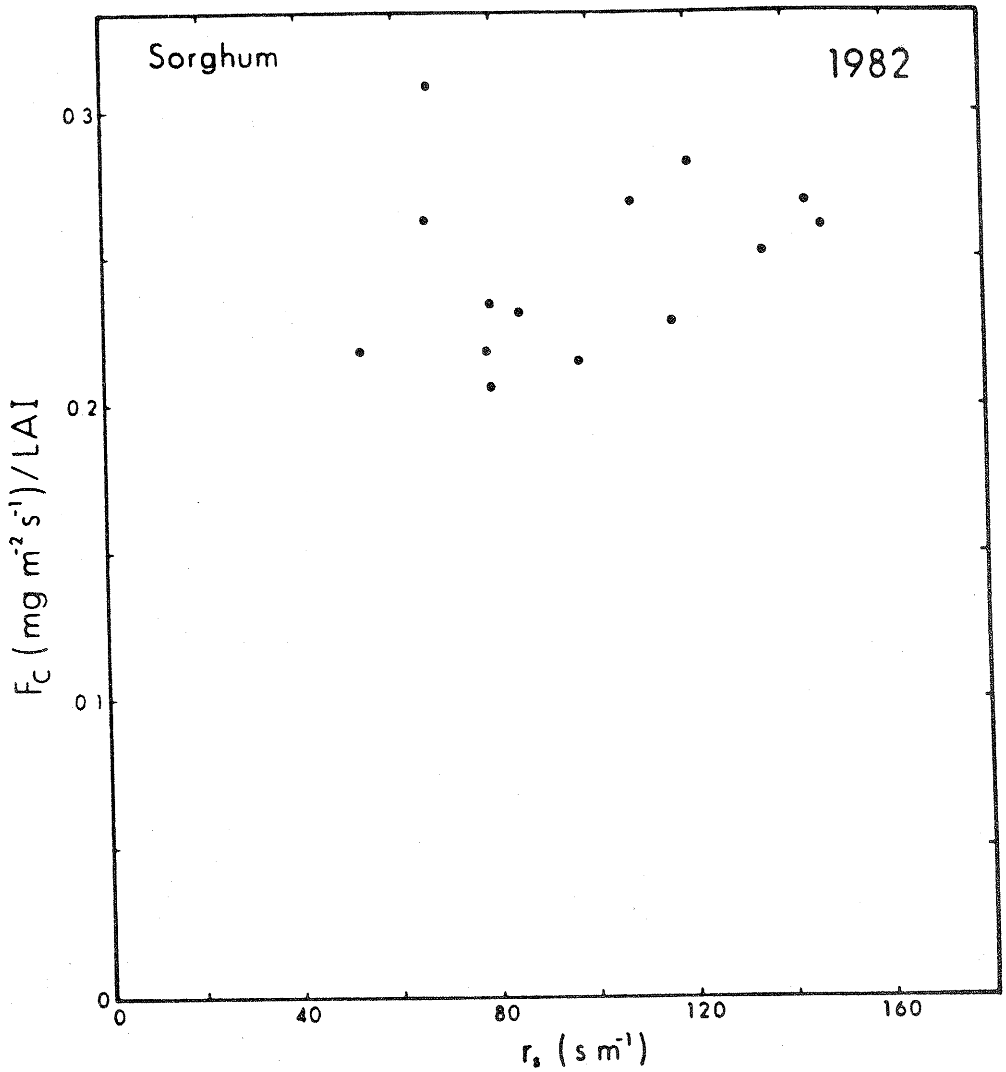

Fig. 4.14 Relationship between CO_2 flux (per unit leaf area) and stomatal resistance (r_s) measured for a sorghum canopy. August 25-September 10, 1982. Mead, Nebraska.

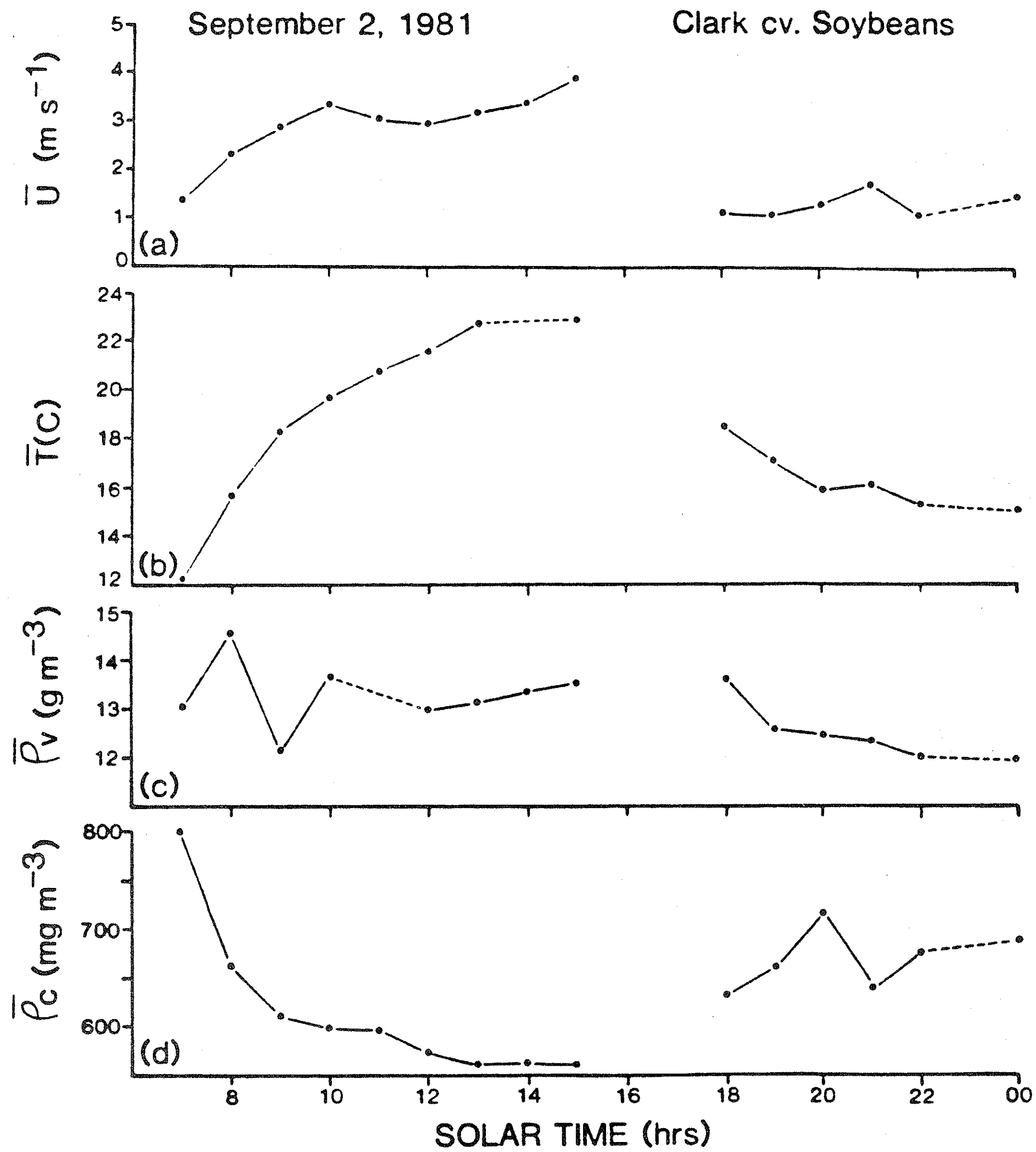

Fig. 4.15 Mean wind quantities (a) Wind Speed ($\overline{U}$), (b) Air temperature ($\overline{T}$), (c) Humidity ($\overline{\rho}_v$) and (d) CO_2 concentration ($\overline{\rho}_c$) measured over a mature soybean canopy. Mead, Nebraska September 2, 1981.

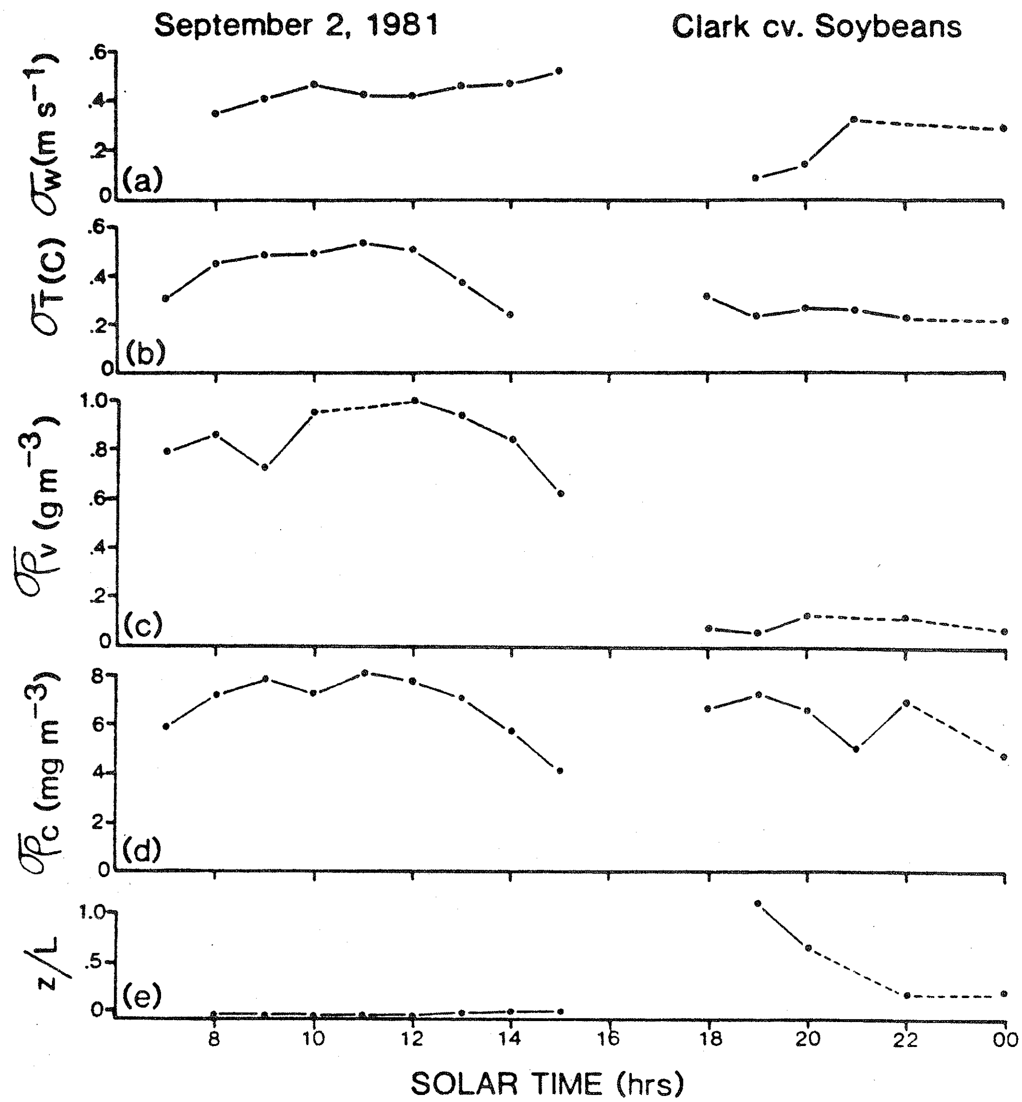

Fig. 4.16 Standard deviations (a) Vertical wind speed (σ_w), (b) Air temperature (σ_t) (c) Humidity (σ_{ρ_v}) (d) CO_2 (σ_{ρ_c}) and (e) the thermal stability parameter z/L, measured over a mature soybean canopy. Mead, Nebraska September 2, 1981.

($\bar{\rho}_c$) had decreased from an early morning maximum of 800 mg m^{-3} to 560 mg m^{-3} by midday. This occurred because the photosynthetically active soybean crop extracts considerable amounts of CO_2 from the air. The CO_2 standard deviation ($\sigma\rho_c$) reached a maximum of 8 mg m^{-3} at 1000 hrs.

During the afternoon hours, $\bar{U}$ and $\bar{T}$ decreased as did the standard deviation of all variables. A decrease in σ_w is expected with a decrease in $\bar{U}$ as a strong linear relationship exists between the two (shown in Figure 4.17). Due to a lessening photosynthetic demand for CO_2, ρ_c began to increase and it continued to rise during nocturnal hours because of respiration. After sunset, $\sigma\rho_c$ began to increase again, between 1700 - 1800 hrs., when the crop canopy changed from a CO_2 sink to a CO_2 source. $\sigma\rho_c$ remained fairly steady between 6 and 7 mg m^{-3} during the night.

A set of mean and standard deviations for a sorghum canopy on August 25-26, 1982 is shown in Figures 4.18 and 4.19. Maxima in $\bar{U}$ and $\bar{T}$, and their standard deviations, occurred at midday. ρ_c reached a minimum of about 530 mg m^{-3} at 1600 hrs. In the afternoon $\bar{U}$ and $\bar{T}$ and all standard deviations decreased in a similar way as seen over the sorghum crop. $\sigma\rho_c$ reached its minimum near sunset, then increased again as the evening progressed. During nocturnal hours, $\sigma\rho_c$ fluctuated near the 4 mg m^{-3} level (about half the midday values of 8.2 mg m^{-3}) seemingly in response to changing thermal stability as indicated by Ri values.

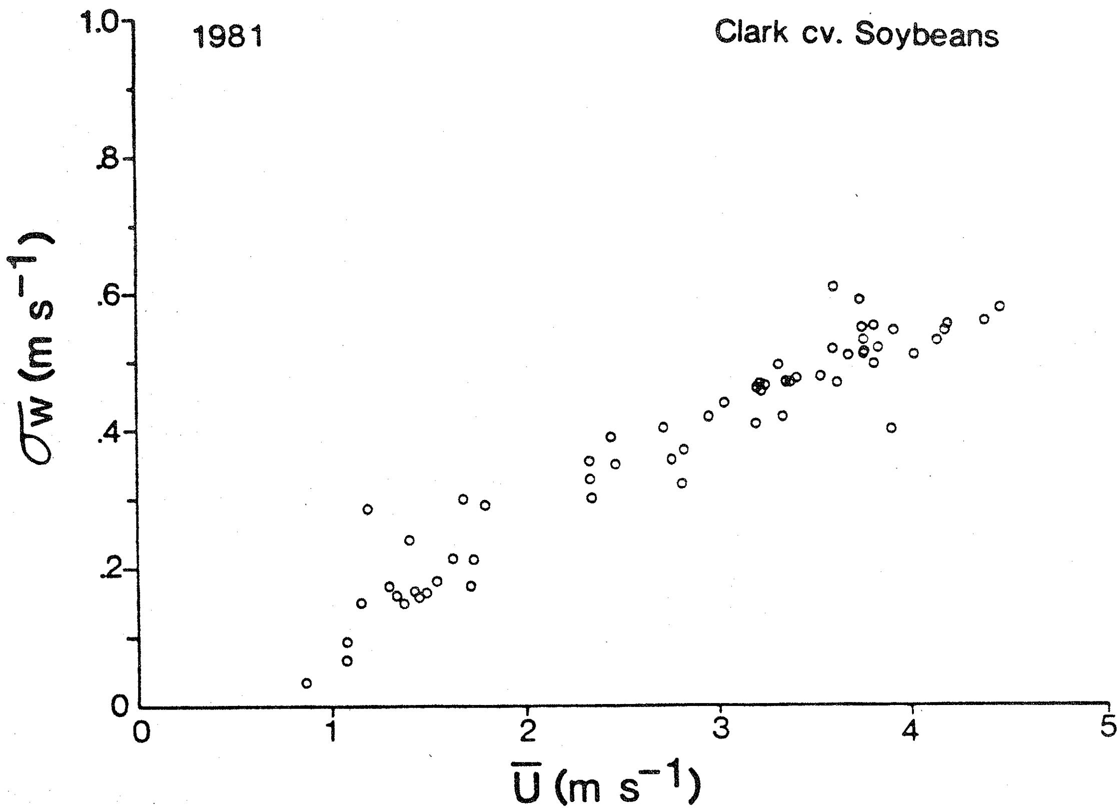

Fig. 4.17 Dependency of standard deviation of vertical wind (σ_w) on mean wind speed ($\overline{U}$). Mead, Nebraska.

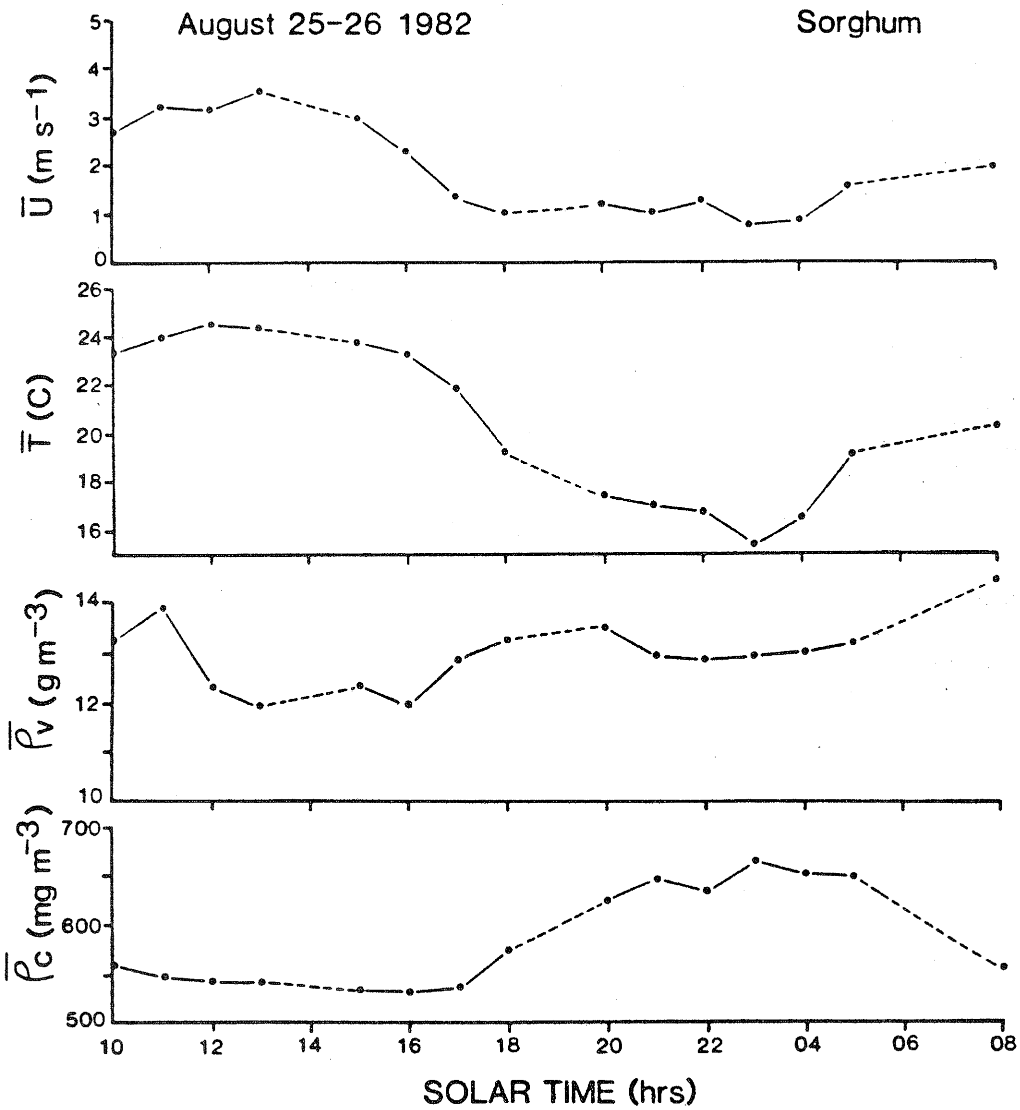

Fig. 4.18 Mean quantities (a) Wind speed ($\overline{U}$), (b) Air temperature ($\overline{T}$), (c) Humidity ($\overline{\rho}_v$), and (d) CO_2 concentration ($\overline{\rho}_c$) measured above a mature sorghum canopy. Mead, Nebraska.

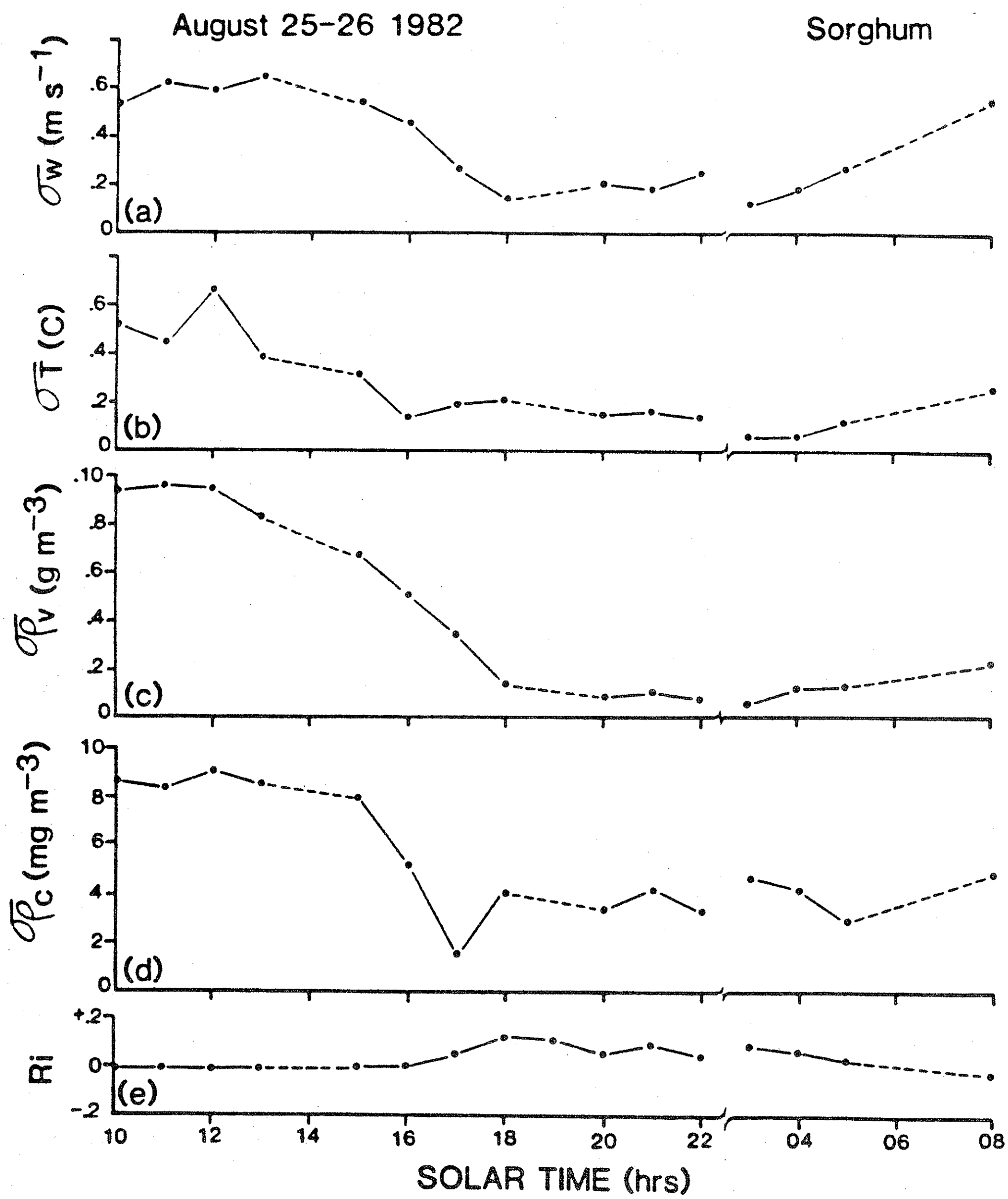

Fig. 4.19 Standard deviations (a) Vertical wind speed (σ_W), (b) Air temperature (σ_T), (c) Humidity (σ_{ρ_V}), (d) CO_2 concentration (σ_{ρ_C}) and (e) Thermal stability index (Ri) above a mature sorghum canopy. Mead, Nebraska.

The ranges in the standard deviations of all measured quantities during three experimental seasons are given in Table 4.1. Values of σ_{ρ_c} are separated into daytime and nighttime values. Daytime ranges were 2.7-10 mg $m^{-2}s^{-1}$ over soybeans and 0.9-9.0 mg $m^{-2}s^{-1}$ over sorghum. Ohtaki (1980) reported σ_{ρ_c} ranges between 5 to 20.5 mg m^{-3} over rice.

4.2.2. Dimensionless Turbulence Integral Statistics

4.2.2.1. Turbulence Intensity

In the study of turbulent fluctuations it is helpful to normalize the standard deviations of quantities with an appropriate scaling parameter to make the statistics more universal in nature. Scaled standard deviations of turbulent quantities are of the form (σ_x/x_*) where x represents the fluctuating parameter and x_* is the scaling parameter (e.g., u_*, T_*, ρ_{v*} and ρ_{c*}, defined in equations (2.22) - (2.25).

According to Monin-Obukhov similarity theory, σ_x/x_* should be a universal function of the stability parameter (z/L). Consequently many studies have expressed σ_w/u_*, along with most of the other scaled parameters enumerated above, as functions of z/L. Hicks (1981), however, has shown that such expressions may be erroneous since, for example, in a σ_w/u_* versus z/L relationship, u_* appears in both the dependent and independent variables. To avoid such autocorrelations, Hicks suggests the use of the gradient Richardson number (Ri) as an independent variable. Ri is given by:

$$Ri = {}^{g}/\overline{T} \left(\frac{\partial \overline{T}v}{\partial z} / \left(\frac{\partial \overline{U}}{\partial z}\right)^2\right) \qquad (4.2)$$

Table 4.1 Range in standard deviations of the turbulent fluctuations of horizontal and vertical windspeed, air temperature, absolute humidity and CO_2 concentration.

YEAR	σ_u ($m\ s^{-1}$)	σ_w ($m\ s^{-1}$)	σ_T (^oC)	$\sigma_{\rho v}$ ($g\ m^{-3}$)	$\sigma_{\rho c}$ ($mg\ m^{-3}$) Day	Night
1980	0.18-1.83	0.14-0.88	0.08-0.64	0.07-1.08	-	-
1981	0.08-1.19	0.04-0.61	0.00-0.57	0.04-3.08	2.70-10.0	4.60-20.9*
1982	0.33-1.60	0.14-0.80	0.06-0.66	0.07-0.97	0.88- 8.97	0.99- 4.72

*Values in the neighborhood of 20 mg m^{-3} were seen only occasionally at night.

where $\frac{\partial \overline{T}v}{\partial z}$ and $\frac{\partial \overline{U}}{\partial z}$ are the vertical gradients of the mean virtual temperature and wind speed, $\overline{T}$ is the mean air temperature and g is the acceleration due to gravity. In view of Hick's arguments integral statistics presented in this section will be considered as functions of Ri rather than z/L.

Vertical Velocity Fluctuations

A plot of σ_w/u_* versus Ri using data collected over sorghum in 1982 appears in Figure 4.20. σ_w/u_* shows little variation over the stability range and values lie at about 1.3. There have been many measurements made of σ_w/u_* and a range of 1.2 to 1.3 has been widely reported, e.g. Mordukhovich and Tsvang (1966), 1.2 over grass; Maitani (1977), 1.27 over wheat; Motha (1978), 1.2 over alfalfa; Ohtaki (1980, 1.2 over a paddy; and Hicks (1981) using Kansas data over wheat stubble, 1.3. Busch (1973) noted that authors working over water or ice have found larger values of σ_w/u_* than those working over land, e.g. Haugen et al. (1971), 1.3-1.4; McBean (1971), 1.4; and Maddukuri and Frisken (1974), 1.4. There is some tendency for σ_w/u_* (Figures 4.21 and 4.22) measured over soybeans, to increase with increasing thermal stability.

Air Temperature Fluctuations

The scaled temperature parameter, σ_T/T_*, exhibits cusp-like behavior near neutral thermal stability as shown in Figure 4.23 with measurements from the 1980 soybean field and in Figure 4.24 from the 1982 sorghum field. McBean (1971), Busch et al. (1970) and Motha (1978) found similar behavior in their results. McBean (1971) and Busch (1973) ascribe this behavior to electronic noise or to lack of stationarity. Outside the

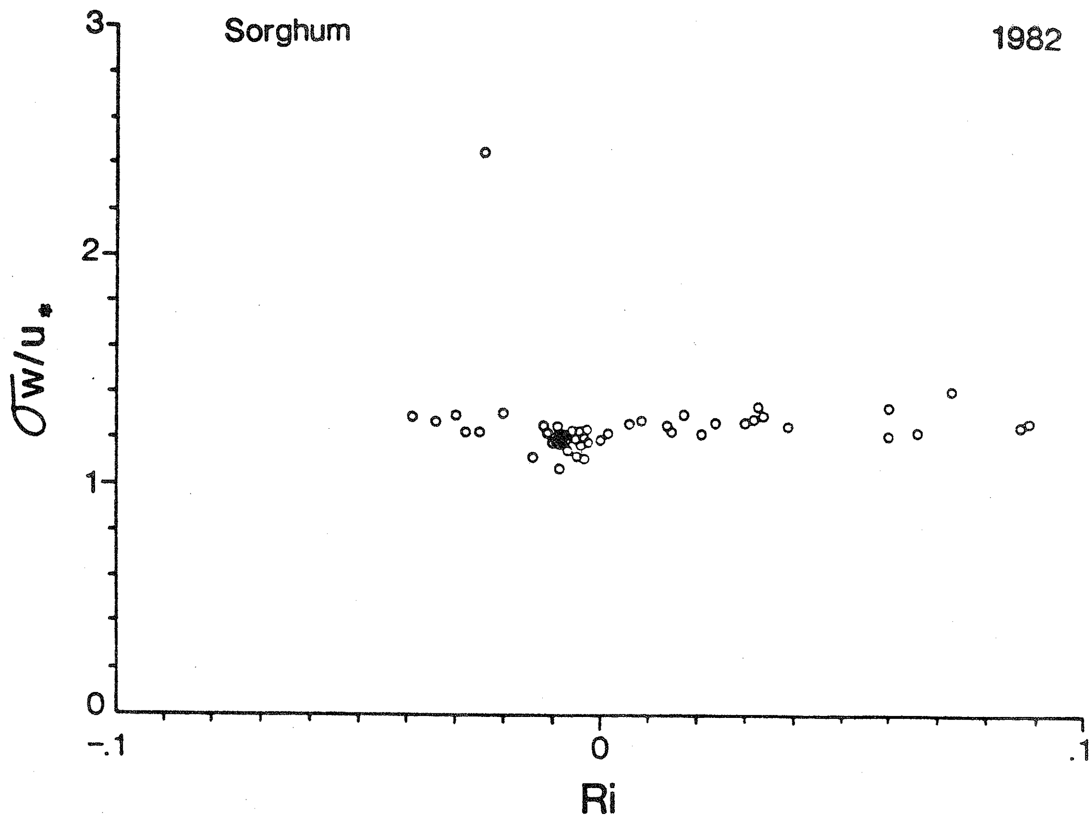

Fig. 4.20 Scaled standard deviation of vertical velocity (σ_w/u_*) as a function of stability (Ri). Sorghum. Mead, Nebraska.

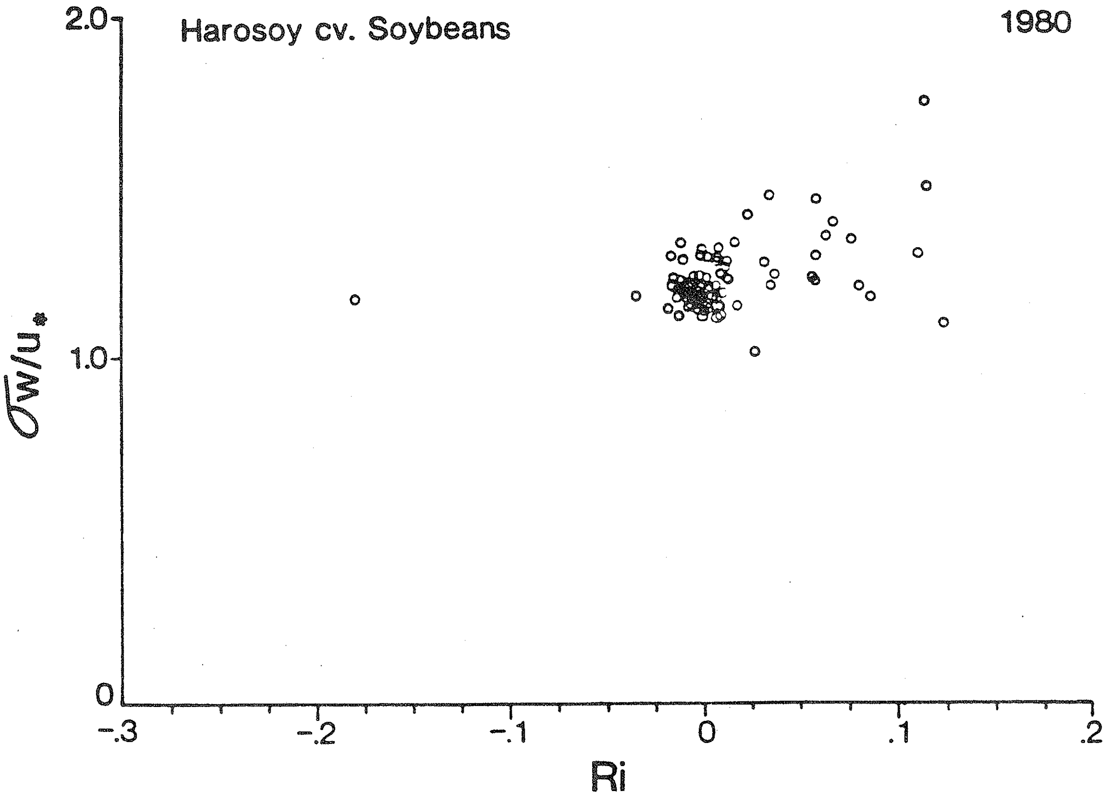

Fig. 4.21 Same as Fig. 4.20 except over a soybean canopy (Harosoy cv.).

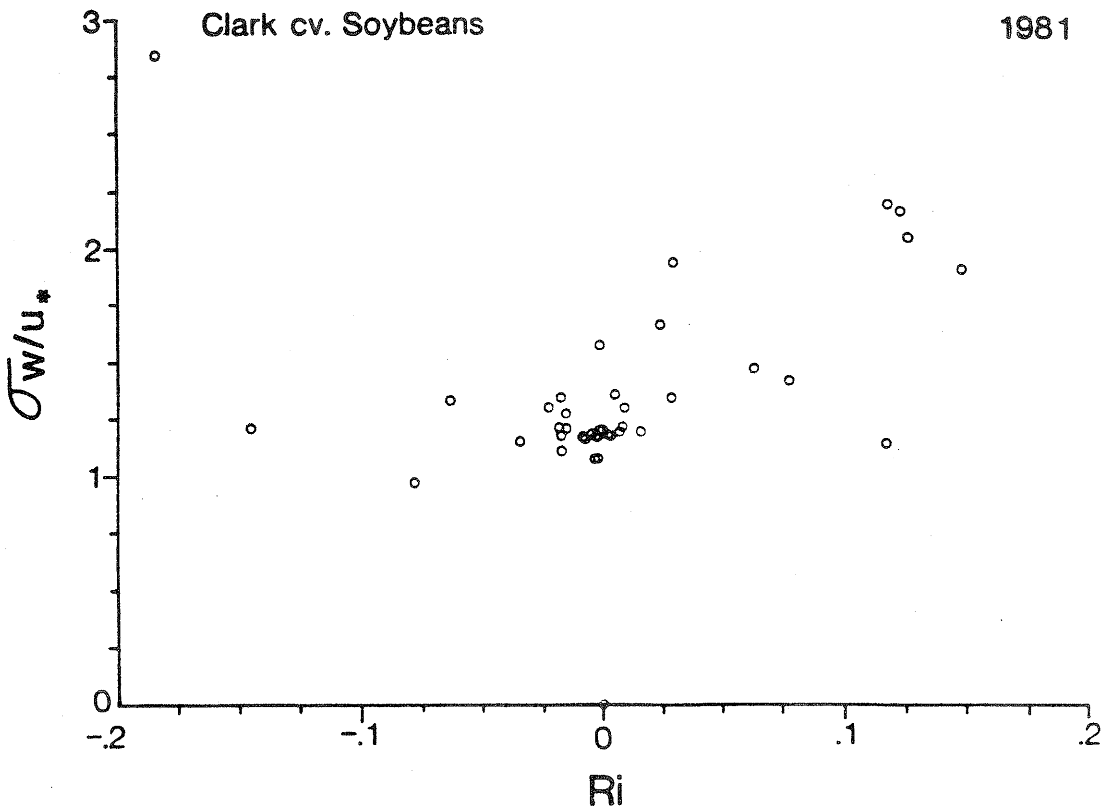

Fig. 4.22 Same as Figs. 4.20 and 4.21 except over a soybean canopy (Clark cv.).

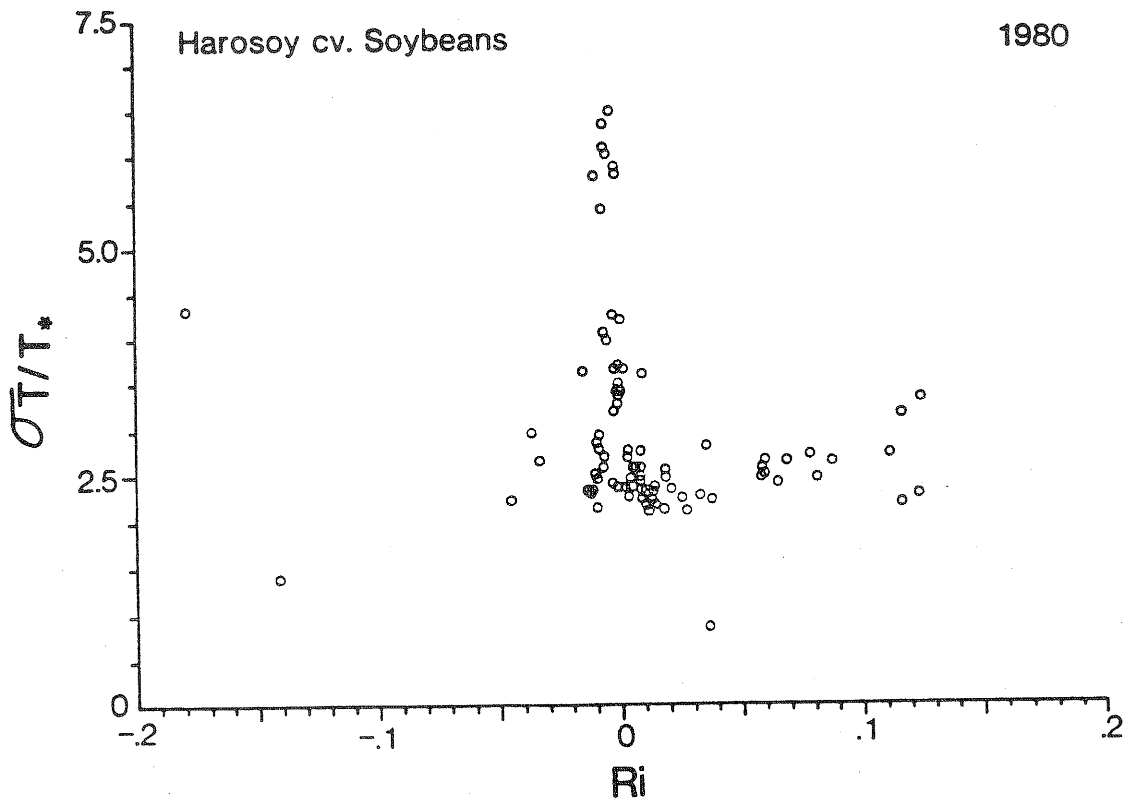

Fig. 4.23 Scaled standard deviation of temperature (σ_T/T_*) as a function of stability over a soybean canopy. Mead, Nebraska.

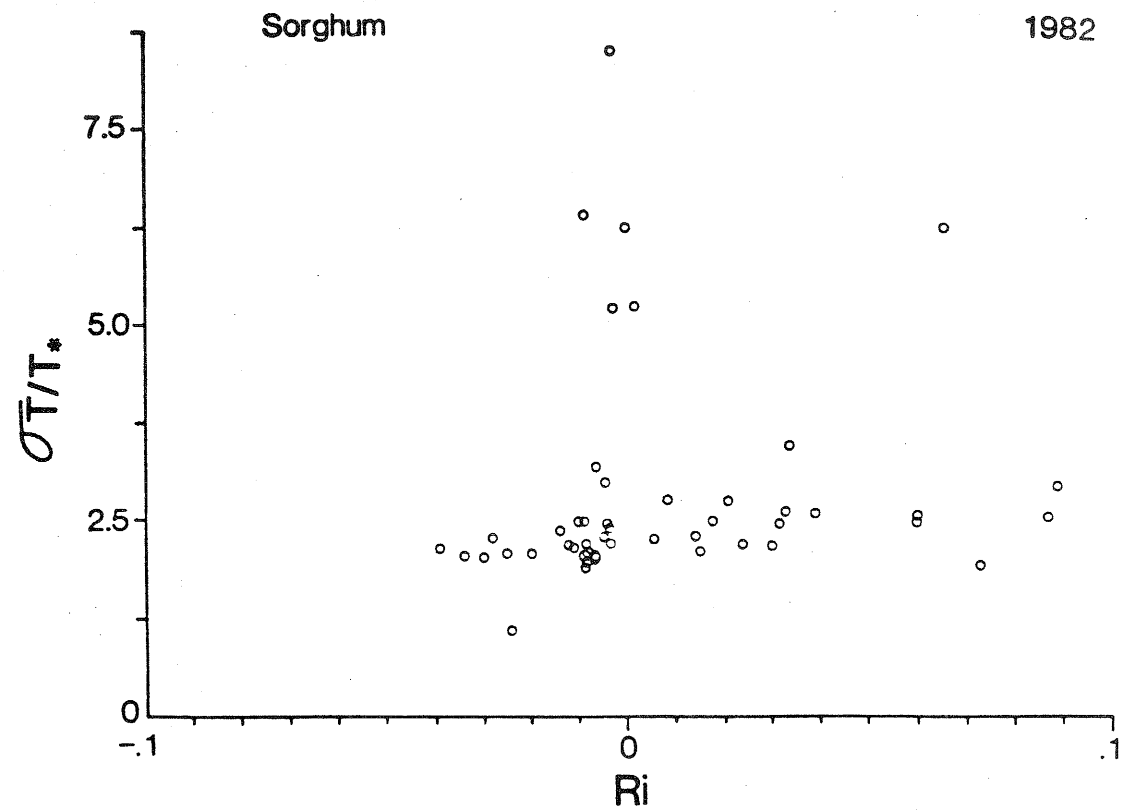

Fig. 4.24 Same as Fig. 4.23 except over a sorghum crop.

range of near neutral stability, temperature fluctuations are larger and noise problems are therefore considerably smaller. Values of σ_T/T_* over soybeans and sorghum appear to be roughly 2.2 for $|Ri| > 0.02$. McBean (1971); Maitani (1977) and Takeuchi et al. (1980) report values near 1.7.

Humidity Fluctuations

There are comparatively few studies reporting moisture fluctuations. A median value of the scaled humidity parameter ($\sigma_{\rho v}/\rho_{v*}$) measured under near neutral conditions over soybeans (Figures 4.25 and 4.26) and over sorghum (Fig. 4.27) is 2.5. This is in agreement with the findings of Motha (1978) over an alfalfa crop, Takeuchi et al. (1980) over wheat, Ohtaki (1980) over a rice paddy and, Phelps and Pond (1971), and McBean (1971) over the ocean.

CO_2 Fluctuations

Scaled turbulent CO_2 fluctuations ($\sigma_{\rho c}/\rho_{c*}$) measured over soybeans and sorghum are shown in Figures 4.28 and 4.29, respectively. Values ranged between 2.0 and 4.2 with median values of 2.7 and 2.9 for near neutral conditions over the two crops. Little tendency is found over the stability range measured. Note that in 1981 $\sigma_{\rho c}/\rho_{c*}$ values are reported as a function of z/L since few Ri calculations were available during the time that the fast response CO_2 sensor was used. In the only other study reporting on CO_2 fluctuations known to the author, Ohtaki (1980) working over a paddy field found $\sigma_{\rho c}/\rho_{c*}$ to be about 3.5 under neutral conditions with considerable scatter. Ohtaki (1980) attributed this scatter to a small correlation between CO_2 and the

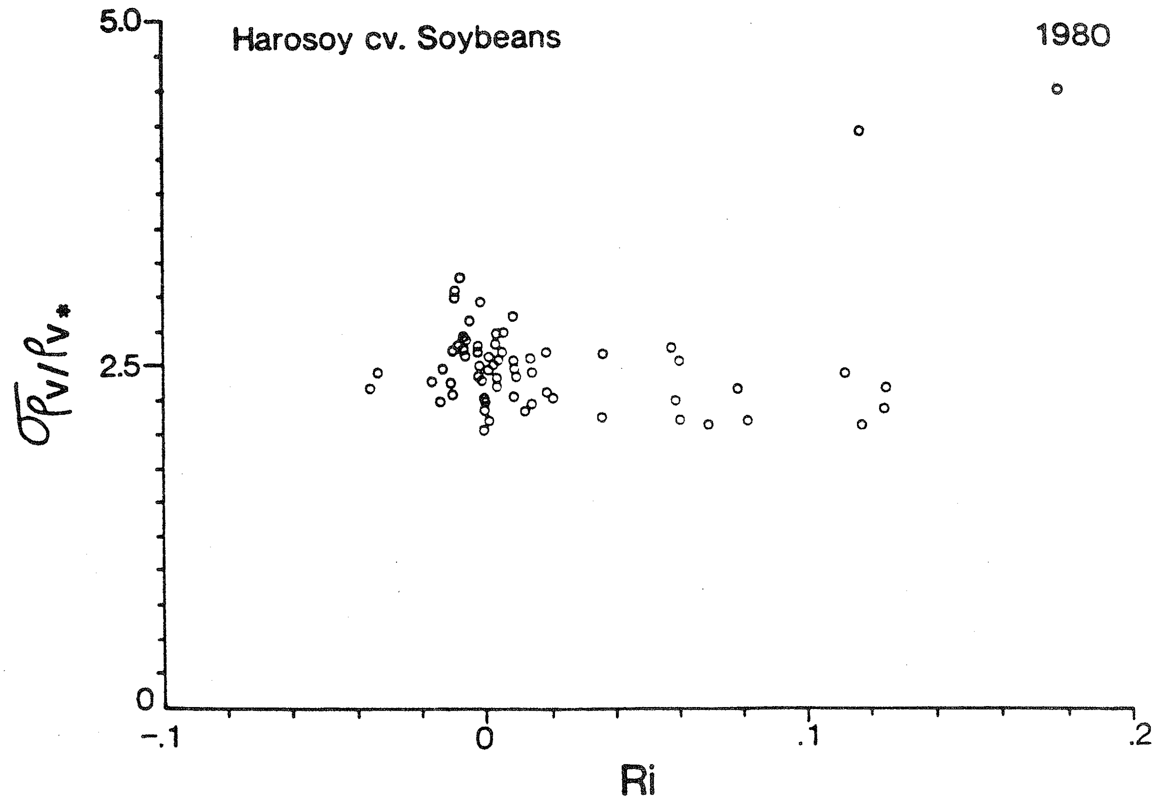

Fig. 4.25 Scaled standard deviation of humidity ($\sigma_{\rho_v}/\rho_{v*}$) as a function of stability (Ri) measured over a soybean canopy. Mead, Nebraska.

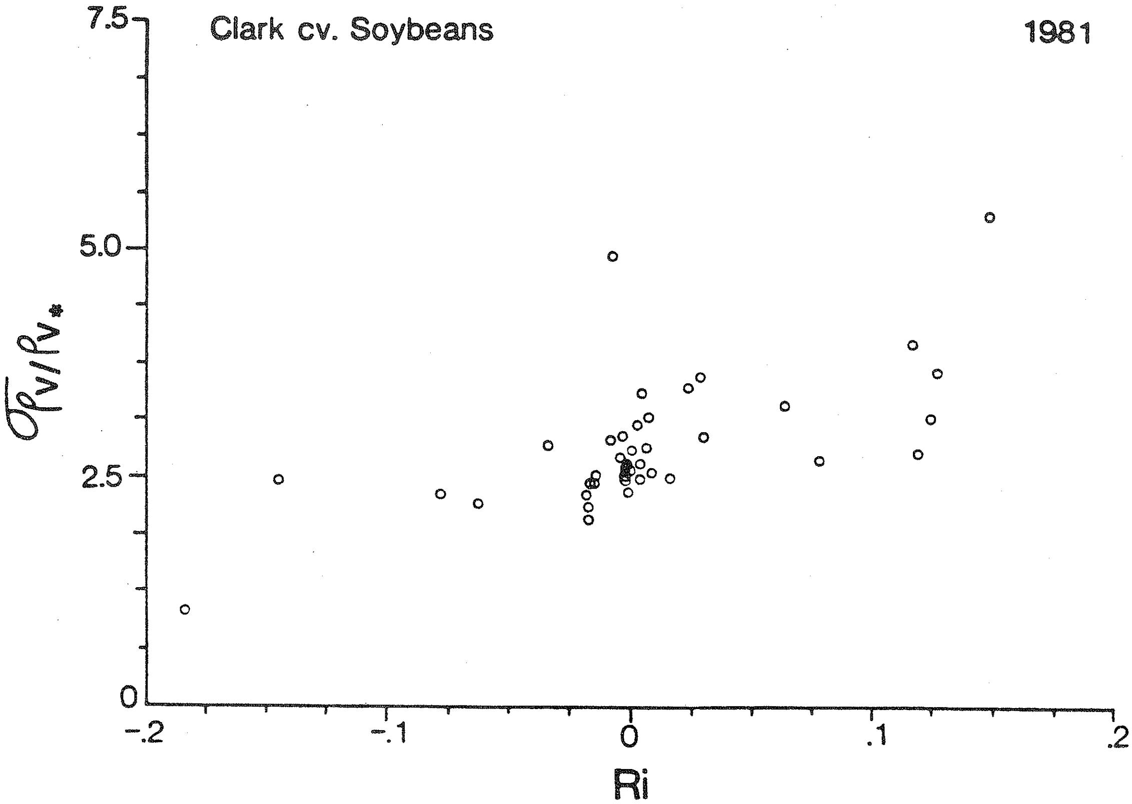

Fig. 4.26 Same as Fig. 4.25 except over a different soybean cultivar.

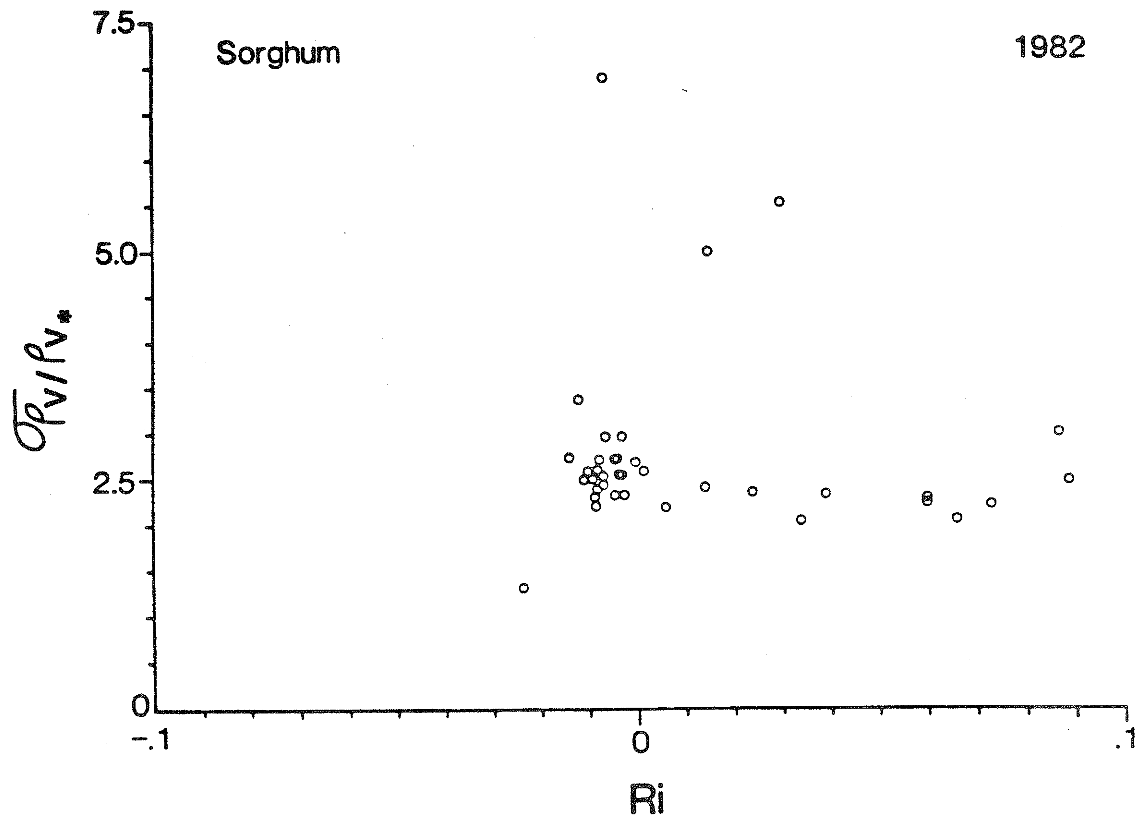

Fig. 4.27 Same as Fig. 4.25 except over a sorghum canopy.

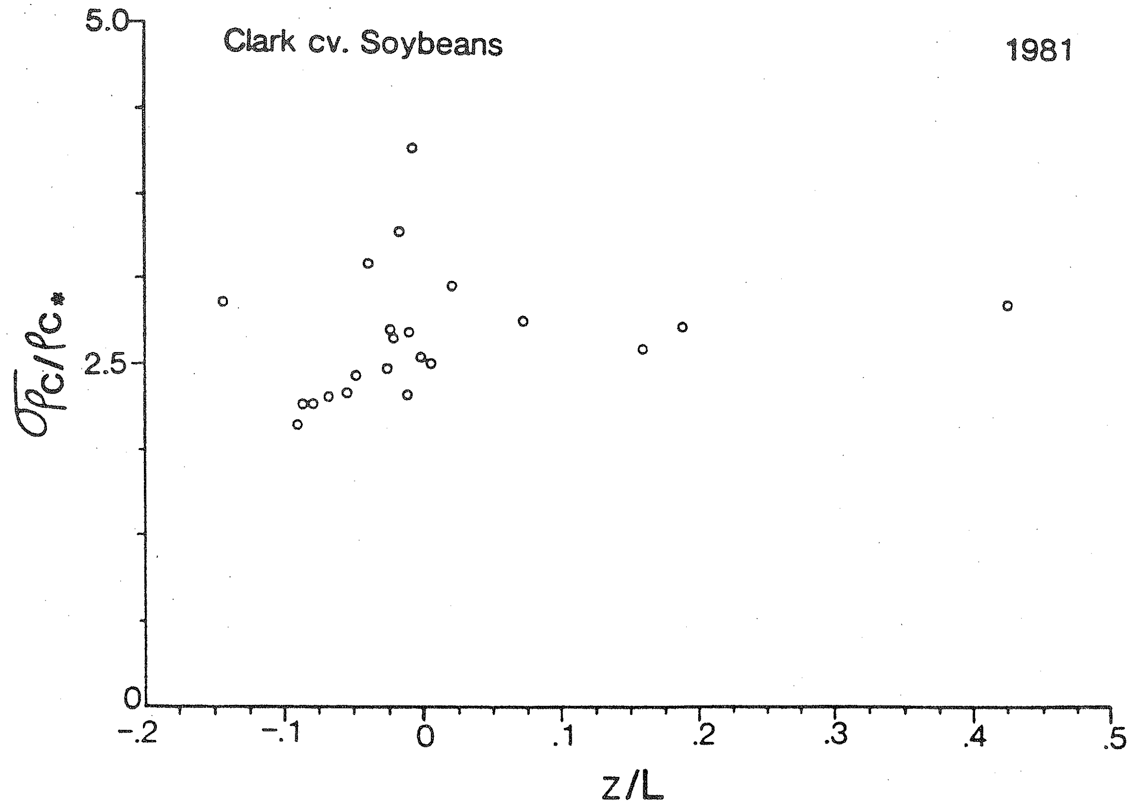

Fig. 4.28 Scaled standard deviation of CO_2 fluctuations ($\sigma_{\rho_c}/\rho_{c*}$) as a function of stability (z/L) over a soybean canopy. Mead, Nebraska.

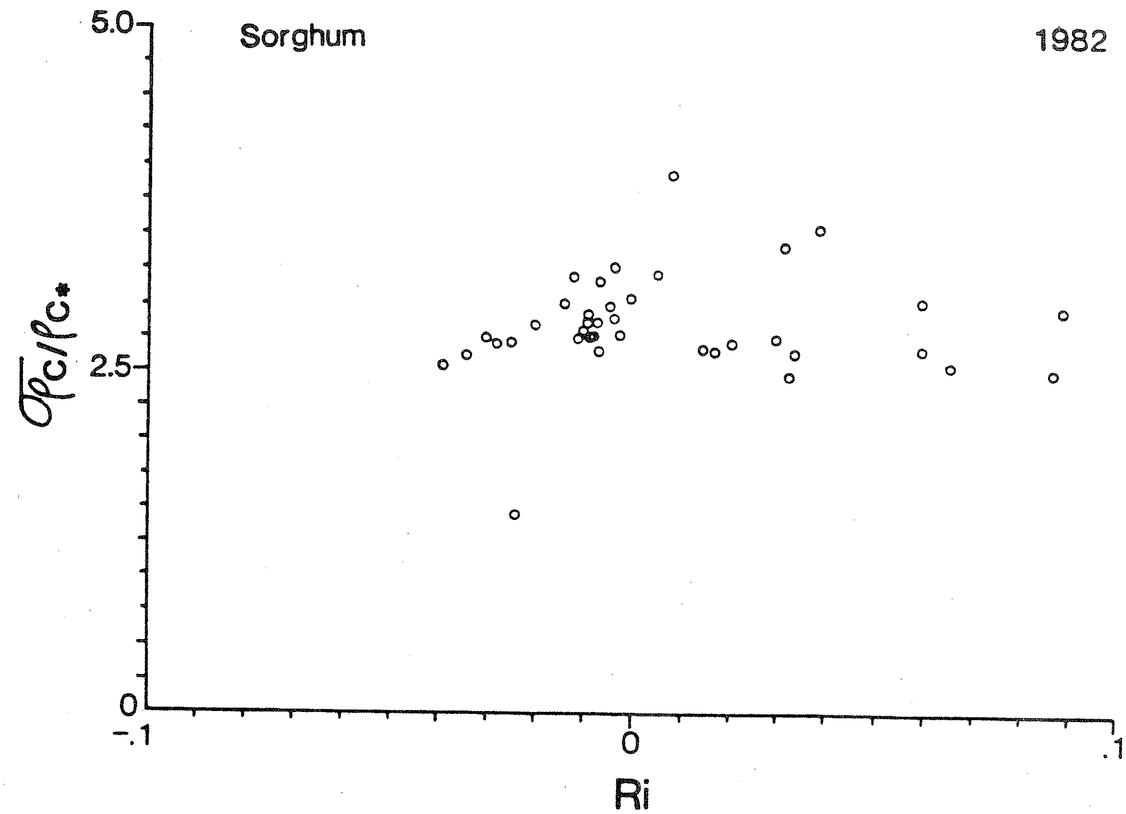

Fig. 4.29 Same as Fig. 4.28 except over a sorghum canopy and plotted with the Ri stability parameter.

vertical velocity ($r_{w\rho_c}$) in the evening hours. This correlation coefficient is discussed below.

4.2.2.2. Integral Correlation Coefficients

The correlation coefficients introduced in Chapter 2 may be written:

$$r_{xy} = \frac{\overline{x'y'}}{\sigma_x \sigma_y} \tag{4.3}$$

where x and y represent atmospheric variables such as u, v, w, t, ρv or ρc. r_{xy} is the correlation of the x-y pair over the entire frequency range of eddies. Correlation coefficients involving w as a variable of the x-y pair represent the efficiency of transport (McBean, 1972). For example, the correlation coefficients of r_{wu}, r_{wT}, $r_{w\rho_v}$ and, $r_{w\rho_c}$ represent the efficiency of transfer of momentum, sensible heat, water vapor and CO_2, respectively.

Correlation Coefficient of Momentum Transfer

The correlation coefficient for momentum transfer (r_{wu}) is shown as a function of Richardson number in Figures 4.30 and 4.31 with data measured over soybeans and sorghum, respectively. Some scatter is seen in the soybean data with Ri > 0 (thermally stable conditions). This may have been a result of poor sensor response at low wind speeds as has also been seen in other studies in the literature under similar conditions. Values of $|r_{wu}|$ under nearly neutral conditions center at about 0.35 for both crops. Such values are in close agreement with those measurements reported by Maitani (1977) over wheat, Takeuchi (1980) over a paddy, Hicks (1981) using Kansas data over wheat stubble, and

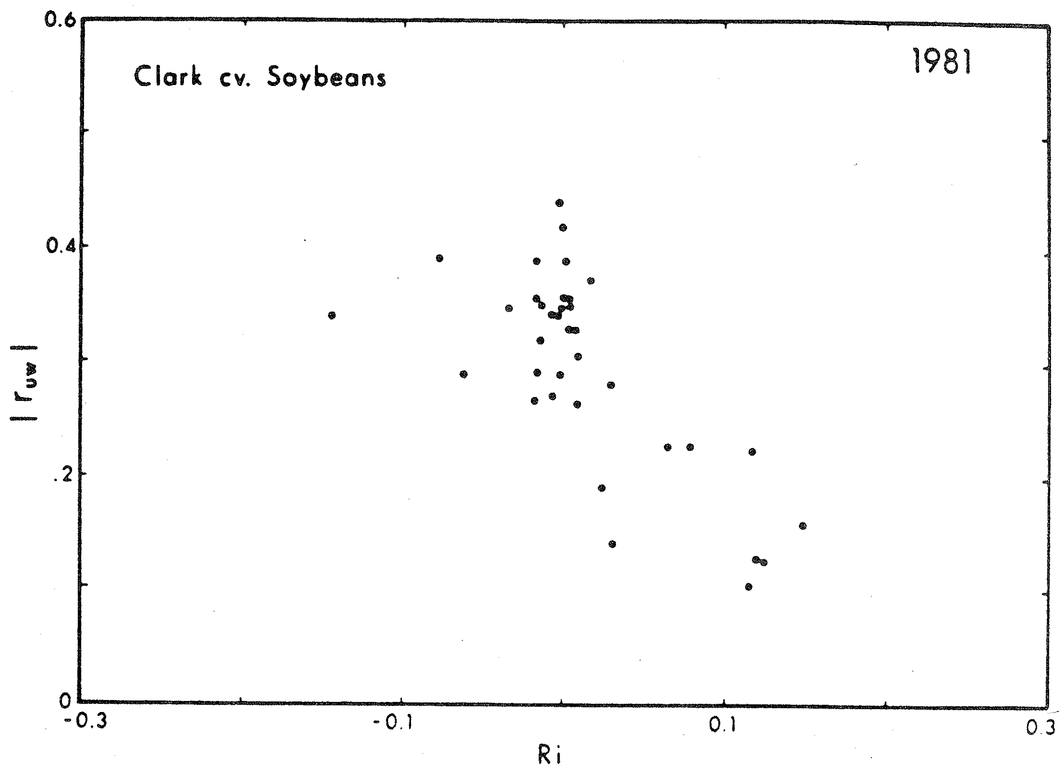

Fig. 4.30 Correlation coefficient of momentum transfer (r_{uw}) as a function of stability (Ri) over a soybean canopy.

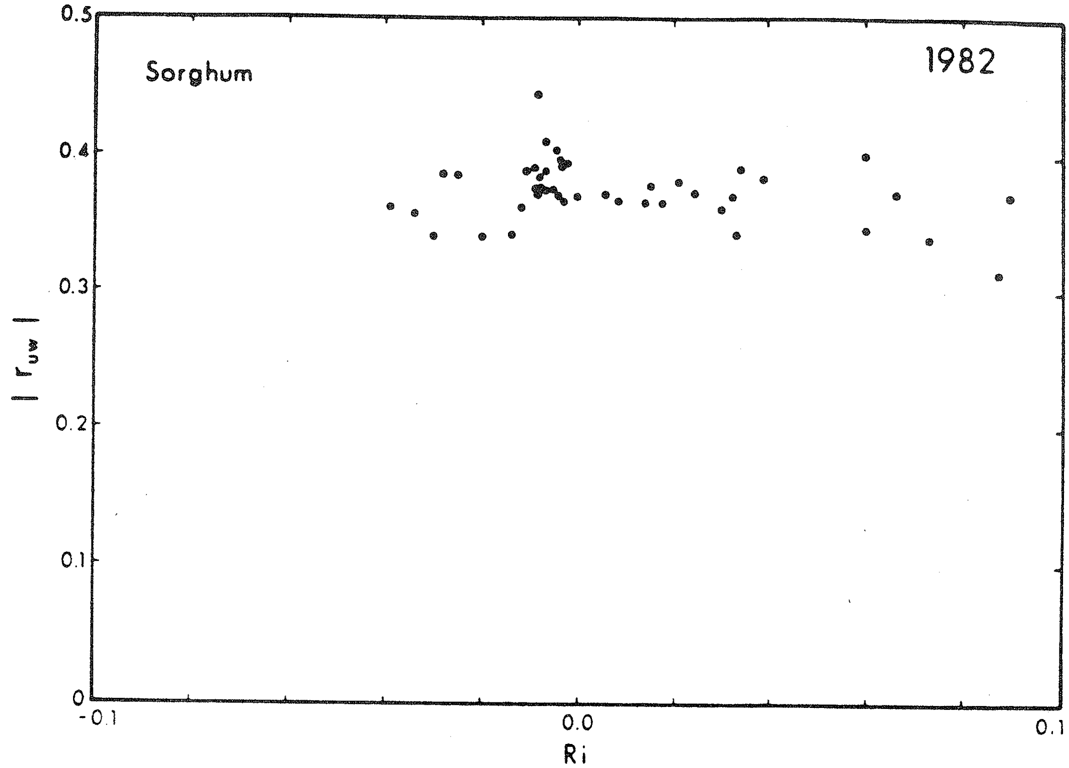

Fig. 4.31 Same as Fig. 4.30 except over a sorghum canopy.

by, McBean (1970) and Thorpe et al. (1973) over oceanic surfaces.

Correlation Coefficient of Heat Transfer

If buoyant motion is dominant in thermally unstable air then one would expect the correlation coefficient $|r_{wT}|$ to be largest in unstable stratification and to become progressively smaller as stability increases. These tendencies are found in data collected over sorghum, shown in Figure 4.32. McBean (1970), Thorpe et al. (1973), Takeuchi et al. (1980) and Hicks (1981) report similar trends. Values of $|r_{wT}|$ are about 0.38 for $-.04 < Ri < 0.01$. For $0.01 < Ri < 0.1$, values lie at about 0.34. The scatter near $Ri = 0$ is probably a result of the difficulty in maintaining sufficiently high signal to noise ratio when temperature fluctuations (T') are very small.

Correlation Coefficient of Water Vapor Transfer

Moisture is a passive scalar although it does influence atmospheric motions somewhat through its effect upon air density. Very few measurements are available in the literature that describe the behavior of the correlation coefficient for moisture transfer ($r_{w\rho_v}$) as a function of thermal stability. Data on $|r_{w\rho_v}|$ plotted in Figure 4.33 and 4.34, were collected over soybeans in 1981 and over sorghum in 1982. Values of $|r_{w\rho_v}|$ in near neutral stability range between 0.2 and 0.4 for the two crops. McBean (1970), Maitani (1977), Thorpe et al. (1973), Takeuchi et al. (1980) and Motha (1978) also found values within this range. Interestingly, a tendency for $|r_{w\rho_v}|$ to decrease with increasing stability is seen in Figure 4.33. A similar trend has been observed by McBean (1970) and Thorpe et al. (1973).

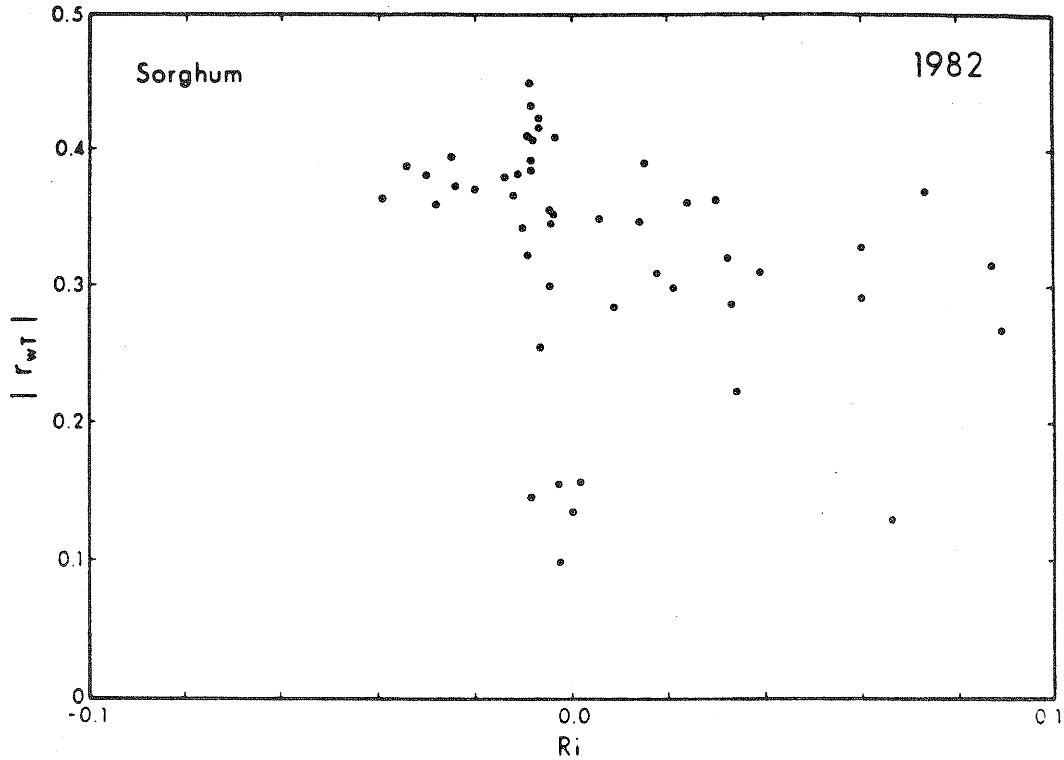

Fig. 4.32 Correlation coefficient for heat transfer (r_{WT}) as a function of stability (Ri) over a sorghum canopy. Mead, Nebraska.

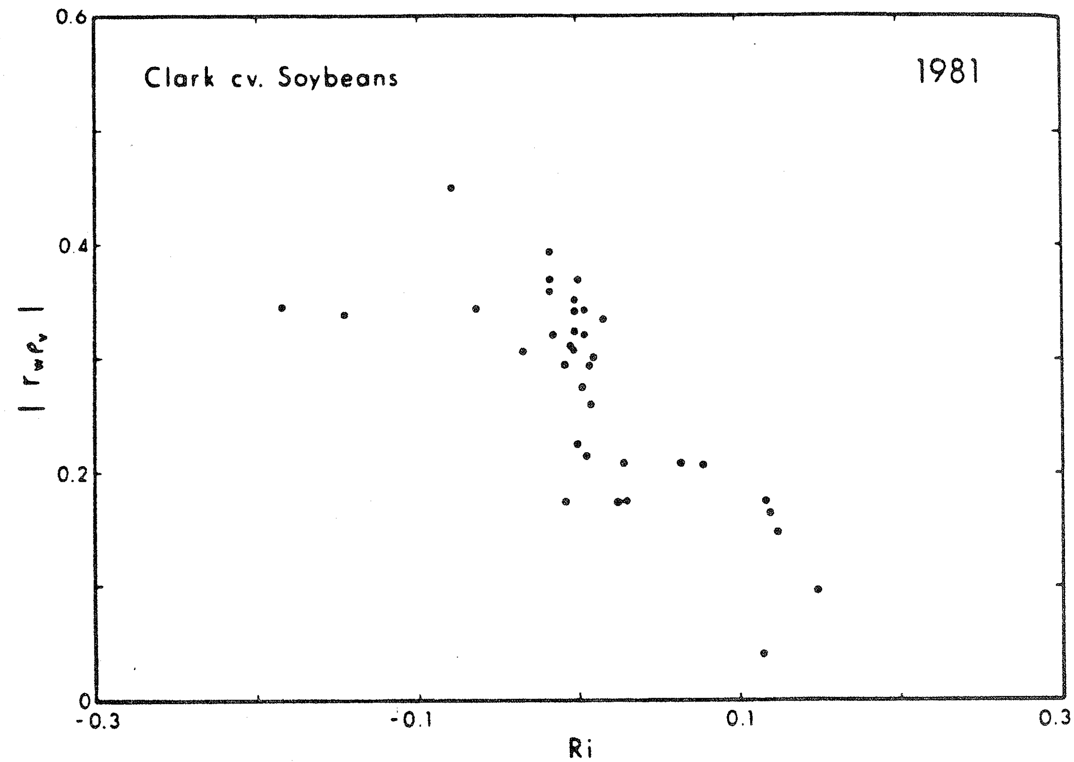

Fig. 4.33 Correlation coefficient for water vapor transfer ($r_{w\rho_v}$) as a function of stability (Ri) over a soybean canopy. Mead, Nebraska.

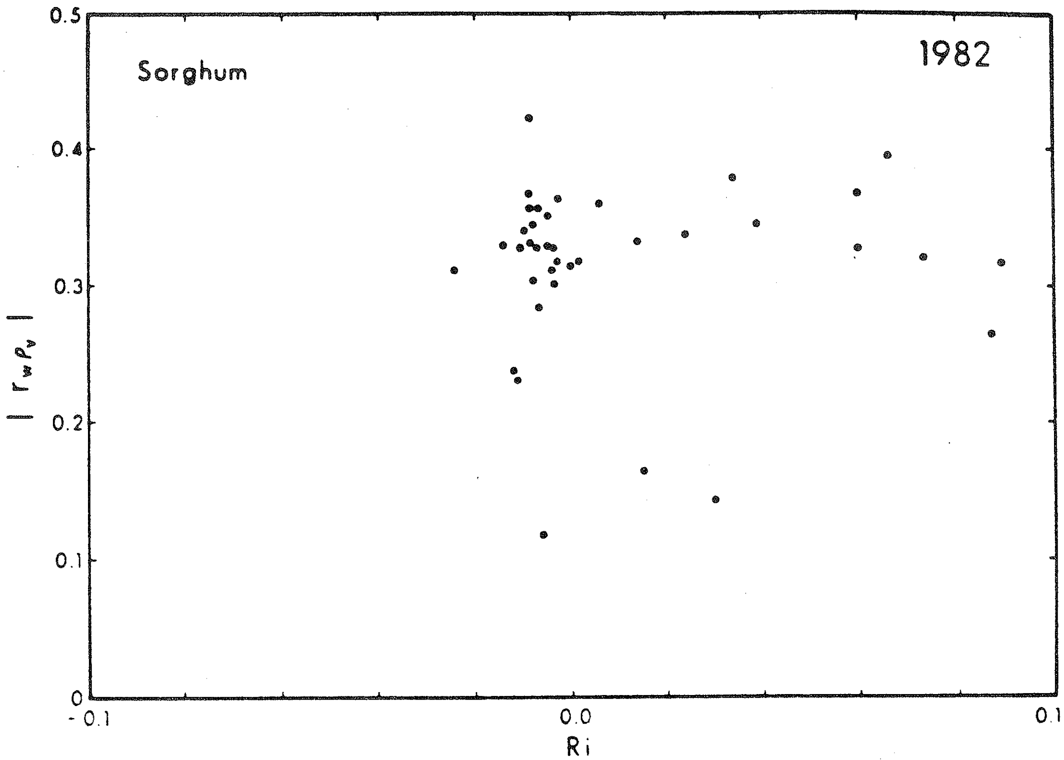

Fig. 4.34 Same as Fig. 4.33 except over sorghum.

Correlation Coefficient of CO_2 Transfer

The value of the correlation coefficient for CO_2 transport over soybeans and sorghum is plotted as a function of thermal stability in Figures 4.35 and 4.36, respectively. The stability parameter (z/L) was used in Figure 4.35 instead of Ri. Values of $|r_{w\rho_c}|$ generally lie between 0.2-0.4 with a mean of 0.28. Similar results were obtained by Ohtaki (1980) over a paddy field in the only study known to the author in which $r_{w\rho_c}$ was measured.

Other Correlation Coefficients

It is interesting to examine the correlation between scalar quantities such as T, ρ_v and ρ_c. The largest correlations were found to be the pairs formed from this group. High correlations were found between temperature and water vapor ($|r_{T\rho_v}|$) and, temperature and CO_2 ($|r_{T\rho_c}|$ as is shown in Figures 4.37 and 4.38, respectively. The scatter near Ri = 0 probably results from the difficulties in the measurement of temperature fluctuations (T'). In the region $|Ri| > 0.015$ mean $|r_{T\rho_v}|$ and $|r_{T\rho_c}|$ values of 0.68 and 0.67 were obtained from data reported in Figures 4.37 and 4.38, respectively. The correlation coefficient $|r_{\rho_v\rho_c}|$ for measurements made over sorghum is shown in Figure 4.39. A mean value of 0.68 is found from the data shown in this figure, very comparable to that of $|r_{T\rho_v}|$ and $|r_{T\rho_c}|$. Ohtaki (1980) who measured $|r_{\rho_v\rho_c}|$ values between 0.7-0.8 found this correlated pair to be the largest he studied.

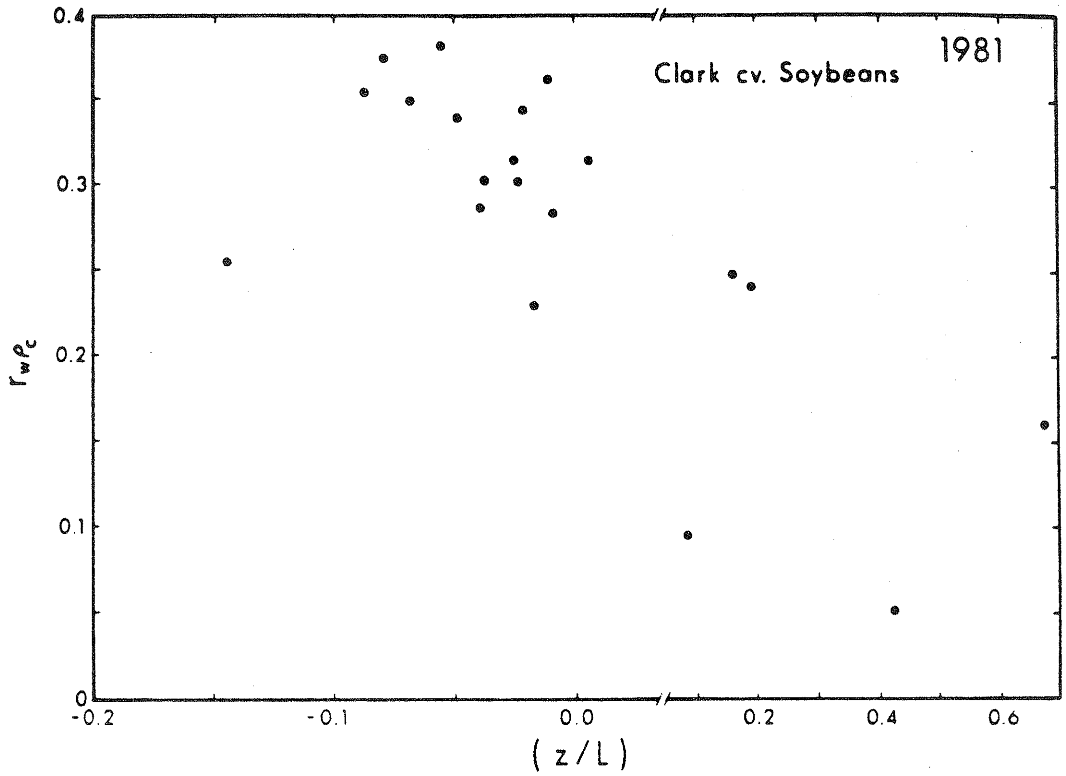

Fig. 4.35 Correlation coefficient for CO_2 transfer ($r_{w\rho_c}$) as a function of stability (z/L) over a soybean canopy. Mead, Nebraska.

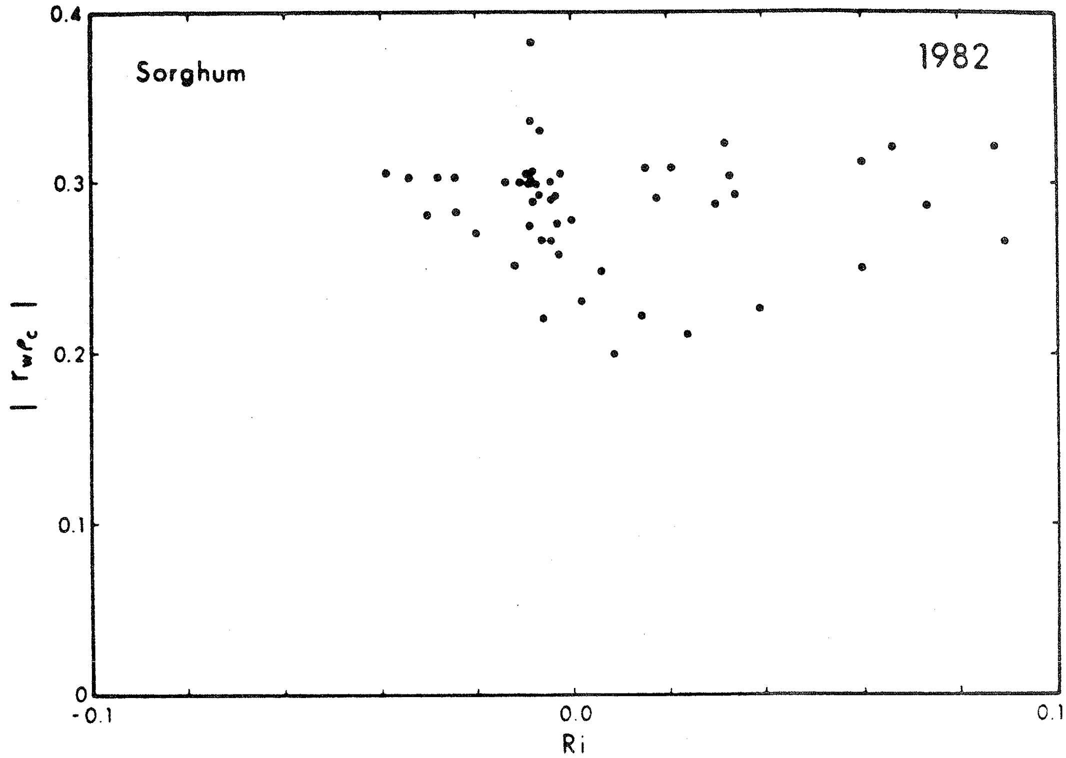

Fig. 4.36 Same as Fig. 4.35 except over a sorghum canopy and plotted against Richardson number.

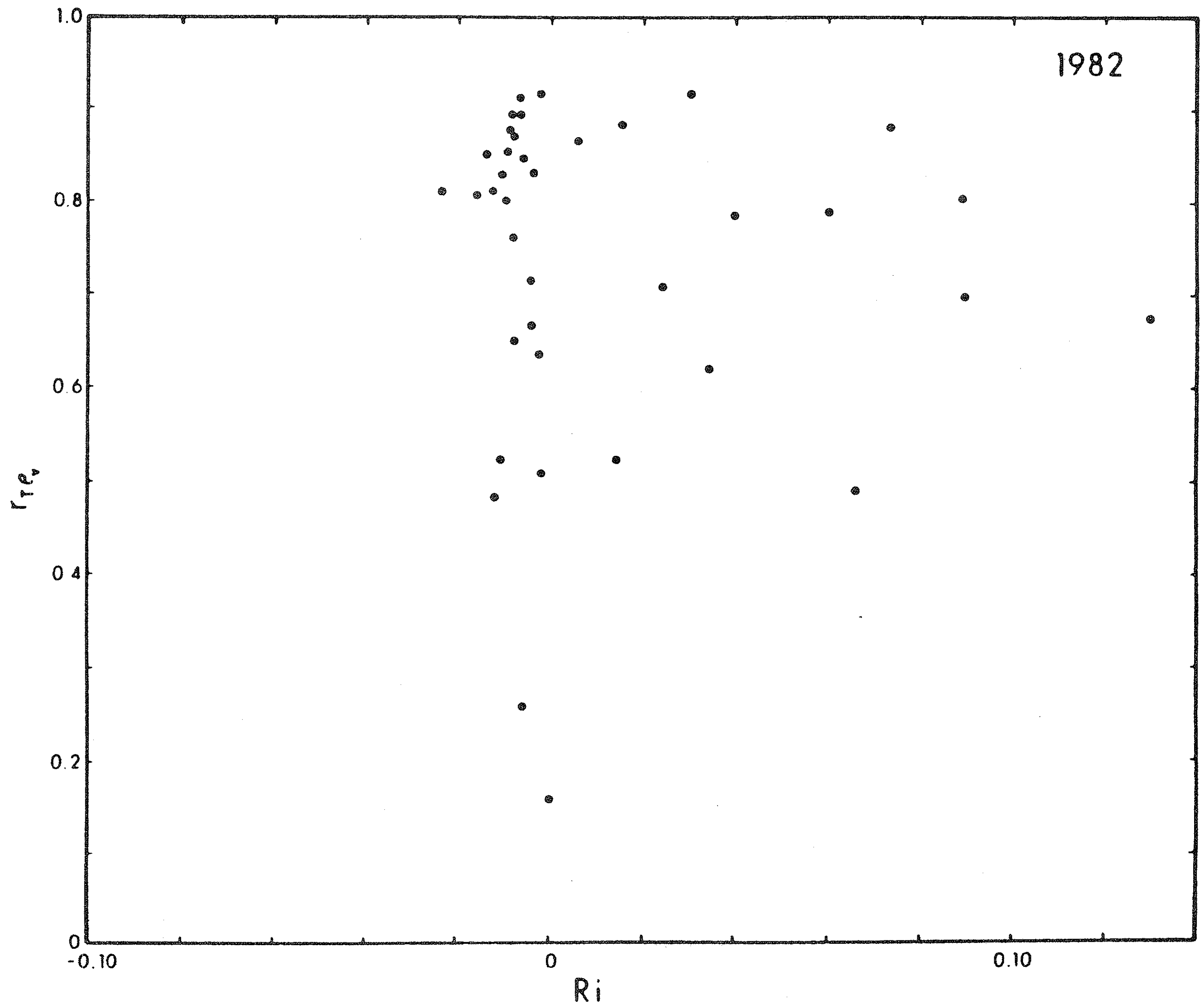

Fig. 4.37 Correlation coefficient between temperature and humidity fluctuations ($r_{T\rho_v}$) as a function of stability (Ri) over a sorghum canopy. Mead, Nebraska.

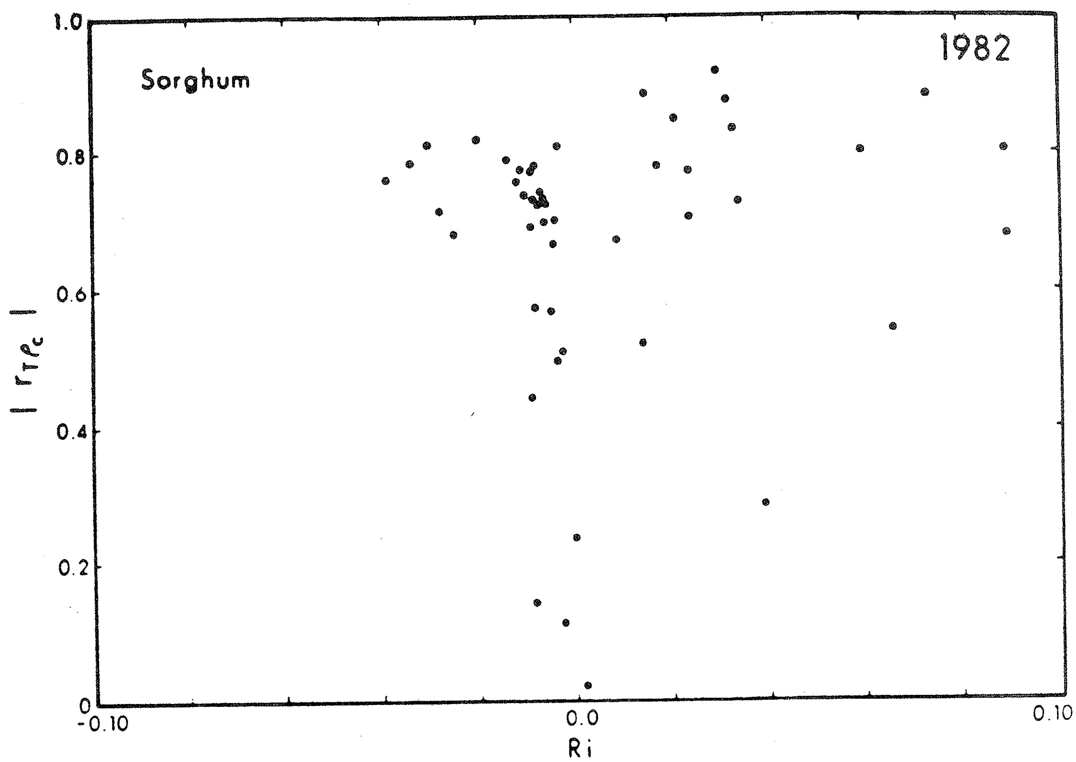

Fig. 4.38 Correlation coefficient between temperature and CO_2 fluctuations ($r_{T\rho_c}$) as a function of stability (Ri) over a sorghum canopy. Mead, Nebraska.

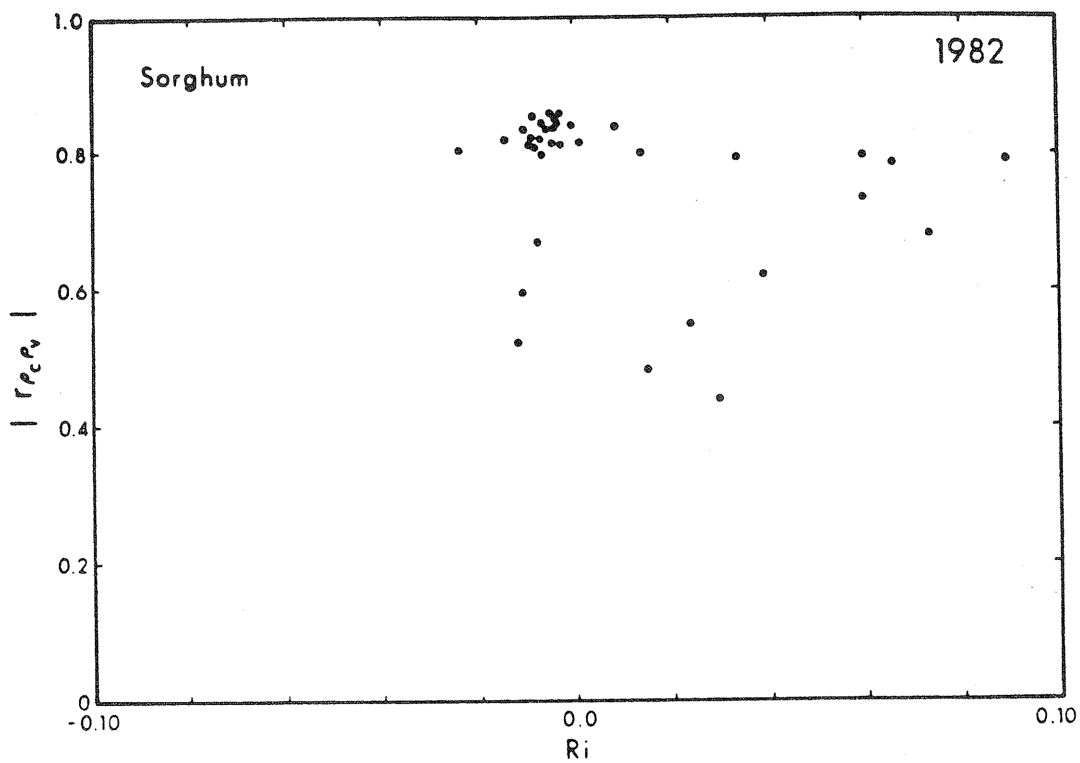

Fig. 4.39 Correlation coefficient between humidity and CO_2 fluctuations ($r_{\rho_v \rho_c}$) as a function of stability (Ri) over a sorghum canopy.

4.3. Spectral Analysis of Turbulence

Buoyancy and mean wind shear are responsible for turbulence in the atmospheric surface layer. It is convenient to consider turbulence as an ensemble of periodic entities or eddies. The relatively large scale eddies produced by buoyancy or wind shear effects are dynamically unstable. The eddies break up into succeedingly smaller eddies until they reach such a small size that they are dominated by viscous forces and at last are dissipated as heat. The energy contained or transported by various eddies may be analyzed by spectral analysis methods described in Chapter 2.

In Chapter 2, Eq. 2.43 was used to describe eddies in the inertial subrange. No significant amounts of energy are created or destroyed in this subrange; energy is merely transported by inertial forces and redistributed isotropically by pressure forces (Busch, 1973). The eddies exhibit isotropic characteristics and a universal, non-linear cascade. Spectral energy or density may be represented by Eq. 2.43 or, alternatively, in terms of frequency by the following equation:

$$S_i\ (n) = \alpha_i \varepsilon^{2/3} n^{-5/3} \tag{4.4a}$$

where n is natural frequency which is related to κ (wave number) and λ (wave length) by Taylor's hypothesis:

$$\kappa = \lambda^{-1} = n/\overline{U} \tag{4.4b}$$

α_i is the Kolmogorov constant, where $i = u, v$ or w. Equation 4.4a applies only to the inertial subrange. Higher frequencies, those in the dissipation range, are governed by molecular diffusion where S (n) falls at a rate faster than -5/3. Lower frequencies, those of the energy containing eddies are dominated by large scale effects.

By examining turbulence in the frequency domain, it is possible to evaluate the most significant scales of motion for the turbulent transport of CO_2, water vapor, heat and momentum, and to gain a better understanding of the transport mechanism involved. As noted by Busch (1973), an extension of Monin-Obukhov similarity theory suggests that properly scaled spectra of turbulent fluctuations should be functions of the stability parameter (z/L) and the non-dimensional frequency:

$$f = n \frac{(z - d)}{\overline{U}} \tag{4.5}$$

where n is the natural frequency, z is measurement height, d is the zero plane displacement and $\overline{U}$ is mean wind speed. McBean (1971) had pointed out that wavelength (λ) used in equation 4.4b can be considered to represent the scale of fluctuations. Using equations 4.4b and 4.5, a relationship between f and λ may be found such that:

$$f = {}^{z}/\,\lambda \tag{4.6}$$

This indicates that the non-dimensional frequency at a given height is inversely proportional to the scale of fluctuations.

In the discussion that follows, the results of spectral analysis of the u, v, w, T, ρ_v and ρ_c fluctuations and covariances (fluxes) of CO_2, water vapor, heat and momentum will be given. Turbulence spectra and cospectra are first analyzed for neutral thermal stability. This affords an opportunity to develop a basis of understanding of the character of turbulence as a function of frequency. Next, an examination of stability effects upon spectra is undertaken. The final sections of this analysis include an evaluation of the spectral correlation coefficient describing the efficiency of mass or energy transport in the frequency domain and the determination of the Kolmogorov constants for wind velocity, temperature, humidity, and CO_2 fluctuations.

4.3.1. Turbulence Spectra and Cospectra in Neutral Thermal Stability

Velocity Spectra

Logarithmic velocity spectra ($nS_u(n)$, $nS_v(n)$, $nS_w(n)$) measured over soybeans are plotted as a function of non-dimensional frequency (f) in Figures 4.40-4.42. These spectra have been normalized with their respective variances σ_u^2, σ_v^2, and σ_w^2. The majority of mechanical and thermal production of turbulence occurs at low frequencies, near the peak of the longitudinal velocity spectrum ($S_u(n)$). The peak frequency of the u spectrum in this study occur near f = 0.02. Near the inertial subrange a -2/3 slope* is found at about f = 0.1. This is in agreement with results obtained by Busch and Panofsky (1968), Sitaraman (1970) and Kaimal et al. (1972). It may be noted in Figure 4.40 that the collapse of u spectra into one curve by normalization with σ_u^2 does not always happen (runs 67B and 68A). Busch and Panofsky (1968) have made similar observations which they attribute to a breakdown of similarity theory due to large scale inhomogeneities.

The lateral velocity (v) spectra $S_v(n)$ under nearly neutral thermal stability in Figure 4.41 appear to be better behaved than do the u spectra although v spectra may also vary in a manner similar to the u component (Busch, 1973). The peak frequency of $S_v(n)$ appears to be about f = 0.05 and the inertial subrange appears to begin near f = 0.3. The

---

*The Kolmogorov -5/3 relationship becomes -2/3 when nS(n) is plotted instead of S(n).

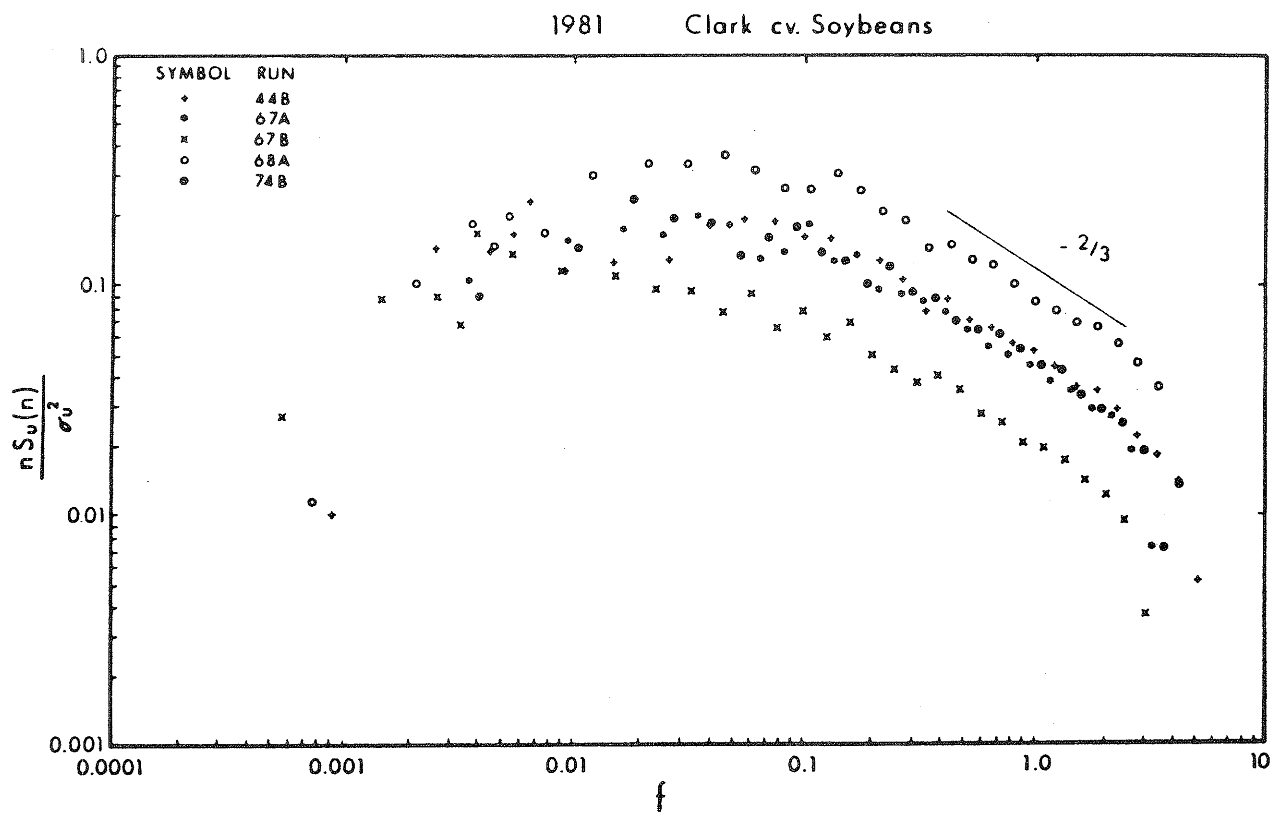

Fig. 4.40 Normalized logarithmic spectra for the U wind component as a function of non-dimensional frequency for neutral stability. Mead, Nebraska.

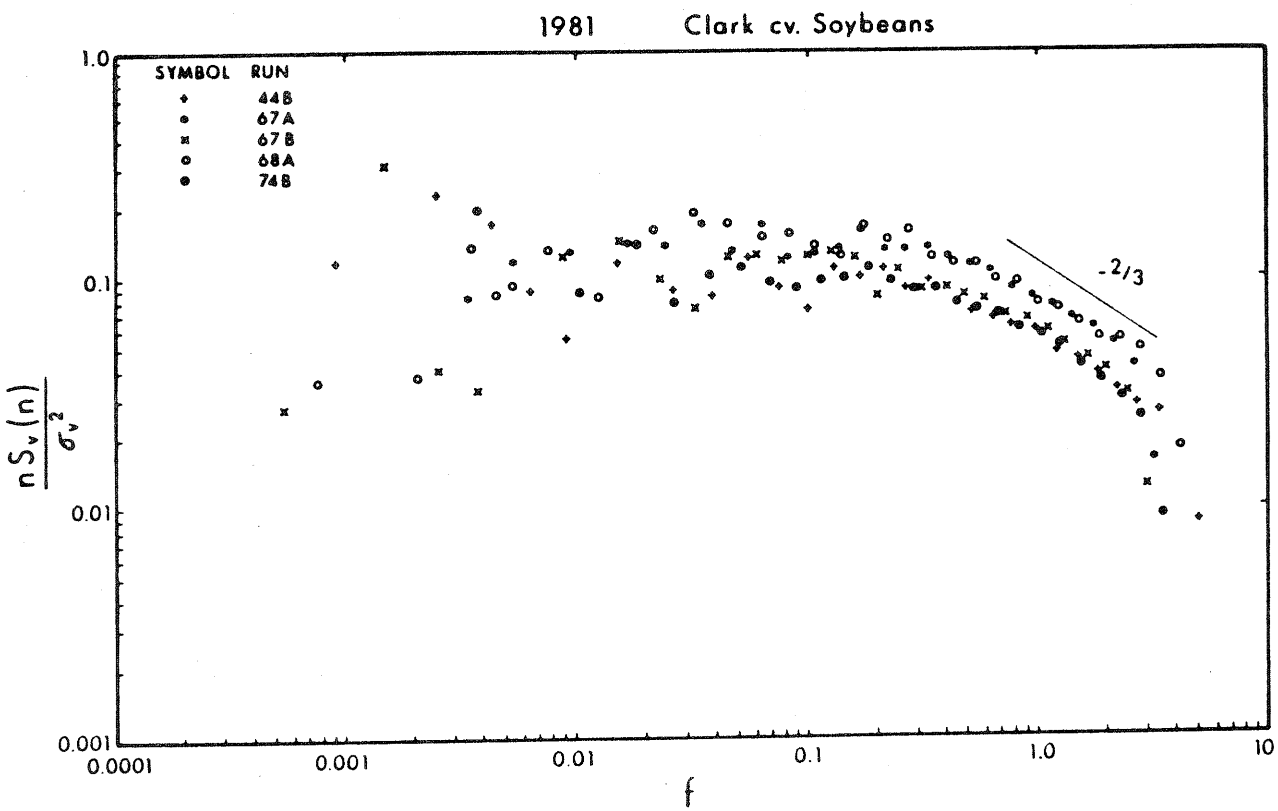

Fig. 4.41 Same as Fig. 4.40 except for V component.

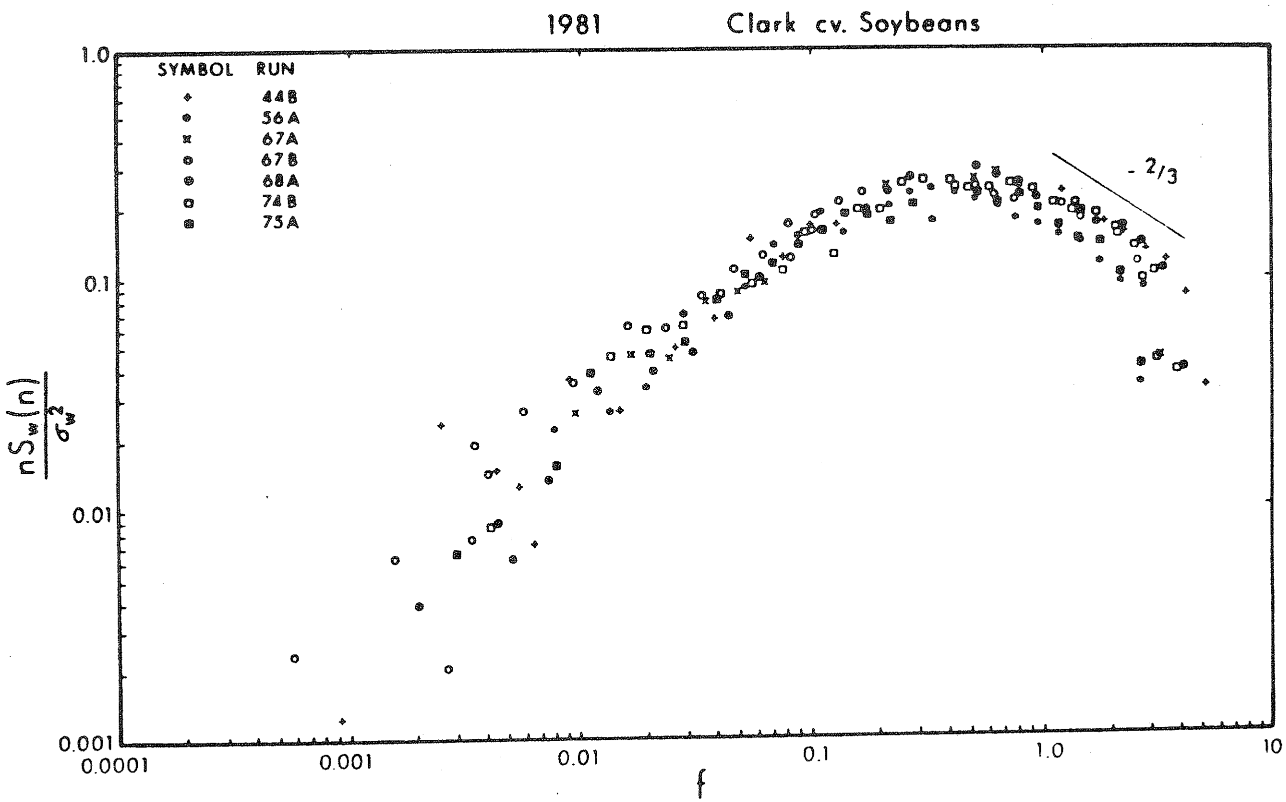

Fig. 4.42 Same as Fig. 4.40 except for W component.

peak frequency of the v spectra is higher than that of the u spectra, a result in agreement with Busch and Panofsky (1968). The relative differences between u and v in spectral peaks and shapes as well as those of others to be discussed later, are shown in Figure 4.46.

Spectra of the vertical velocity component (w) for near neutral thermal stability appear in Figure 4.42. The peak frequency is obviously much higher for the w spectra than that of the u or v components. The spectral peak occurs near f = 0.5 and the inertial subrange begins near f = 1.0. These results compare favorably with those obtained by Busch and Panofsky (1968) at Round Hill and with those of Kaimal et al. (1972) which indicate a spectral peak at f = 0.5 and an intertial subrange beginning at f = 1.0. The spectral shape of the w component measured under nearly neutral conditions in this study is similar to that reported by Kaimal et al. (1972) measured over wheat stubble. It does not indicate a peakiness as observed by Shaw et al. (1974) over corn and by Thompson (1979) over a forest. These latter surfaces are rougher and more effective exchange of energy over these surfaces may be responsible for the greater peakiness in the w spectra.

Spectra of Scalar Quantities

A set of equations similar to (4.4a) may be written for T, ρ_v, or ρ_c spectra as developed by Corrsin (1951):

$$S_\zeta(n) = \alpha_\zeta \varepsilon^{-1/3} N_\zeta n^{-5/3} \tag{4.7}$$

where ζ = T, ρ_v, or ρ_c and N_ζ is the dissipation rate of the variance ($\overline{T'^2}/2$, $\overline{\rho_v'^2}/2$, $\overline{\rho_c'^2}/2$).

Temperature Spectra

The spectral peak for temperature under slight thermally unstable conditions* occurs near f = 0.06 with the lower end of the inertial subrange beginning near f = 0.8 (Figure 4.43). These results are in close agreement with the measurements of Kaimal et al. (1972) over wheat stubble. Sitaraman (1970) indicates a peak between f = 0.2-0.6 and Motha's (1979) temperature spectra under slight thermal instability show a peak at f = 0.02 over alfalfa. Phelps and Pond's (1971) data indicate a peak at f = 0.5 over the ocean and f = 0.14 over land. McBean (1971) found a peak of f = 0.02-0.03 over the ocean under unstable and near neutral conditions.

Humidity Spectra

Humidity spectra for near neutral thermal stability are given in Figure 4.44. Their shape is similar to that for temperature. A spectral peak occurs at f = 0.05 with the low end of the inertial subrange near f = 0.4. Data from Ohtaki and Matsui (1982) taken over a paddy indicate a peak at n = 0.4 (natural frequency). Takeuchi et al. (1980) reports a peak frequency over wheat near f = 0.54.

CO_2 Spectra

CO_2 spectra shown in Figure 4.45 appear similar to those for temperature and humidity. The similarity between humidity and CO_2 spectra was also noted in Ohtaki and Matsui (1982) over a paddy field, the only other study known to the author in which simultaneous CO_2 and humidity

---

*To avoid excessive scatter, temperature spectra are plotted for slightly unstable conditions.

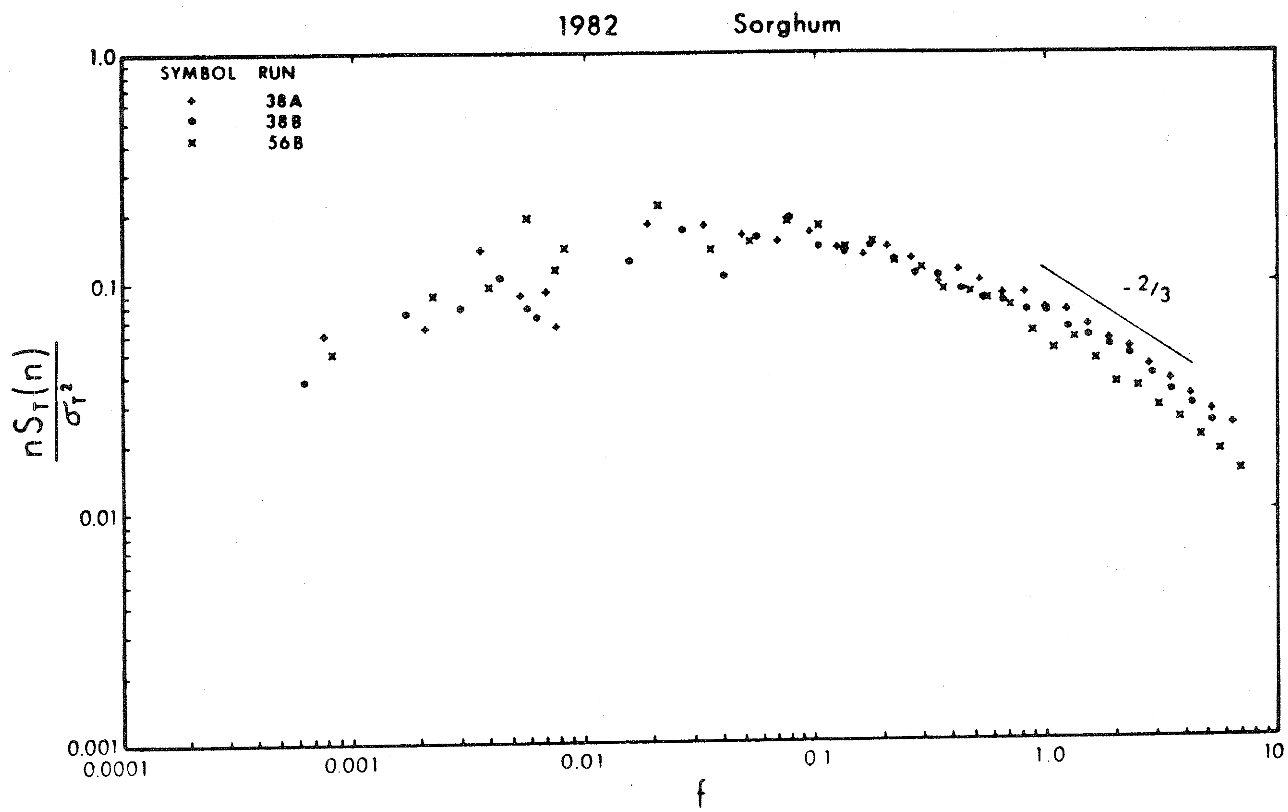

Fig. 4.43 Normalized logarithmic temperature spectra as a function of non-dimensional frequency for neutral stability. Mead, Nebraska.

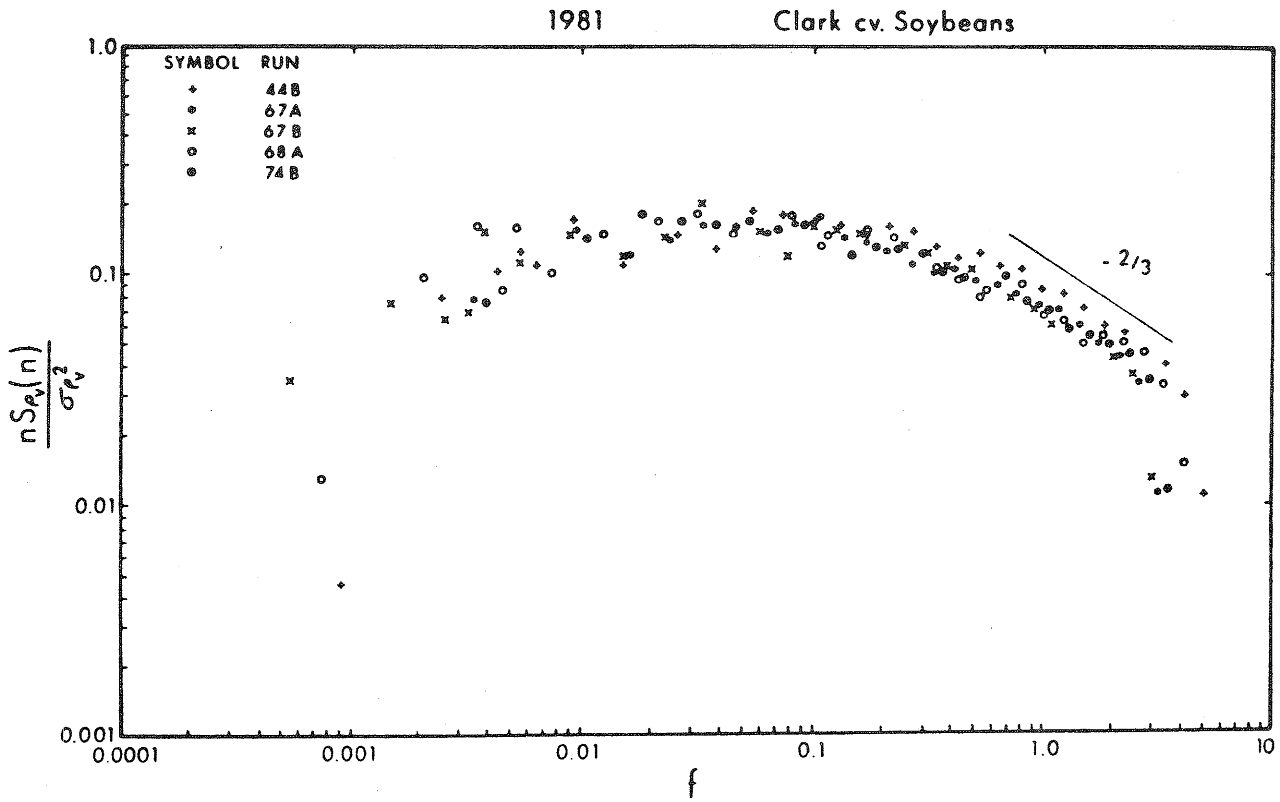

Fig. 4.44 Normalized logarithmic humidity spectra as a function of non-dimensional frequency for neutral stability. Mead, Nebraska.

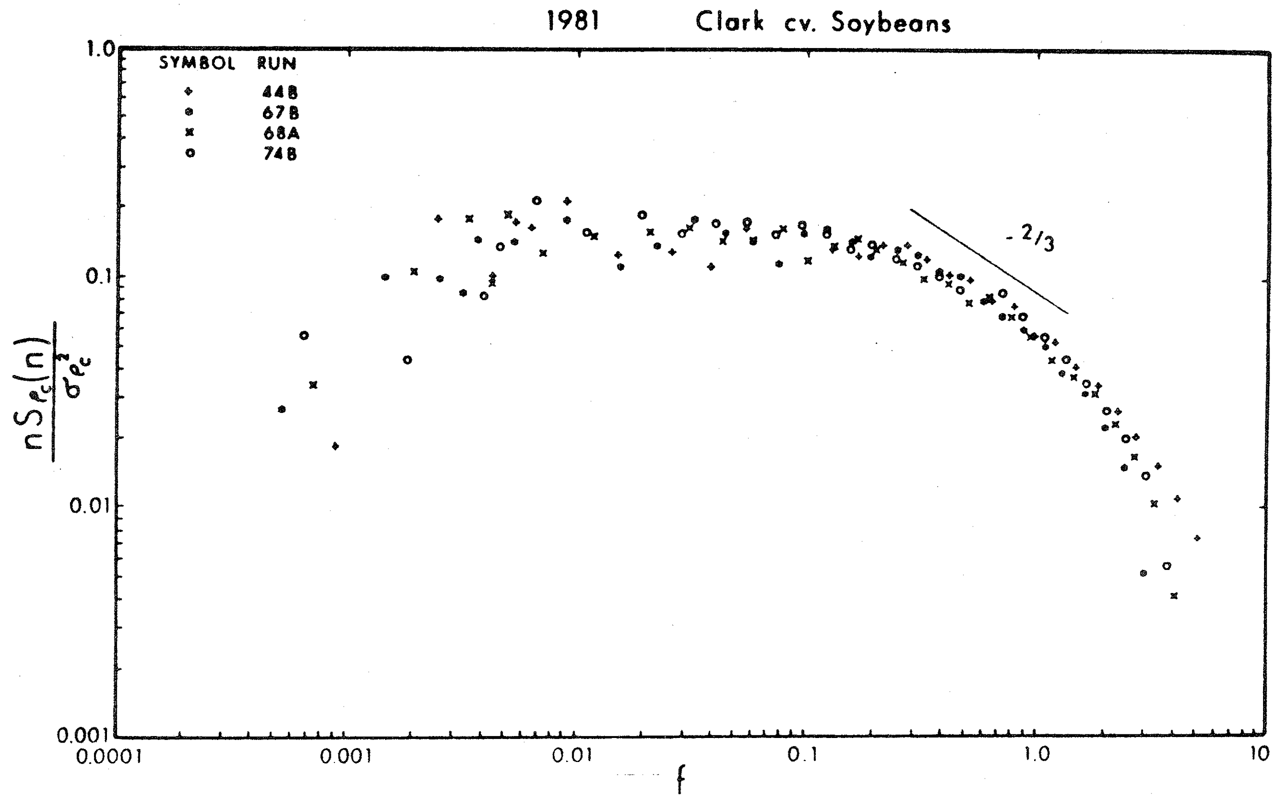

Fig. 4.45 Normalized logarithmic CO_2 spectra as a function of non-dimensional frequency for neutral stability. Mead, Nebraska.

measurements were made.

The spectral peak for CO_2 occurs near f = 0.03 although there appears to be some evidence of another peak near f = 0.009. The spectra follow a -2/3 slope from about f = 0.2 to f = 1.7. Ohtaki and Matsui (1982) and Ohtaki (1980) have similar results with peak frequencies near 0.05 HZ (natural frequency). Ohtaki (1980) found u component and CO_2 spectra to have similar shapes in contrast to w component spectra which are more peaked and shifted to higher frequencies. Data presented in Figure 4.46 agree with this finding.

The spectral shapes and peaks of T, ρ_v and ρ_c are very similar as is shown in Figure 4.46. These spectra are somewhat broader and flatter than those of the u and v components. Kaimal et al. (1972) noted similar characteristics in their T spectra. However, based upon the character of their spectra, Phelps and Pond (1971) conclude that, while humidity spectra had universal forms in the Monin-Obukhov framework, temperature spectra did not. Phelps and Pond found temperature and humidity spectra to be similar over land but different over the ocean. As Busch (1973) has noted one would expect moisture and temperature spectra to be very similar since both may be considered passive scalars. Indeed, governing equations of motion (equations 2.9 and 2.10) are similar, except for a radiative flux divergence term in the equation for thermal transport. Phelps and Pond consider this term responsible for the dissimilarity between temperature and humidity spectra on certain occasions. They add, however, that radiative flux divergence effects on temperature spectra had negligible influence on vertical velocity spectra.

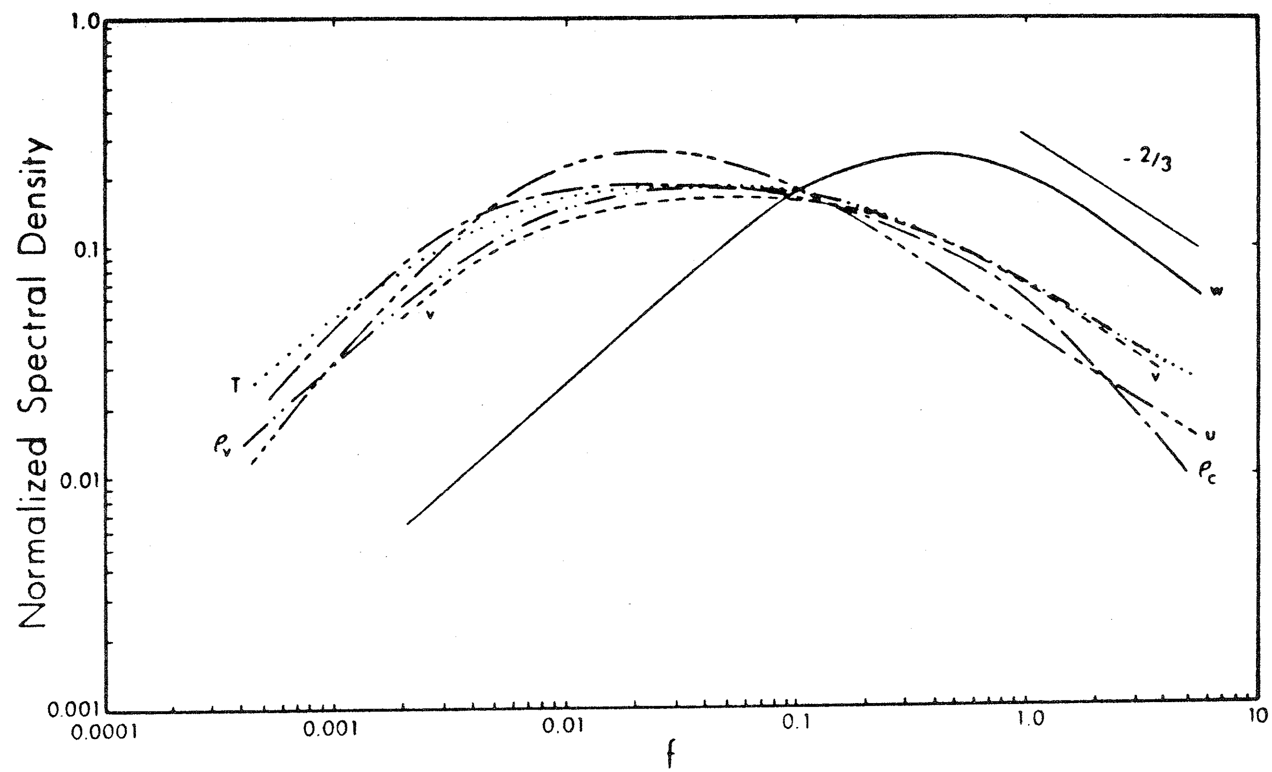

Fig. 4.46 Eye fit curves of normalized U, V, W, T, ρ_V and ρ_C spectra as a function of non-dimensional frequency for neutral stability. Mead, Nebraska.

Cospectra of Momentum, Sensible Heat, Water Vapor and CO_2

Cospectra are useful in describing the relative contributions of various frequencies to total covariances (or fluxes). In this section, the cospectra of uw, wT, $w\rho_v$ and $w\rho_c$ pairs are examined since they relate directly to the fluxes of momentum, heat, water vapor and CO_2. As compared with the -5/3 slope of spectra in the inertial subrange, cospectra typically exhibit a -7/3 slope (Wyngaard and Cote, 1972). However, the -7/3 relationship for cospectra is not as firmly established in theory as is the -5/3 law of spectra (Busch, 1973). Kaimal et al. (1972) indicate that the -7/3 relationship is not consistently found in cospectra data. Busch (1973) and Kaimal et al. (1972) mention that cospectra are generally more difficult to measure than are spectra for a number of reasons. These include weak correlations between variables and an increased sensitivity to errors associated with instrument levelling and alignment and spatial separation between sensors.

Cospectra of momentum (C_{wu}), heat (C_{wT}) water vapor ($C_{w\rho_v}$) and CO_2 ($C_{w\rho_c}$) are shown in Figures 4.47-4.50, respectively. Eyefit curves for all cospectra appear in Figure 4.51, for comparative purposes. The peak frequency in (C_{wu}) occurs near f = 0.08 while those for C_{wT}, $C_{w\rho_v}$ and $C_{w\rho_c}$ occur at a higher frequency, near f = 0.15. This result is consistent with the findings of Kaimal et al. (1972) for C_{wu} and C_{wT} cospectra over wheat stubble. The similarity of the shapes of C_{wu} and C_{wT} cospectra measured in this study agrees with observations over grass by Panofsky and Mares (1968).

While C_{wT}, $C_{w\rho_v}$, $C_{w\rho_c}$ have nearly the same spectral peaks they do differ somewhat in shape. C_{wT}, $C_{w\rho_v}$ and $C_{w\rho_c}$ are very similar in low

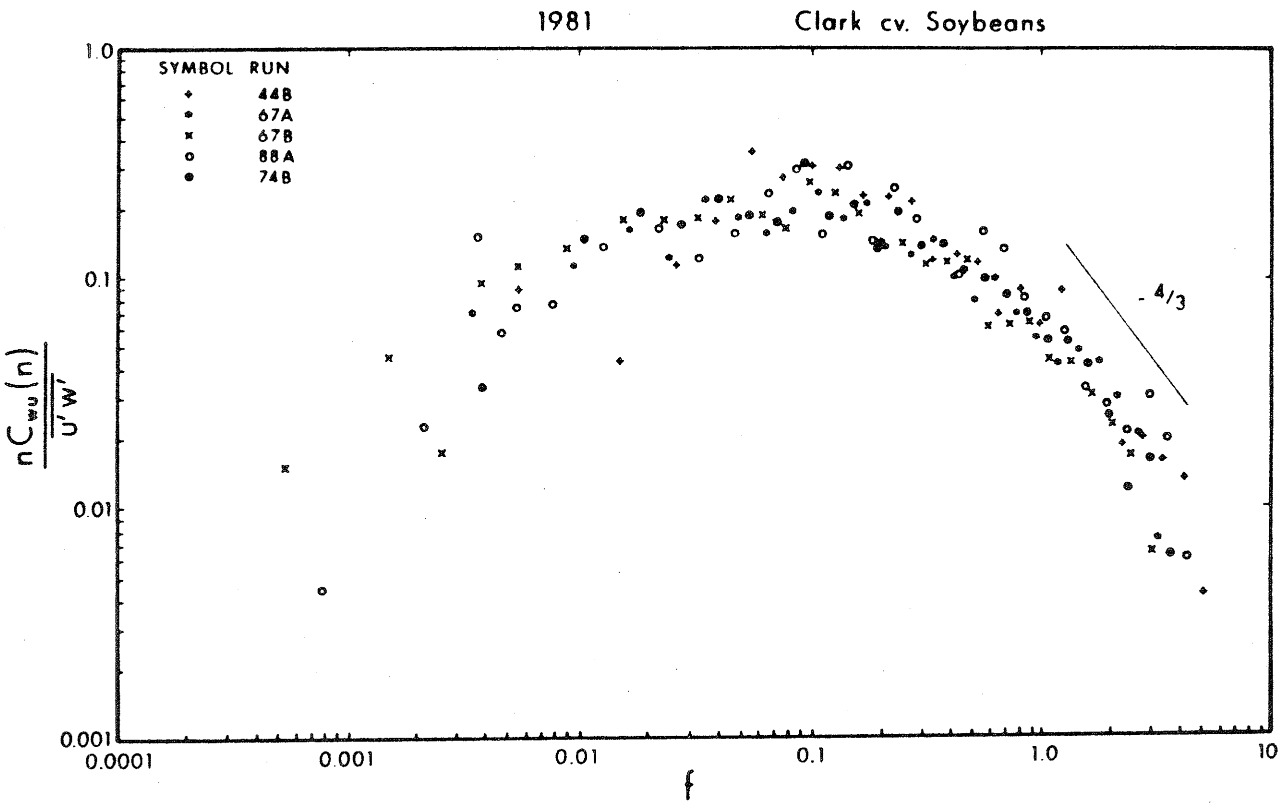

Fig. 4.47 Normalized logarithmic cospectra of momentum as a function of non-dimensional frequency for neutral stability. Mead, Nebraska. The -7/3 law for C(n) becomes -4/3 law when nC(n) is plotted on the ordinate.

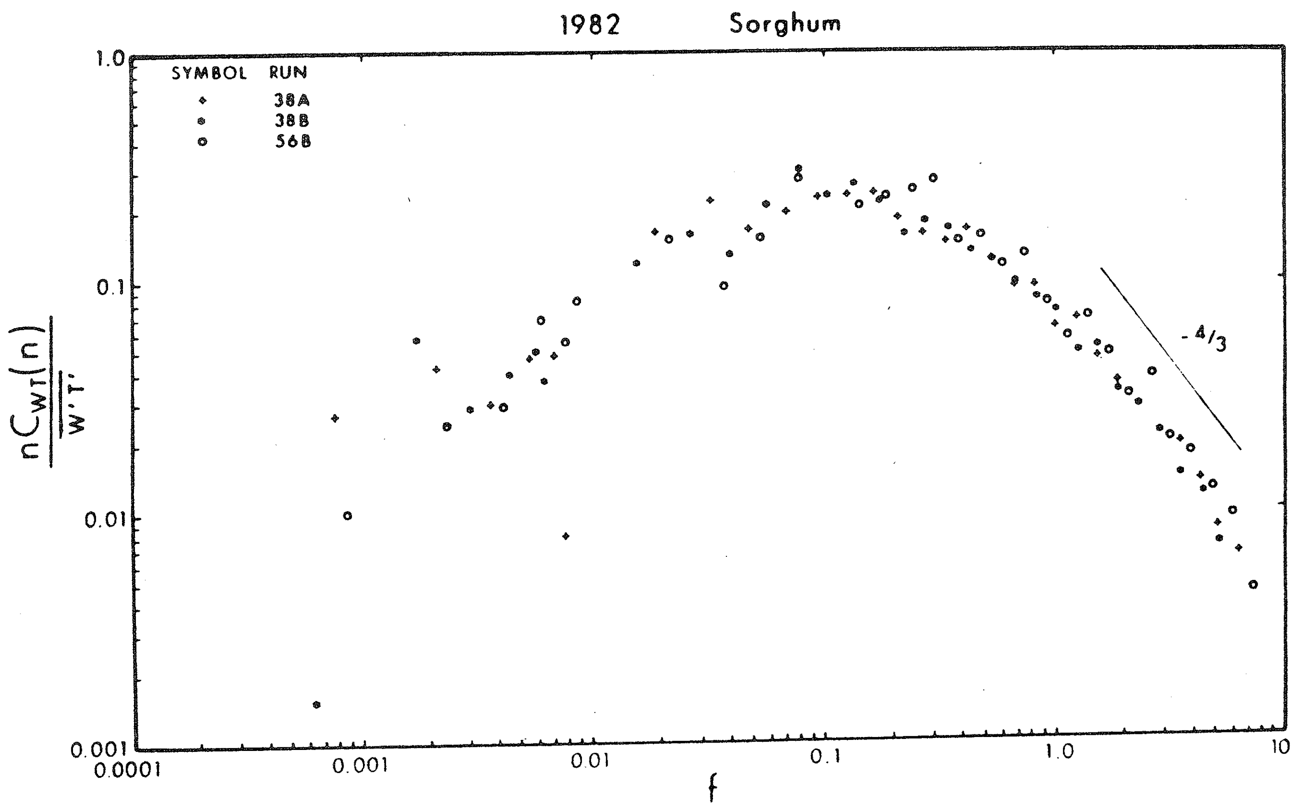

Fig. 4.48 Normalized logarithmic cospectra of heat as a function of non-dimensional frequency under slightly unstable stratification. Mead, Nebraska.

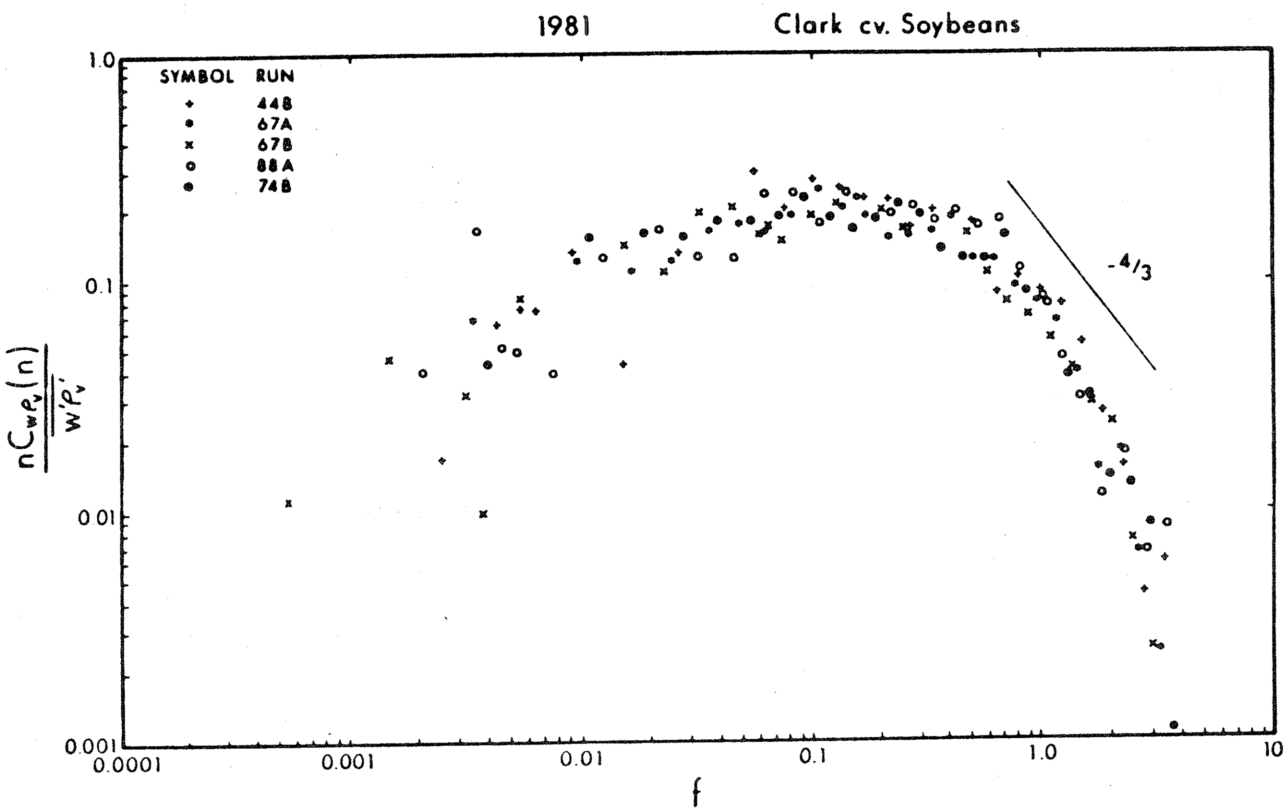

Fig. 4.49 Same as Fig. 4.48 except for water vapor cospectra.

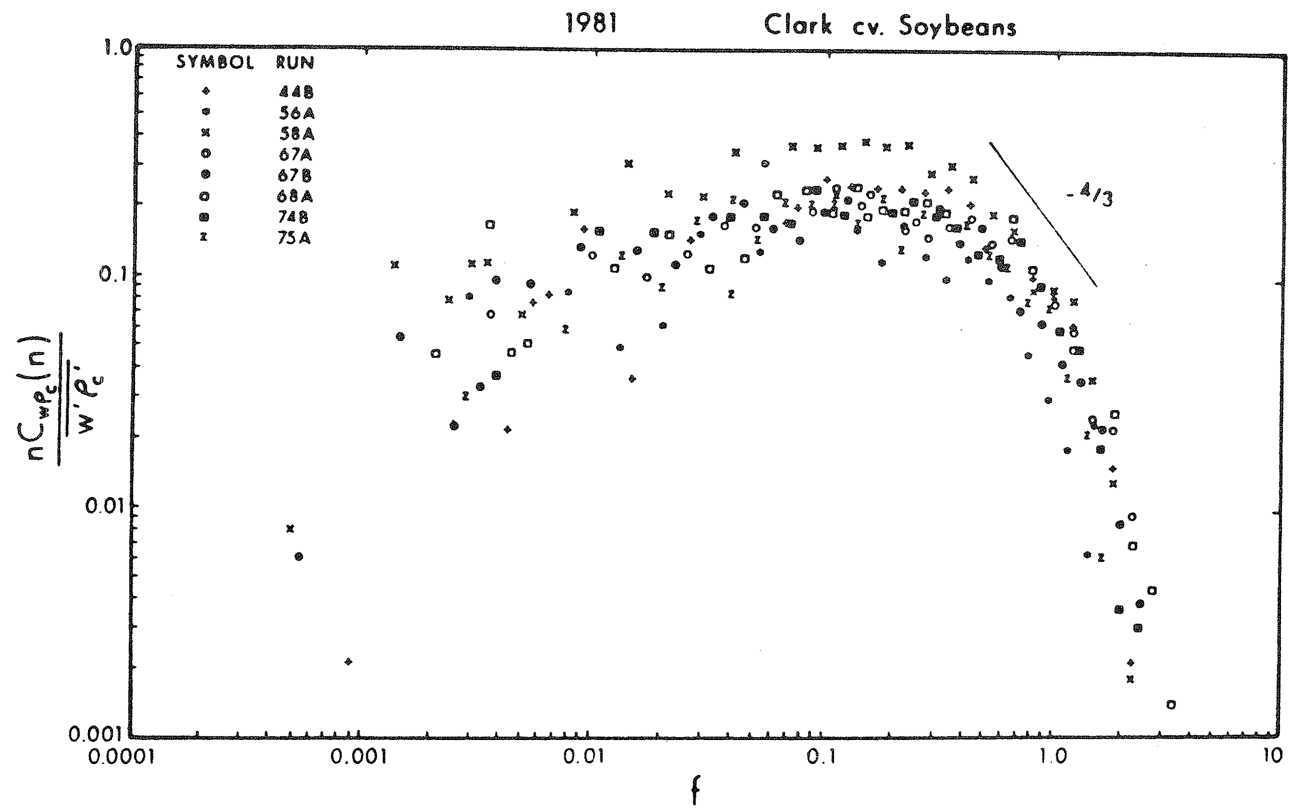

Fig. 4.50 Same as Fig. 4.48 except for CO_2 cospectra.

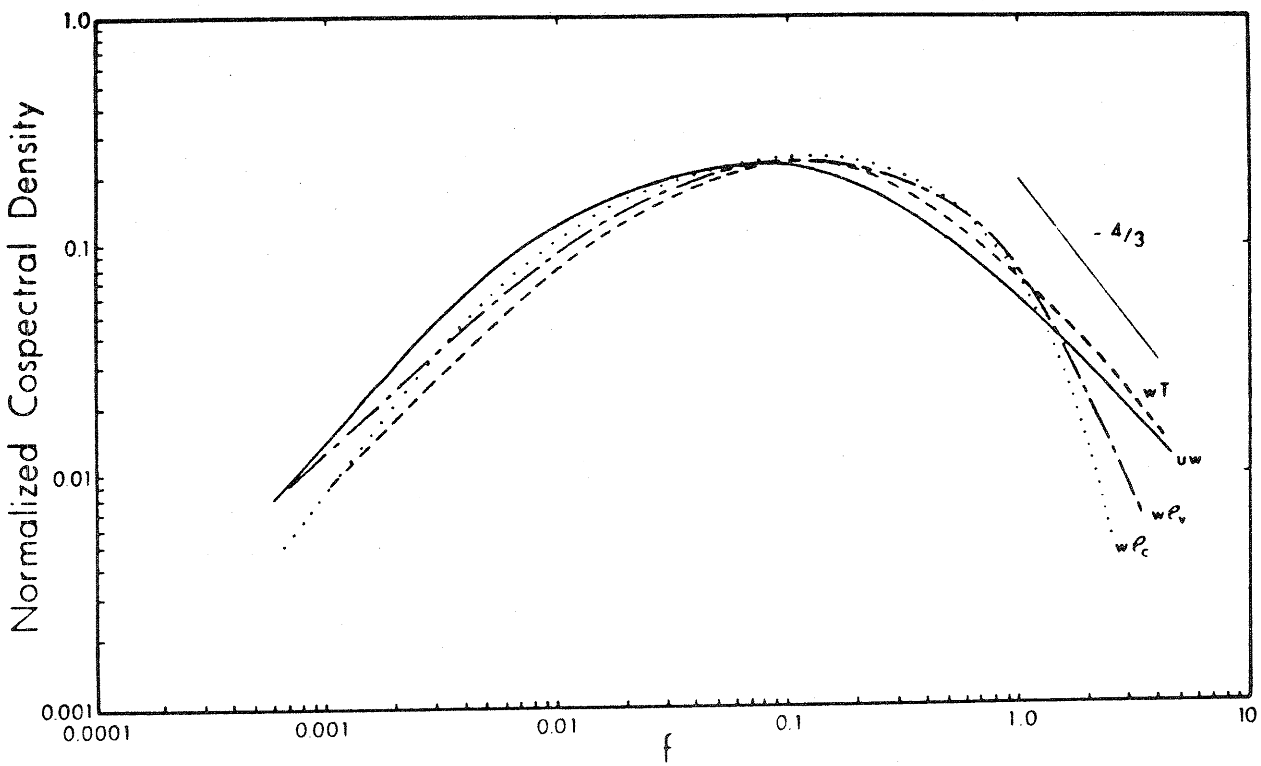

Fig. 4.51 Eye fit curves of normalized CO_2 ($w\rho_c$), water vapor ($w\rho_v$), heat (wT) and momentum (uw) cospectra as a function of non-dimensional frequency for neutral stability. Mead, Nebraska.

and middle frequencies. However, some differences are apparent near and within the inertial subrange. C_{wT} data aligns with the -4/3 slope (inertial subrange) from about f = 1.0 to the frequency limit of measurement. However, $C_{w\rho_v}$ and $C_{w\rho_c}$ become aligned with the -4/3 slope near f = 0.4. The $C_{w\rho_v}$ and $C_{w\rho_c}$ data finally separate from each other near f = 2 when $C_{w\rho_c}$ data fall off from the -4/3 slope at a rate faster than that of $C_{w\rho_v}$. Frequencies higher than f = 2 contribute relatively little to the total covariance (or flux). The similarity between $C_{w\rho_v}$ and $C_{w\rho_c}$ was also noted by Ohtaki and Matsui (1982). They report peaks at n = 0.02 Hz and an alignment with the inertial subrange (-4/3 slope) for frequencies ranging from 0.5 to 2.0 Hz. This peak is exactly that of run #44B shown in Figure 4.50 of this study, in which (z-d) = 1.74 and $\overline{U}$ = 2.33 m s^{-1}. The departure from the -4/3 slope seen in this study for $C_{w\rho_v}$ and $C_{w\rho_c}$ was also observed by Ohtaki and Matsui (1982). The departure may be a result of the spatial resolution of the instruments or spatial separation of w and ρ_c or ρ_v sensors.

4.3.2. Effects of Stability on Spectra

The effects of stability on the spectra of longitudinal velocity, vertical velocity, humidity and CO_2 fluctuations is examined in this section. Various stability classes were used and a cross reference to z/L values may be found in Table 4.2. In order to study the stability effects on spectra an approach used by Kaimal et al. (1972) was followed.

Table 4.2

Thermal Stability Classes Defined in Terms of z/L

Stability Class	z/L Range
A	0.006 to -0.011
B	-0.055 to -0.079
B_1	-0.079
D	-0.209
E	0.073 to 0.160
E_1	0.160
F	1.13

The equation

$$S_u(n) = \alpha_u \, \varepsilon^{2/3} n^{-5/3} \tag{4.8}$$

is normalized as follows:

$$\frac{nSu(n)}{u_*^2} = \alpha_u \, (2\,\pi\,\kappa\,f)^{-2/3} \, \phi_\varepsilon^{-2/3} \tag{4.9}$$

where
$$\phi_\varepsilon = \frac{\varepsilon k\,(z-d)}{u_*^3} \quad ,$$

k is von Karman's constant, and ε is the dissipation rate of $\overline{u'^2}/2$.
The non-dimensional spectral density $\left(\frac{nSu(n)}{u_*^2\phi_\varepsilon^{2/3}}\right)$ found from this equation may be considered to be a function of f. Equations for normalized temperature, humidity, and CO_2 spectra, developed in a similar manner are:

$$\frac{nS_T(n)}{T_*^2} = \alpha_T \, (2\,\pi\,\kappa\,f)^{-2/3} \, \phi_{N_T}\phi_\varepsilon^{-1/3} \tag{4.10}$$

$$\frac{nS\rho_v(n)}{\rho_{v*}^2} = \alpha_{\rho_v} \, (2\,\pi\,\kappa\,f)^{-2/3} \, \phi_{N\rho_v}\phi_\varepsilon^{-1/3} \tag{4.11}$$

$$\frac{nS\rho_c(n)}{\rho_{c*}^2} = \alpha_{\rho_c} \, (2\,\pi\,\kappa\,f)^{-2/3} \, \phi_{N\rho_c}\phi_\varepsilon^{-1/3} \tag{4.12}$$

where ϕ_{N_T}, $\phi_{N\rho_v}$ and $\phi_{N\rho_c}$ are non-dimensional quantities given by:

$$\phi_{N_T} = \frac{N_T\kappa\,(z-d)}{u_*T_*^2} \tag{4.13}$$

$$\phi_{N\rho_v} = \frac{N_T\kappa\,(z-d)}{u_*\,\rho_{v*}^2} \tag{4.14}$$

$$\phi_{N\rho_c} = \frac{N_{\rho_c} \kappa (z-d)}{U_* \rho_{c*}^{2}} \tag{4.15}$$

N_T, N_{ρ_v} and N_{ρ_c} are the dissipation rates of temperature, humidity and CO_2 variances, respectively. Non-dimensional wind velocity, temperature, humidity and CO_2 spectra when plotted as functions of f, collapse in the inertial subrange, regardless of thermal stability.

Non-dimensional u spectra as a function of f are shown in Figure 4.52. Note that as stability increases from neutral (Class A, $z/L \simeq 0$ used here as a reference) spectral energy decreases, the shapes of the curves become more peaked and spectral peaks shift toward higher frequencies. A spectral peak near f = 0.03 is found for near neutral stability (class A, $z/L \simeq 0$) and a peak near f = 0.09 occurs in stable stratification (Class F, $z/L \simeq 1.1$). The tendencies described above are in general agreement with those found by Kaimal et al. (1972) although in the latter case, they found spectral peaks near f = 0.06 for z/L = 0 and f = 0.3 for z/L = 1.0. As thermal stability decreases from neutral, spectral peaks shift to lower frequencies and the spectral curves broaden. A similar finding was reported by Kaimal et al. (1972).

w spectra do not exhibit as wide a range in peak frequencies as do u spectra (Figure 4.53). This was also observed by Kaimal et al. (1972). The spectral peak for class B (z/L = -0.055 to -0.079, slightly unstable thermal stability) occurs near f = 0.5 while that of stable stratification (class E_1, z/L = 0.16) occurs near f = 0.9.

In a similar way to the normalized u and w spectra, ρ_v and ρ_c spectra experience consistent changes into higher peak frequency as stability increases from neutral conditions (Figure 4.54 and 4.55). Peak frequencies increase from f = 0.05 for ρ_v and f = 0.06 for ρ_c spectra for Class A

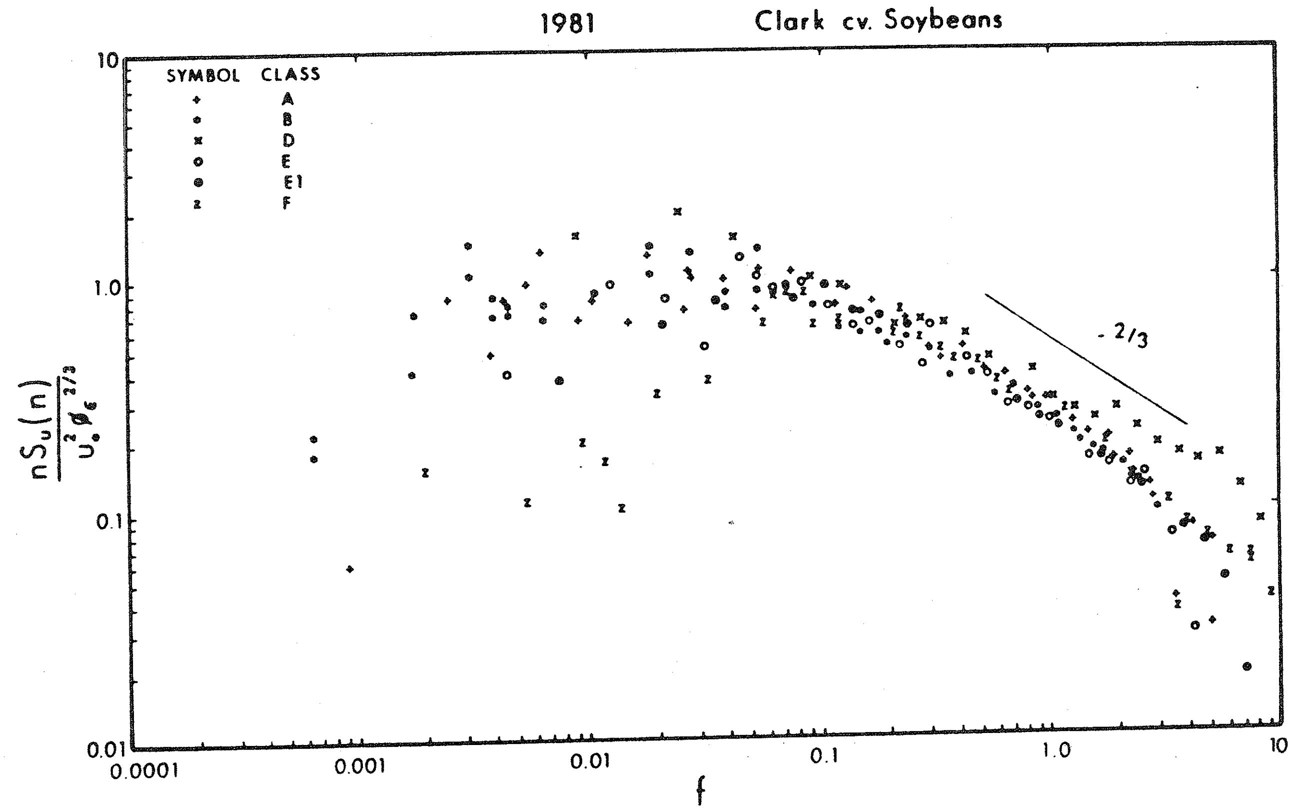

Fig. 4.52 Non-dimensional logarithmic U wind component spectra as a function of non-dimensional frequency for various stabilities. Mead, Nebraska.

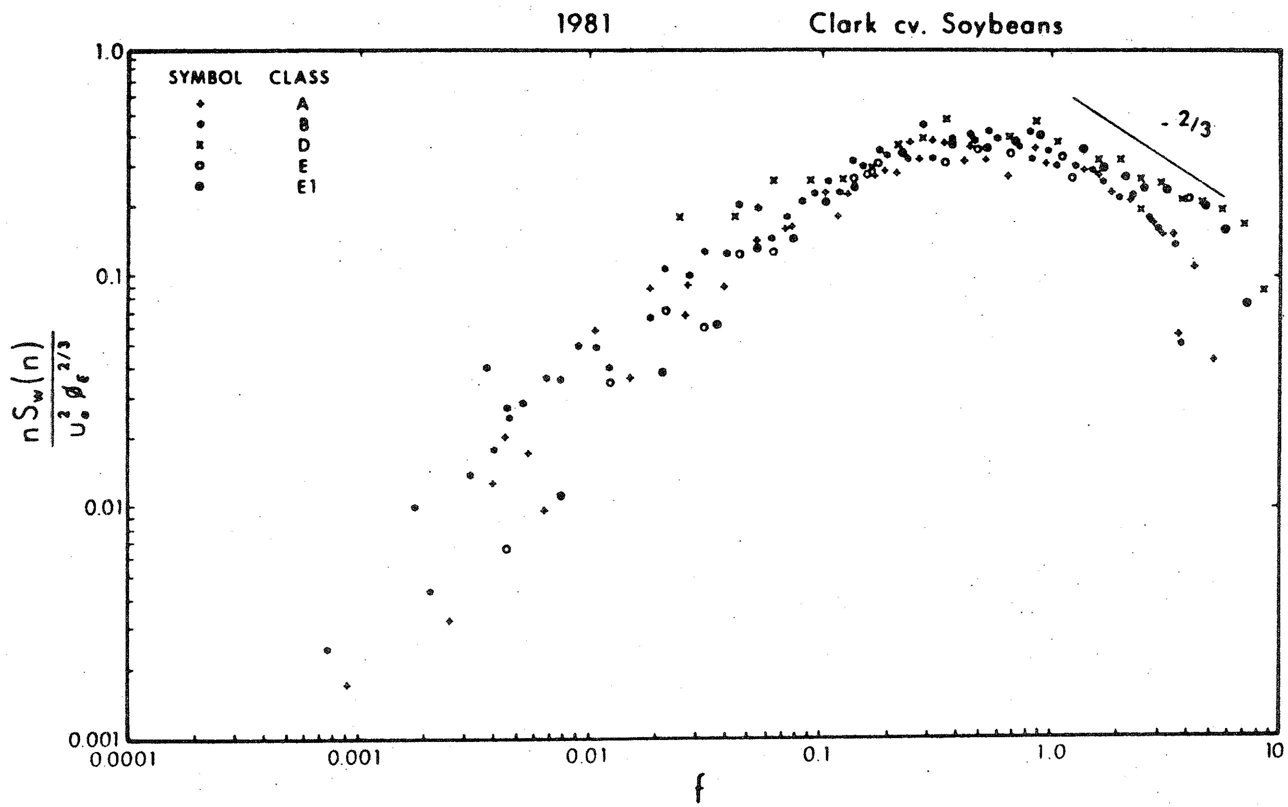

Fig. 4.53 Same as Fig. 4.52 except for W component spectra.

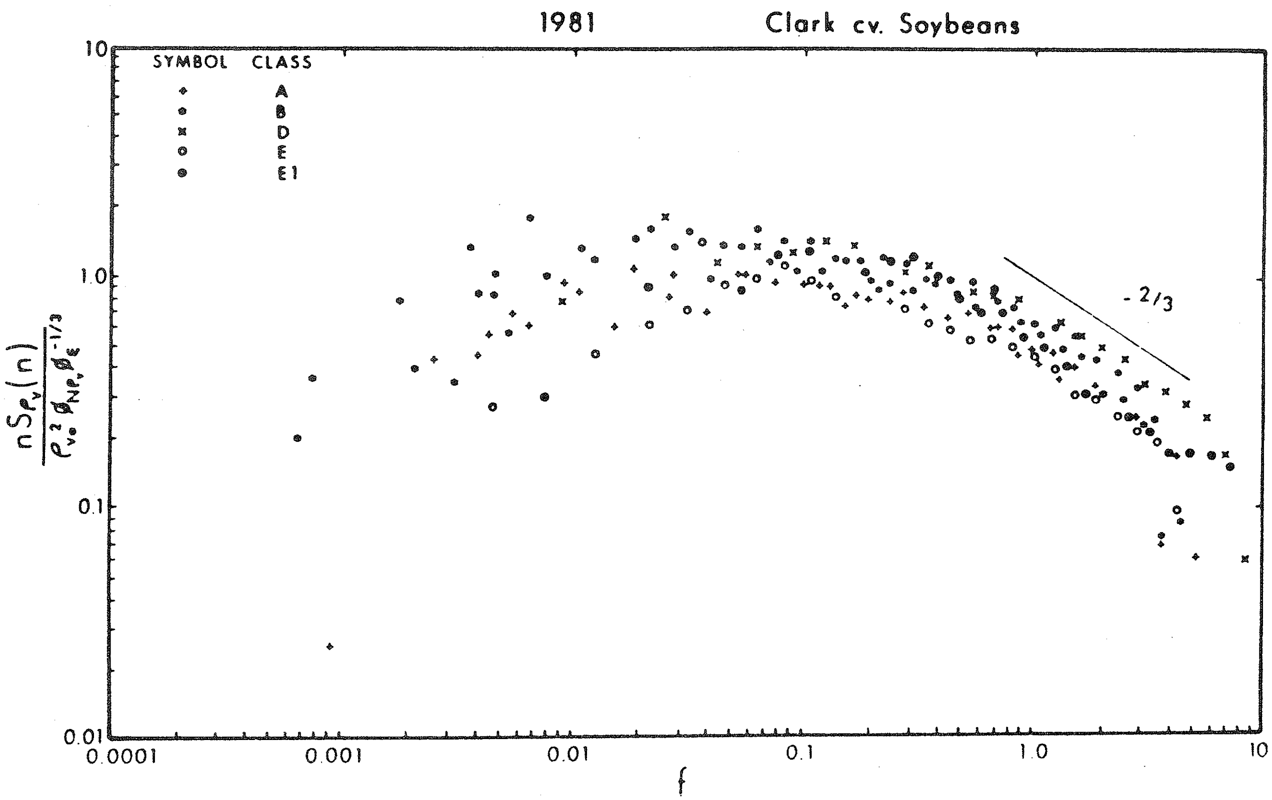

Fig. 4.54 Same as Fig. 4.52 except for humidity spectra.

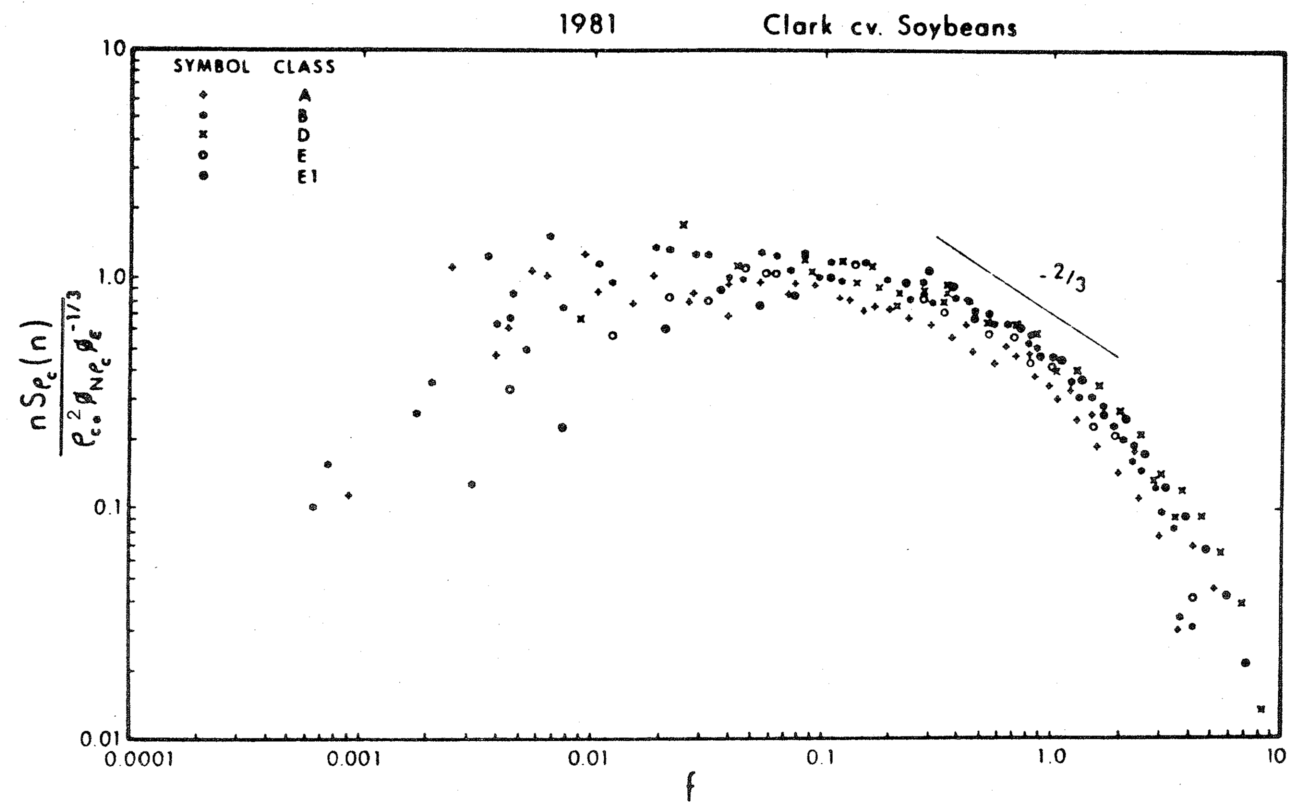

Fig. 4.55 Same as Fig. 4.52 except for CO_2 spectra.

($z/L \simeq 0$) to near $f = 0.15$ for both spectra in Class E_1 (stability) ($z/L \simeq 0.16$). Again in a manner similar to u and w, spectra of ρ_v and ρ_c become more peaked with increasing stability. As thermal stability decreases from neutral, spectra become flatter. The spectral peaks for both ρ_v and ρ_c shift toward lower frequencies. Due to the greater scatter in data at low frequencies it is difficult to exactly determine the location of spectral peaks. For Class B stratification ($z/L = -0.055$ to -0.079) peaks for both ρ_v and ρ_c appear in the neighborhood of $f = 0.02$.

4.3.3. Spectral Correlation Coefficients

The spectral correlation coefficient is defined as:

$$R_{xy}(f) = \frac{C_{xy}(f)}{[S_x(f)\; S_y(f)]^{1/2}} \qquad (4.16)$$

where C and S are cospectral and spectral densities, respectively, of variable x and y at non-dimensional frequency, f. If x is replaced by the vertical wind component (w), then $R_{wy}(f)$ can be thought of as the efficiency of vertical transfer of the appropriate entity y at frequency f (McBean, 1972). Values of R_{wy} (f) near unity imply excellent transfer efficiency while values near zero are associated with poor transfer efficiency.

Spectral correlation coefficients* for momentum transfer (R_{wu}) are shown in Figure 4.56. Above $f = 0.05$ an overall trend is apparent which indicates that correlation coefficient R_{wu} decreases in magnitude and variability as the non-dimensional frequency (f) increases. Similar

*Negative values indicate downward transfer. Note that $-R_{wu}$ is plotted since momentum transfer is normally downward.

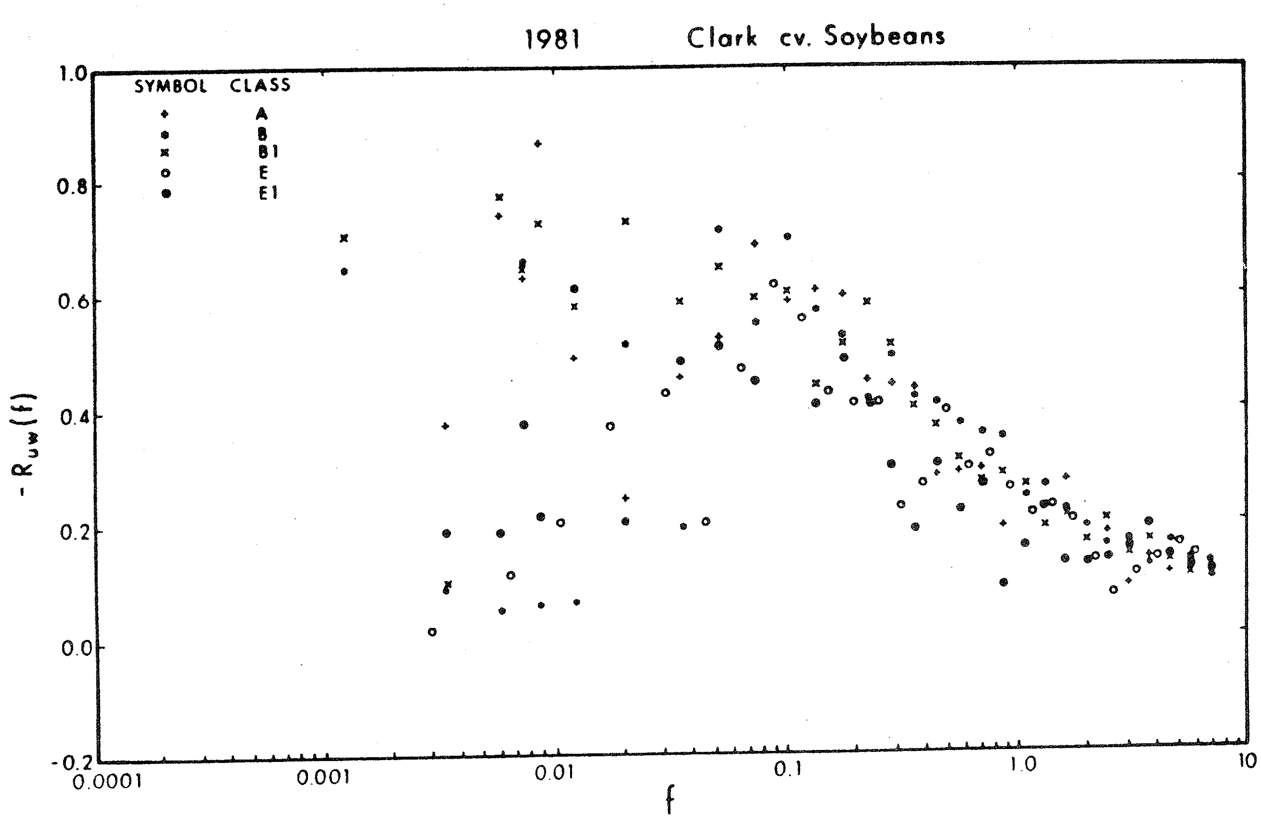

Fig. 4.56 Spectral correlation coefficient for momentum transfer as a function of non-dimensional frequency for various stability classes. Mead, Nebraska.

findings are reported in McBean and Miyake (1972). There appear to be peaks in R_{wu} near f = 0.006 and f = 0.05 indicating maxima in transfer efficiency at these frequencies. McBean and Miyake (1972) found a peak near f = 0.02 in their data. Examining R_{wu} by thermal stability classification, the correlation appears to decrease in magnitude at all frequencies as stability increases from neutral or unstable stratification to more stable stratification. Results reported in McBean (1970) and McBean and Miyake (1972) show similar tendencies of R_{uw} with thermal stability.

Spectral correlation values for water vapor transfer ($R_{w\rho_v}$) are given in Figure 4.57 as a function of f for various stability classes. The same general tendencies of decreasing magnitude of the correlation with increasing f are seen in Figure 4.57 for frequencies above f = 0.05. Similar to the findings for R_{wu}, values of $R_{w\rho_v}$ obtained under thermally stable conditions are lower than those obtained in neutral or unstable stratification. A greater number of high correlation coefficients are seen in the $R_{w\rho_v}$ data as compared with R_{wu} in the low frequency range, indicating that water vapor is transferred more efficiently than momentum by large eddies. Similar to R_{wu}, $R_{w\rho_v}$ has peak frequencies near f = 0.006 and near f = 0.04. In contrast, distinct valleys occur near f = 0.02 and f = 0.2 Data of Phelps and Pond (1971) also have a valley near f = 0.2.

The spectral correlation coefficient for CO_2 transfer ($R_{w\rho_c}$) is presented in Figure 4.58. Note that values plotted are in terms of ($-R_{w\rho_c}$) since CO_2 flux is downward during daylight hours when most of the

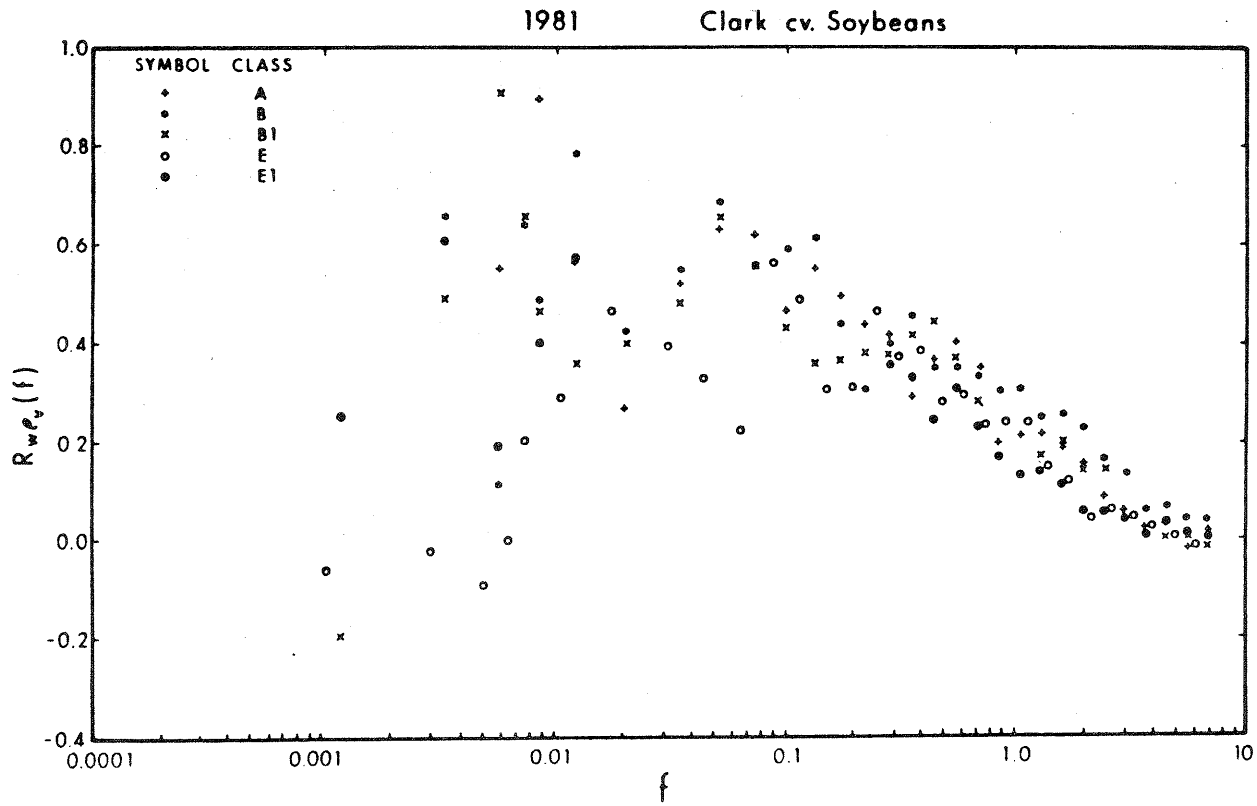

Fig. 4.57 Same as Fig. 4.56 except for water vapor transfer.

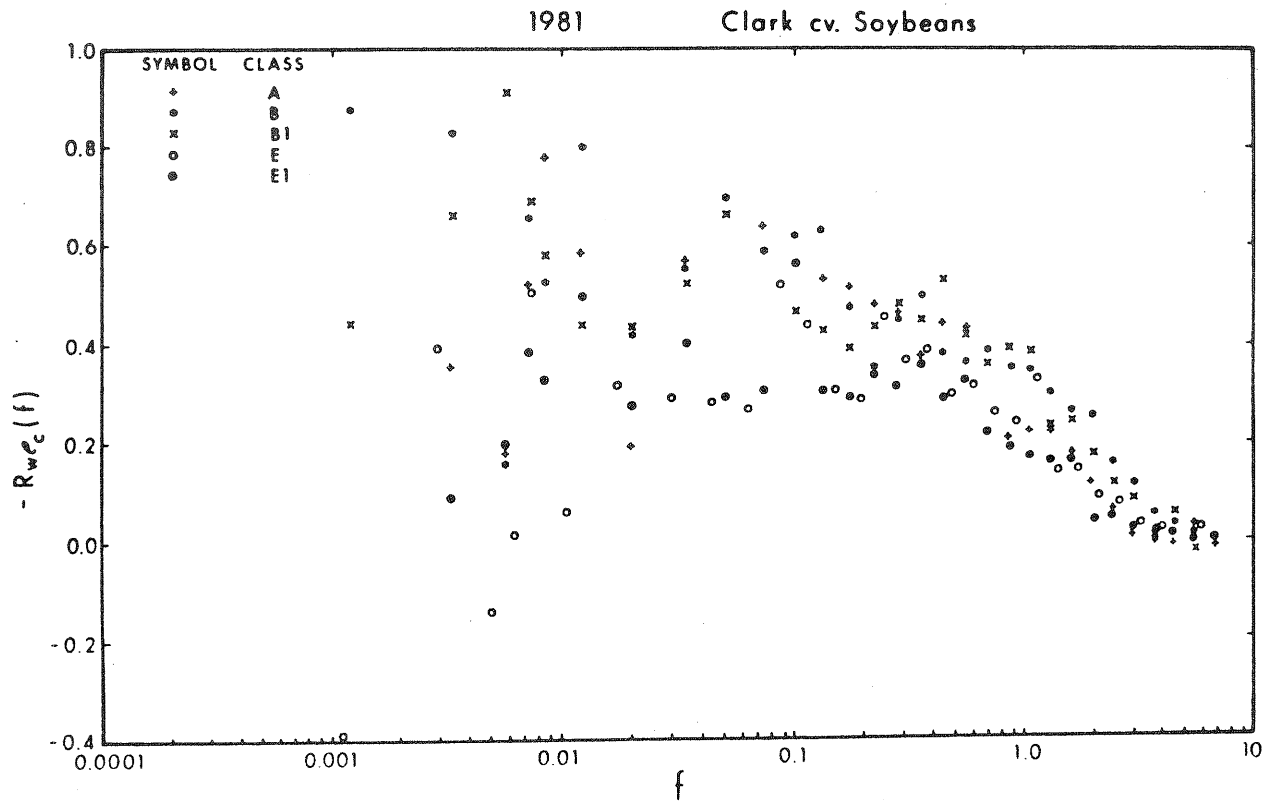

Fig. 4.58 Same as Fig. 4.56 except for CO_2 transfer. Data for classes E and E_1 are from nocturnal conditions and are multiplied by (-1).

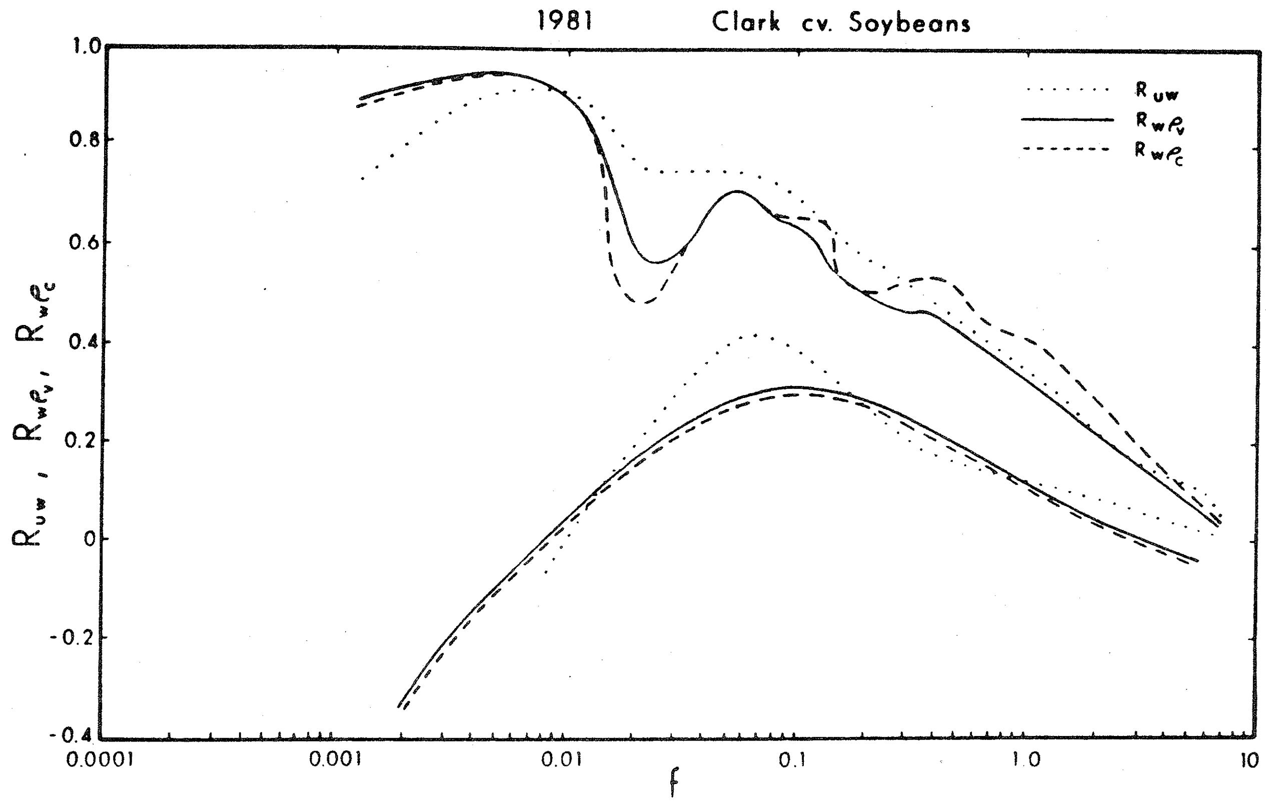

Fig. 4.59 Envelopes (ranges) of momentum (R_{uw}), water vapor ($R_{w\rho_v}$) and CO_2 ($R_{w\rho_c}$) spectral correlation coefficients as a function of non-dimensional frequency. Mead, Nebraska.

measurements were made.* The overall trends in R_{wu} and $R_{w\rho_v}$ discussed above are apparent in $R_{w\rho_c}$ data. $R_{w\rho_c}$ decreases in magnitude with increasing frequency above f = 0.05. Similar to the $R_{w\rho_v}$ data, $R_{w\rho_c}$ decreases in magnitude with increasing stability over all values of f. The peak frequencies and valleys found in $R_{w\rho_v}$ data are also found in $R_{w\rho_c}$ data and occur at very nearly the same frequencies. No data on $R_{w\rho_c}$ is available in the literature to allow comparison with results obtained in this study.

The envelopes (ranges) of R_{wu}, $R_{w\rho_v}$, and $R_{w\rho_c}$ data points over the frequency domain are given schematically in Figure 4.59 in order to facilitate comparisons. Except for a somewhat more distinct valley near f = 0.02 in the $R_{w\rho_c}$ data, there is a strong similarity between $R_{w\rho_v}$ and $R_{w\rho_c}$ indicating a corresonding similarity in the transfer mechanisms for water vapor and CO_2.

4.3.4. Kolmogorov Constants

The behavior of velocity, temperature, humidity, and CO_2 spectra in the inertial subrange has been presented earlier with the help of equation (4.4). The Kolmogorov constants were used to relate the non-dimensional spectral densities, dissipation rates and frequencies. In recent years, there has been considerable interest in the Kolmogorov constants for wind velocity, temperature, and humidity fluctuations (Hicks and Dyer, 1972; Dyer and Hicks, 1982). However the Kolmogorov constant for CO_2 has not been studied, except in one recent study over a paddy field (Ohtaki, 1982).

---

*Nocturnal CO_2 fluxes and the corresponding values of $R_{w\rho_c}$ are positive; these values, as noted in the caption of Figure 4.58 are multiplied by (-1).

Hicks and Dyer (1972) described the utility of the Kolmogorov constant in the determination of turbulent fluxes by a spectral density technique over the ocean. Flux measurements made from floating platforms on the ocean must be corrected for three dimensional motions. This would require careful monitoring of the platform's motion. A means by which the turbulence instrumentation may be used to measure fluxes in this type of situation was outlined in Hicks and Dyer (1972) and in Dyer and Hicks (1982). Using their method instrumentation along with a narrow band pass electronic filter may be employed to measure fluxes. The band pass filter may be used to eliminate frequency contributions from the supporting structure or platform. In the case of an ocean surface, it would be important to filter out the contributions of surface waves. The flux computation described by Hicks and Dyer requires knowledge of the Kolmogorov constant (α) of the fluctuating parameter with the appropriate spectral density value. The inertial subrange equations of spectral density for velocity, temperature, humidity and CO_2 fluctuations in non-dimensional form are given in Equations (4.9) - (4.12).

By assuming incompressible, stationary, horizontally homogeneous conditions and neglecting flux divergence terms, the turbulent kinetic energy budget may be written in non-dimensional form as:

$$\phi_\varepsilon = \phi_m - z/L \qquad (4.17)$$

and similarly for temperature, humidity and CO_2 variance budgets:

$$\phi_{N_T} = \phi_H \qquad (4.18)$$

$$\phi_{N\rho_v} = \phi_{\rho_v} \qquad (4.19)$$

$$\phi_{N\rho_c} = \phi_{\rho_c} \qquad (4.20)$$

where terms on the left represent dissipation and those on the right represent production. The terms on the right are well known non-dimensional gradients, given by:

$$\phi_m = \left(\frac{kz}{u_*}\right) \frac{\partial \overline{U}}{\partial z} \tag{4.21}$$

$$\phi_H = \left(-\frac{kz}{T_*} \frac{\partial \overline{T}}{\partial z}\right) \tag{4.22}$$

$$\phi_{\rho_v} = \left(-\frac{kz}{\rho_{v*}}\right) \frac{\partial \overline{\rho}_v}{\partial z} \tag{4.23}$$

$$\phi_{\rho_c} = \left(-\frac{kz}{\rho_{c*}}\right) \frac{\partial \overline{\rho}_c}{\partial z} \tag{4.24}$$

Dyer and Hicks (1970) have determined the following empirical relationships for ϕ_m and ϕ_H in unstable thermal stability:

$$\phi_m = (1 - 16\ z/L)^{-0.25} \tag{4.25}$$

$$\phi_H = \phi_{\rho_v} = (1 - 16\ z/L)^{-0.50} \tag{4.26}$$

For the purpose of determing the Kolmogorov constant in this study it was assumed that $\phi_{\rho_c} = \phi_{\rho_v} = \phi_H$.

It is now possible to solve for the Kolmogorov constants using the relationships presented thus far. By using equation (4.25) in (4.17) a value of ϕ_ε is found for a given value of z/L. This value of ϕ_ε may be used in equation (4.9) with spectral values of Su(n), natural frequency (n), mean wind speed ($\overline{U}$) at the height of measurement (z), and zero plane displacement (d) to solve for α_u. Similar procedures are involved in the calculation of α_T, α_{ρ_v}, α_{ρ_c} where, instead, equations 4.26 and 4.25 are used in 4.18-4.20 to find Kolmogorov constants from equations 4.10-4.12.

The computational procedure of the Kolmogorov constants involved the use of three values of nS(n) in the inertial subrange around a normalized frequency of f= 0.8 - 1.2. Calculations were made on data taken during thermally unstable conditions, preferably, only because the functions ϕ_m and ϕ_H are more accurately established for this stability.

The results of the computations are presented in Figure 4.60 and summarized in Table 4.3. The value of Kolmogorov constant for velocity fluctuation (α_u) was determined to be 0.489 $\pm$ 0.08. This compares closely with the values of Wyngaard and Cote (1971); Kaimal et al. (1972);Hicks and Dyer (1972) and Dyer and Hicks (1982).

The Kolmogorov constant for temperature fluctuations (α_T) was found to be 0.70 $\pm$ 0.15, falling within the range reported by Dyer and Hicks (1982); Kaimal et al. (1972) and Wyngaard and Cote (1971). The Kolmogorov constant for humidity fluctuations (α_{ρ_v}) was found to be 0.99 $\pm$ 0.16, a little larger than those found in the literature (Dyer and Hicks, 1982; Raupach, 1978; Paquin and Pond (1971).

The Kolmogorov constant for CO_2 fluctuations (α_{ρ_v}) was found to be 0.78 $\pm$ 0.11. This is in agreement with a value of 0.89 $\pm$ 0.13 re-reported by Ohtaki (1982) obtained from a narrow stability range. Ohtaki's is the only report in the literature which has found a value of α_{ρ_c}.

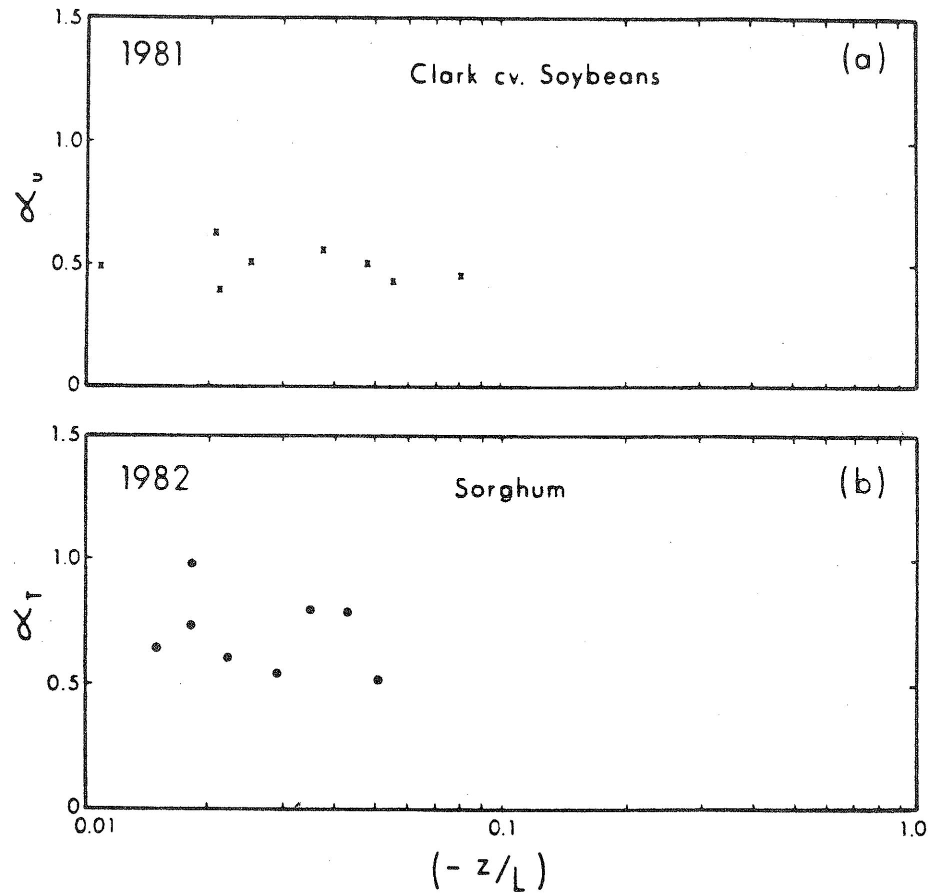

Fig. 4.60 Kolmogorov constant (α) as a function of stability (z/L). (a) Longitudinal wind velocity (U) and (b) Air temperature (T). Mead, Nebraska.

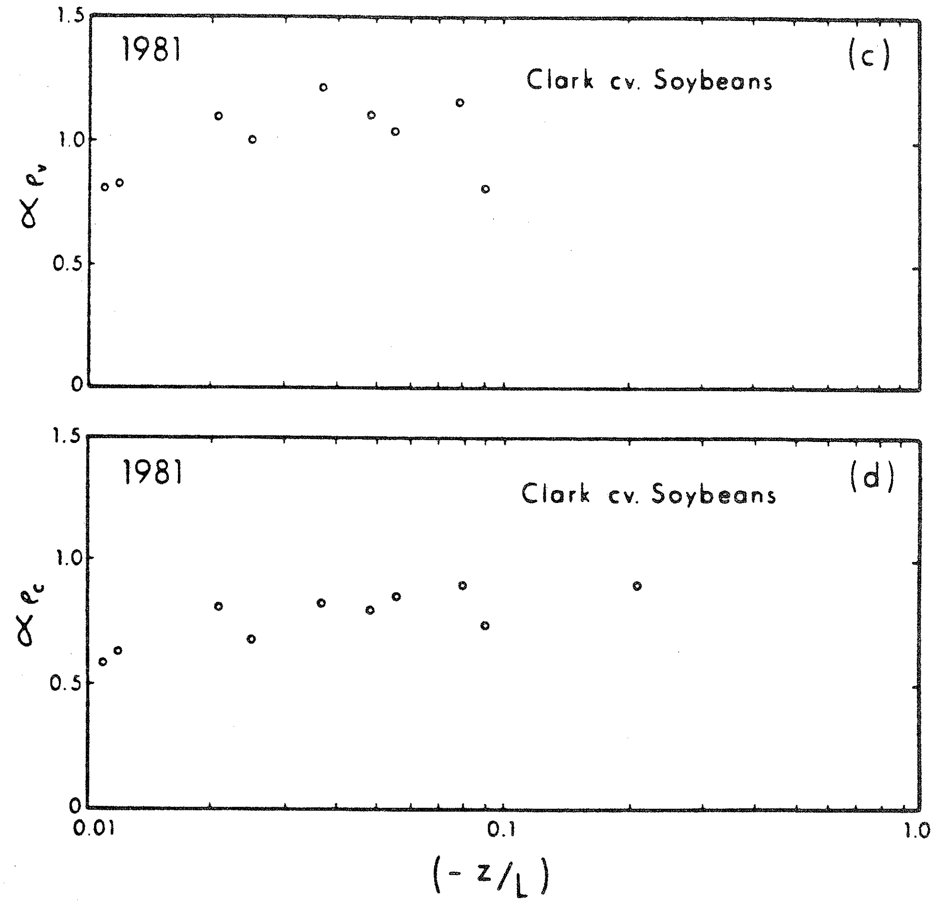

Fig. 4.60 continued. (c) Humidity (ρ_v) and (d) CO_2 (ρ_c).

Table 4.3 Values of Kolmogorov Constants

Fluctuation	Kolmogorov Constants	Value mean	deviation	Study
Velocity		0.489	± 0.08	Present
		0.52	± 0.05	Wyngaard and Cote (1971)
		0.50	± 0.05	Kaimal et al. (1972)
		0.54	± 0.03	Hicks and Dyer (1972)
		0.59	± 0.01	Dyer and Hicks (1982)
Temperature		0.70	± 0.15	Present
		0.68	± 0.02	Dyer and Hicks (1982)
		0.82	± 0.08	Kaimal et al. (1972)
		0.79	± 0.10	Wyngaard and Cote (1971)
Humidity		0.99	± 0.16	Present
		0.88	± 0.26	Raupach (1978)
		0.80	± 0.20	Paquin and Pond (1971)
		0.76	± 0.03	Dyer and Hicks (1982)
CO_2		0.78	± 0.11	Present
		0.89	± 0.13	Ohtaki (1982)

CHAPTER 5

Summary and Conclusions

Turbulence was measured over soybean and sorghum crops at Mead, Nebraska during the growing seasons 1980 to 1982. A prototype, fast response CO_2 sensor employing infrared absorption principles was obtained from the Lawrence Livermore National Laboratory and used to measure fluctuations in CO_2 concentration. Procedures were developed for field calibration and operation of the sensor. A laboratory calibration scheme was devised to determine the water vapor sensitivity of the CO_2 sensor.

The sensor proved to be reliable, provided approximately linear calibration and was easy to maintain in the field. Fluctuations of absolute humidity were measured with a Lyman-alpha hygrometer. Fluctuations of air temperature were measured with fine wire thermocouples. A drag anemometer was used to sense the three wind components. Vertical velocity fluctuations were also measured with a one dimensional sonic anemometer.

Components of the energy budget were observed over crop surfaces. The sum of sensible and latent heat fluxes [-(H + LE)] as measured by the eddy correlation technique compared very well with the sum of net radiation and soil heat flux [(Rn + S)] measured independently.

The diurnal patterns of the turbulent fluxes of CO_2, water vapor, and sensible heat over the soybeans and sorghum crops were analyzed. The integral as well as spectral statistics of turbulent fluctuations were examined.

The primary conclusions derived from this study are given below:

1. On a clear day with moderate temperatures and wind speeds, peak CO_2 flux rates over well-watered mature soybeans (LAI $\simeq$ 3.5) ranged around 1.0 mg $m^{-2}s^{-1}$ (ground area) when flux density of photosynthetically active radiation (PAR) was about 1,750 μEi $m^{-2}s^{-1}$. Under similar environmental conditions with PAR = 1,350 μEi $m^{-2}s^{-1}$, peak CO_2 flux over sorghum (LAI $\simeq$ 3.5) ranged around 1.4 mg $m^{-2}s^{-1}$.

On clear days, CO_2 flux reached a maximum in late morning over soybeans and began to decrease before the midday maximum of PAR was reached. Baldocchi (1982) and Rawson et al. (1978) also observed this behavior in soybeans. Maximum CO_2 fluxes over sorghum occurred at midday near the time of the PAR maximum.

Nocturnal CO_2 flux (plants + soil + root respiration rates) for mature soybeans (LAI $\simeq$ 3.5) were between 0.1-0.2 mg $m^{-2}s^{-1}$. Respiration rates for a sorghum crop between the half-bloom and soft dough stages (LAI $\simeq$ 4.5) were between 0.12-0.25 mg $m^{-2}s^{-1}$.

The carbon water flux ratio (CWFR) for both soybeans and sorghum on clear days reached a mid-morning maximum then decreased throughout the remainder of the day. Maximum CWFR over well watered, mature soybeans (LAI $\simeq$ 3-3.5) on a typical clear day was 12 mg CO_2 (g $H_2O)^{-1}$. A maximum CWFR value of 10 mg CO_2 (g $H_2O)^{-1}$ was measured over well-watered sorghum (LAI $\simeq$ 4-4.5).

2. a. The standard deviation of CO_2 concentration fluctuations (σ_{ρ_c}) reached a midday maximum of about 8 mg m^{-3} over mature soybeans on a typical clear day. The values decreased to a minimum near sundown then increased again to 6-7 mg m^{-3} with the occurrence of dark respiration. Similar trends were observed over the mature sorghum crop. Values near

9 mg m^{-3} occurred at midday, falling to 1 mg m^{-3} near sunset and rising again to about 4 mg m^{-3} at night.

The standard deviation of humidity (σ_{ρ_v}) on a typical clear day was similar in tendency and magnitude over both soybean and sorghum crops. σ_{ρ_v} reached midday values near 1 g m^{-3} and decreased during afternoon hours. Nocturnal values of σ_{ρ_v} remained near 0.1 g m^{-3} over both crops.

The standard deviation of temperature (σ_T) was typically larger over either crop during the day (0.2-0.6 C) than at night (0.2-0.3 C). The standard deviation of the vertical wind speed (σ_w) was found to be linearly related to the mean wind speed.

b. Scaled standard deviation of CO_2 ($\sigma\rho_c/\rho_{c_*}$) was found to have a median value of 2.9. Ohtaki (1980), the only other researcher reporting measurements of this quantity, found a median $\sigma\rho_c/\rho_{c_*}$ near 3.5. Median values of the scaled standard deviations of humidity ($\sigma\rho_v/\rho_{v_*}$), temperature (σ_T/T_*- excluding those under neutral conditions) and vertical wind (σ_w/u_*) were 2.5, 2.2, and 1.3, respectively. These values agree closely with others reported in the literature.

The correlation coefficient for vertical transfer of CO_2 ($r_{w\rho_c}$) ranged between 0.2-0.4, with a median value of 0.28. These values agree with those of Ohtaki (1980). The values of the correlation coefficients of water vapor, heat and momentum transfer were found to be in the neighborhood of the $r_{w\rho_c}$ values. They too compared well with the results reported in the literature.

That correlations between temperature and humidity ($r_{T\rho_v}$), temperature and CO_2 concentration ($r_{T\rho_c}$) and, humidity and CO_2 concentration ($r\rho_v\rho_c$) are large and of approximately equal magnitude indicates the similarity in structure of temperature, humidity, and CO_2 fluctuations. Mean values of these correlations lie between 0.60-0.75. Ohtaki and Matsui (1982) reported that $|r_{\rho_v \rho_c}|$ was the largest correlation, with values typically in the range of 0.7-0.8.

3. a. Spectral shapes and peak frequencies of air temperature, humidity and CO_2 fluctuations were somewhat similar under neutral thermal stability conditions. The shapes of these three spectra were found to be broader than those of the longitudinal (U) or vertical (W) velocity spectra and peak frequencies were found to lie between those of lateral velocity (V) and (W). Kaimal et al. (1972) report a similar finding for the temperature spectra. The peak frequency of CO_2 spectra was near 0.03 (non-dimensional frequency, f).

b. The cospectra of heat, water vapor, and CO_2 transport were similar for frequencies above $f \simeq 0.4$. These cospectra had peak frequencies near $f = 0.15$. Near $f = 2.0$, water vapor and CO_2 cospectra begin to decrease at a faster rate than do those of momentum and heat. Water vapor and CO_2 cospectra are very similar in shape and peak frequencies. Similar results were reported in Ohtaki and Matsui (1982), the only other study on this subject known to the author. The cospectra of momentum were found to be centered over lower frequencies than were those for heat, water vapor, and CO_2.

c. An investigation was made of thermal stability effects on wind velocity (U and W), humidity, and CO_2 spectra. Spectral peaks were shifted toward higher frequencies, spectral densities were reduced, and spectral shapes became more peaked as stability increased from the neutral condition. As the air became thermally unstable, spectral peaks were shifted toward lower frequencies and shapes became flatter for all spectra. These results are consistent with those of Kaimal et al. (1972) for U and W spectra and, with those of Phelps and Pond (1971) who reported on ρ_v spectra. No data reporting on stability effects on CO_2 spectra are available in the literature. The effects of thermal stability upon humidity and CO_2 spectra were found to be quite similar.

d. Spectral correlation coefficients for the transfer of CO_2, water vapor and momentum indicate a trend of decreasing correlation with increasing frequency above about f = 0.05. A large scatter of values were found below f = 0.05. In general, spectral correlations of all transfers decreased with increasing thermal stability from near neutral conditions. A strong similarity was found between the distribution of water vapor and CO_2 spectral correlation coefficients, indicating the existence of similar transport mechanisms. The trends found in momentum and water vapor spectral correlation coefficients are in agreement with those reported in McBean and Miyake (1972). However, no data is available in the literature for a comparison of results on CO_2 data.

e. The Kolmogorov constant for CO_2 fluctuations was found to be 0.78 ± 0.11 in agreement with Ohtaki (1982). The Kolmogorov constants for humidity, temperature and longitudinal velocity fluctuations were found to be 0.99 ± 0.16, 0.70 ± 0.15 and 0.49 ± 0.08 respectively; in close agreement with other values reported in the literature.

REFERENCES

Allen, K. H. 1971. Variations in carbon dioxide concentration over an agricultural field. Agric. Meteorol. 8:5-24.

Allen, L. H., R. J. Hanks, J. K. Aase and H. R. Gardner. 1974. Carbon dioxide uptake by wide-row grain sorghum computed by the profile Bowen ratio. Agron. J. 66:35-41.

Baes, C. F., H. E. Goeller, J. S. Olson and R. M. Rotty. 1976. The Global Carbon Dioxide Problem. Oak Ridge Nat. Lab. Report #ORNL-5194, 72 pp, Oak Ridge, TN.

Bakan, S. 1978. Note on the eddy correlation method for CO_2 flux measurements. Boundary-Layer Meteorol. 14:597-600.

Baldocchi, D. D. 1982. Mass and Energy Exchanges of Soybeans: Microclimate-Plant Architectural Interactions. Ph.D. Dissertation. UNL, Lincoln, NE. 265 pp.

Beadle, C. L., K. R. Stevenson, H. H. Neumann, G. W. Thurtell, and K. M. King. 1973. Diffusive resistance, transpiration, and photosynthesis in single leaves of corn and sorghum in relation to leaf water potential. Can. J. Plant Sci. 53:537-544.

Berkowicz, R. and L. P. Prahm. 1981. Note on turbulent scaling parameters for the convective planetary boundary layer. Boundary-Layer Meteorol. 21:215-222.

Bingham, G. E., C. H. Gillespie and J. H. McQuaid. 1978. Development of a miniature, rapid response CO_2 sensor. Lawrence Livermore National Laboratory, Rept. UCRL-52440.

Bird, R. B., W. E. Steward and E. N. Lightfoot. 1960. Transport Phenomena. John Wiley and Sons, NY. 980 pp.

Biscoe, P. V., J. A. Clark, K. Gragson, M. McGowan, J. L. Monteith and R. K. Scott. 1975. Barley and its environment. I. Theory and Practice. J. Appl. Ecol. 12:227-257.

Boussinesq, J. 1877. Essai sur la theorie des eaux courantes. Mein. pres. apr div. savants a'l' Acad. Sci. Paris. 23:1-680.

Boussinesq, J. 1897. Theorie de l'ecoulement tourbillonnant et tumulteux des liquides daus les lits rectilignes a' grande section. I-II. Gautheir-Villars, Paris.

Brach, E. J., R. L. Desjardins, G. T. St. Amour. 1981. Open path CO_2 analyzer. J. Phys. Elec. Sci. Instrum. 14:1415-1419.

Brakke, T. W. 1977. Local and regional components of sensible heat advection. M.S. Thesis. UNL, Lincoln, NE. 75 pp.

Broecker, W. S., T. Takashi, J. H. Simpson and T. H. Peng. 1979. Fate of fossil fuel carbon dioxide and the global carbon budget. Science 206:409-418.

Brown, K. W. and N. J.Rosenberg. 1971. Energy and CO_2 balance of an irrigated sugar beet field in the Great Plains. Agron. J. 63: 207-312.

Brutsaert, W. 1975. The roughness length for water vapor, sensible heat, and other scalars. J. Atmos. Sci. 32:2028-2031.

Buck, A. 1975. Variable-path Lyman-alpha hygrometer opearting and maintenance manual 023032002, NCAR, Boulder, CO. 116 pp.

Buck, A. 1976. The variable path Lyman-alpha hygrometer and its operating characteristics. Bull. Amer. Meteorol. Soc. 57:1113-1118.

Busch, N. E. 1973. On the Mechanics of Atmospheric Turbulence pp. 1-65 in Workshop on Micrometeorology. D. Haugen, (ed.). Amer. Meteorol. Soc., Boston, MA. 392 pp.

Busch, N. E. and H. A. Panofsky. 1968. Recent spectra of atmospheric turbulence. Quart. J. Roy. Meteorol. Soc. 94:132-148.

Busch, N. E., R. M. Brown, and J. A. Frizzola. 1970. Vertical velocity variance and Reynolds stresses at Brookhaven. J. Appl. Meteorol. 9:583-87.

Businger, J. A., J. C. Syngaard, Y. Izumi and E. F. Bradley. 1971. Flux-profile relationship in the atmospheric surface layer. J. Atmos. Sci. 28:181-189.

Campbell, G. S. and M. H. Unsworth. 1979. An inexpensive sonic anemometer for eddy correlation. J. Appl. Meteorol. 18:1072-1077.

Champagne, F., G. Sleicher and O. Wehrman. 1967. Turbulence measurements with inclined hot wires. J. Fluid Mech. 28:153-175.

Chen, J.-Y., S. B. Verma and D. E. Anderson. 1983a. Computation of humidity fluctuations using a Lyman-alpha hygrometer with decaying output. (In Preparation).

Chen, J.-Y., S. B. Verma and D. E. Anderson. 1983b. An evaluation of frequency response and phase shift characteristics of numerical filters. (In Preparation).

Clough, J. M., M. M. Peet and P. J. Kramer. 1981. Effects of high atmospheric CO_2 sink size or rates of photosynthesis for soybean cultivar. Plant Physiol. 67:1007-1010.

Cooley, J. W. and J. W. Tukey. 1965. An algorithm for the machine calculation of complex Fourier series. Mathematics of Computation 19:297-301.

Corrsin, S. 1951. On the spectrum of isotropic temperature fluctuations in an isotropic turbulence. J. Appl. Phys. 22:469-473.

DaCosta, J. M. N., S. B. Verma and N. J. Rosenberg. 1981. Dark Respiration of Soybeans (Glycine Max (L.) Merr.). 15th Conference on Agriculture and Forest Meteorology, American Meteorological Society, Anaheim, CA. p. 49.

Denmead, O. T. 1966. CO_2 exchange in the field: its measurement and interpretation. Agric. Meteorol. Proc. of WMO, Melbourne. pp 442-482.

Desjardins, R. L. and E. R. Lemon. 1974. Limitations of an eddy-correlation technique for the determination of the carbon dioxide and sensible heat fluxes. Boundary-Layer Meteorol. 5:475-488.

Dyer, A. J. 1968. An evaluation of eddy flux variation in the atmospheric boundary layer. J. Appl. Meteorol. 1:845-850.

Dyer, A. J. 1981. Flow distortion by supporting structures. Boundary-Layer Meteorol. 20:243-251.

Dyer, A. J. 1982. 'Reply' Boundary-Layer Meteorol. 22:267-268.

Dyer, A. J. and B. B. Hicks. 1970. Flux-gradient relationships in the constant flux layer. Quart. J. Roy. Meteorol. Soc. 96:715-721.

Dyer, A. J. and B. B. Hicks. 1972. The spatial variability of eddy fluxes in the constant flux layer. Quart. J. Roy. Meteorol. Soc. 98:206-212.

Dyer, A. J. and B. B. Hicks. 1982. Kolmogoroff constants at the 1976 ITCE. Boundary-Layer Meteorol. 22:137-150.

Egli, D. B., J. W. Pendleton and D. B. Peters. 1970. Photosynthetic rate of three soybean communities as related to CO_2 levels and solar radiation. Agron. J. 62:411-414.

Funk, J. P. 1960. Measured radiative flux divergence near the ground at night. Quart. J. Roy. Meteorol. Soc. 86:382-389.

Funk, J. P. 1964. Comparison of measured and computed radiative flux divergence profiles near the ground. Presented at I.A.M.A.P. Radiation Symp., Leningrad, 1964.

Garay, A. 1981. Physical characteristics of the soil of the Agricultural Meteorology field laboratory at Mead, NE: Results and some measurements. CAMaC Progress Report 81-2.

Garratt, J. R. 1975. Limitations of the eddy-correlation technique for the determination of turbulent fluxes near the surface. Boundary-Layer Meteorol. 8:255-259.

Gill, G. C. 1975. Development and use of the Gill UW anemometer. Boundary-Layer Meteorol. 8:475-495.

Gill, G. G. and P. L. Hexter. 1972. Source instrumentation definitions for use by meteorologists and engineers. Bull. Amer. Meteorol. Soc. 53:846-850.

Gjessing, D. T., T. Lanes and A. Tangerud. 1969. A hotwire anemometer for the measurement of the three orthogonal components of wind velocity and also directly the wind direction, employing no moving parts. J. Sci. Instr. 2:51-54.

Haugen, D. A., J. C. Kaimal, and E. F. Bradley. 1971. An experimental study of Reynolds stress and heat flux in the atmospheric surface layer. Quart. J. Roy. Meteorol. Soc. 97:168-80.

Hicks, B. B. 1972. Propellor anemometers as sensors of atmospheric turbulence. Boundary-Layer Meteorol. 3:214-228.

Hicks, B. B. 1977. Some effects of displacement height variability in tall vegetation. Radiological and Environmental Research Div. Ann. Report ANL-77-65 Part IV Argonne Nat. Lab.

Hicks, B. B. 1981. An examination of turbulence statistics in the surface boundary layer. Boundary-Layer Meteorol. 21:389-402.

Hicks, B. B. and A. J. Dyer. 1972. The spectral density technique for the determination of eddy fluxes. Quart. J. Roy. Meteorol. Soc. 98:838-844.

Hicks, B. B., P. Hyson and C. J. Moore. 1975. A study of eddy fluxes over a forest. J. Appl. Meteorol. 14:58-66.

Hinze, J. O. 1959. Turbulence. McGraw-Hill. NY. 586 pp.

Hogstrom, U. 1982. A critical evaluation of the aerodynamical error of a turbulence instrument. J. Appl. Meteorol. 21:1838-1844.

Hyson, P. and B. B. Hicks. 1975. A single-beam infrared hygrometer for evaporation measurement. J. Appl. Meteorol. 14:301-307.

Inoue, E. 1957. An aerodynamic measurement of photosynthesis over a paddy field. Proc. 7th Japan National Congress Appl. Mech. pp 211-214.

Inoue, E. 1965. On the CO_2 concentration profiles with crop canopies. J. Agric. Met., Tokyo 20:137-140.

Jeffers, D. L. and R. M. Shibles. 1969. Some effects of leaf area, solar radiation, air temperature and variety on net photosynthesis in field grown soybeans. Crop Sci. 9:762-764.

Jones, E. P. and S. D. Smith. 1977. A first measurement of sea-air CO_2 flux by eddy correlation. J. Geophys. Res. 82:5990-5992.

Jones, E. P. and S. D. Smith. 1978. The air density correction to eddy flux measurements. Boundary-Layer Meteorol. 15:357-360.

Jones, E. P., T. V. Ward, and H. H. Zwick. 1978. A fast response atmospheric CO_2 sensor for eddy correlation flux measurements. Atmos. Env. 12:845-851.

Kaimal, J. C. 1975. Sensor and techniques for direct measurement of turbulent fluxes and profiles in the atmospheric surface layer. Atmospheric Technology, NCAR, pp 7-23.

Kaimal, J. C. and J. A. Businger. 1963. A continuous wave sonic anemometer-thermometer. J. Appl. Meteorol. 2:156-164.

Kaimal, J. C., J. C. Wyngaard, Y. Izumi and O. R. Coté. 1972. Spectral characteristics of surface layer turbulence. Q. J. Roy. Meteorol. Soc. 98:563-589.

Kanemasu, E. T., M. L. Wesely, B. B. Hicks and J. L. Heilman. 1979. Techniques for calculating energy and mass fluxes. p. 156-182 in Modification of the Aerial Environment of Planrs, B. J. Barfield and J. F. Gerber (ed.) Am. Soc. of Agr. Eng., St. Joseph, MI. 538 pp.

Keeling, C. 1973. Industrial production of carbon dioxide from fossil fuels and limestone. Tellus 25:174-198.

Keeling, C. D., J. A. Adams, C. A. Ekdahl, P. R. Guenthner. 1976. Atmospheric carbon dioxide variations at the South Pole. Tellus 28:552-564.

Kolmogorov, A. N. 1941. The local structure of turbulence. Compt. rend. Acad. Sci. URSS 30:301-305.

Kolmogorov, A. N. 1962. A refinement of previous hypothesis concerning the local structure of turbulence in viscous, incompressible fluids at high Reynolds number. J. Fluid Mech. 13:82-85.

Landsberg, H. E. 1970. Man-made climatic changes. Science 170: 1265-1274.

Lang, A. R. G. and R. Leuning. 1981. New omnidirectional anemometer with no moving parts. Boundary-Layer Meteorol. 20:445-457.

Larson, E. M., J. D. Hesketh, J. T. Wooley and D. B. Peters. 1981. Seasonal variations in apparent photosynthesis among plant stands of different soybean cultivars. Photosyn. Res. 2:3-20.

Lemon, E. R. 1960. Photosynthesis under field conditions, II. An aerodynamic method for determining the turbulent carbon dioxide exchange between the atmosphere and a corn field. Agron. J. 52:697-703.

Liepmann, H. W. 1979. The rise and fall of ideas in turbulence. Amer. Scientist 67:221-228.

Ling, S. C. and P. G. Hubbard. 1956. The hot-film anemometer - A new device for fluid mechanics research. J. Aerosp. Sci. 23:890-891.

Long, R. R. 1982. A new theory of the energy spectrum. Boundary-Layer Meteorol. 24:137-160.

Long, R. R. and T. C. Chen. 1981. Experimental evidence for the existence of the mesolayer in turbulent systems. J. Fluid Mech. 105:19-59.

Lumley, J. L. and H. Panofsky. 1964. The Structure of Atmospheric Turbulence. John Wiley & Sons. NY. 231 pp.

Machta, L. 1972. Mauna Loa and global trends in air quality. Bull. Amer. Meteorol. Soc. 53:402.

Maddukuri, C. S. and W. R. Frisken. 1974. Turbulent kinetic energy balance near the frozen surface of eastern Lake Ontario. Proc. 17th Conf. Great Lakes Res. 1974:288-295. Internat'l Assoc. Great Lakes Res.

Maitani, T. 1977. Some turbulence characteristics in the surface layer over a wheat field. Berichte des Ohara Institute fur landwirt schaftliche Biologie, Okayama Universtat. 17:29-46.

Martin, H. C. 1971. The humidity microstructure: A comparison bebetween a refractometer and a Lyman-alpha humidiometer. Boundary-Layer Meteorol. 2:167-172.

Mauney, J. R., G. Grimm, K. E. Fry and J. D. Hesketh. 1979. Correlation of photosynthetic carbon dioxide uptake and carbohydrate accumulation in cotton, soybean, sunflower, and sorghum. Photosynthesis 13:260-266.

McBean, G. 1970. The Turbulent Transfer Mechanisms in the Atmospheric Surface Layer. Ph.D. Dissertation. University of British Columbia. 119 p.

McBean, G. 1971. The variation of statistics of wind temperature and humidity fluctuations with stability. Boundary-Layer Meteorol. 1:438-457.

McBean, G. 1972. Instrument requirements for eddy correlation measurement. J. Appl. Meteorol. 11:1078-1084.

McBean, G. A. and M. Miyake. 1972. Turbulent transfer mechanisms in the atmospheric surface layer. Q. J. Roy. Meteorol. Soc. 98: 383-398.

Mitsuta, Y. 1966. Sonic anemometer-thermometer for general use. J. Meteorol. Soc. Japan, Ser. II 44:12-24.

Monin, A. S. 1965. On the symmetry properties of turbulence in the surface layer of air. Izv. Atm. and Oceanic Phys. Ser., 1:45-54.

Monin, A. S. and A. M. Obukhov. 1954. Basic turbulent mixing laws in the atmospheric surface layer. Trudy Geofiz. Inst. AN SSSR 151:163-187.

Monin, A. S. and A. M. Yaglom. 1971. Statistical Fluid Mechanics: Mechanics of Turbulence. Vol. I. M.I.T. Press, Cambridge, MA. 769 pp.

Monteith, J. L. and G. Szeicz. 1960. The CO_2 flux over a field of sugar beets. Q. J. Roy. Meteorol. Soc. 86:205-214.

Mordukhovich, M. I. and L. R. Tsvang. 1966. Direct measurements of turbulent fluxes at two heights in the atmospheric surface layer. Izvestiya AN SSSR, Series, fiz atmosf. okeana. 2:786-803.

Motha, R. P. 1978. Turbulent Transfer Over An Irrigated Crop Under Conditions of Sensible Heat Advection. Ph.D. Dissertation, UNL, 194 pp.

Motha, R. P., S. B. Verma, and N. J. Rosenberg. 1979. Exchange coefficients under sensible heat advection determined by eddy correlation. Agric. Meteorol. 20:273-280.

Munn, R. E. 1966. Descriptive Micrometeorology. Academic Press, NY. 245 pp.

Munro, D. S. and T. R. Oke. 1975. Aerodynamic boundary-layer adjustment over a crop in neutral stability. Boundary-Layer Meteorol. 9:53-61.

Nafziger, E. D. and H. R. Koller. 1976. Influence of leaf starch concentrates on CO_2 assimilation in soybean. Plant Physiol. 57:560-563.

Norman, J. M., S. G. Perry and H. A. Panofsky. 1976. Measurement and theory of horizontal coherence at a two meter height. 3rd Symposium on Atmospheric Turbulence, Diffusion and Air Quality, Raleigh, NC, AMS preprint pp 19-22.

Ohtaki, E. 1980. Turbulent transport of carbon dioxide over a paddy field. Boundary-Layer Meteorol. 19:315-336.

Ohtaki, E. 1982. The Kolmogorov constant for carbon dioxide in the atmospheric surface layer over a paddy field. Boundary-Layer Meteorol. 23:153-159.

Ohtaki, E. and T. Matsui. 1982. Infrared device for simultaneous measurement of fluctuations of atmospheric carbon dioxide and water vapor. Boundary-Layer Meteorol. 24:109-119.

Olin, J. G. and R. B. Kiland. 1970. Split-film anemometer sensors for three-dimensional velocity vector measurement. Symposium on Aircraft Wake Turbulence, Sept., 1970, Seattle, WA.

Panofsky, H. A. and E. Mares. 1968. Recent measurements of cospectra for heat flux and stress. Q. J. Roy. Meteorol. Soc. 94:581-582.

Paquin, J. E. and S. Pond. 1971. The determination of the Kolmogoroff constants for velocity, temperature and humidity fluctuations from second and third-order structure functions. J. Fluid Mech. 50: 257-269.

Parhami, B. 1971. Spectral analysis by fast Fourier transform. Contributed computer program and write-up to the Computation Center, Department of Meteorology, The Pennsylvania State University. 24 pp.

Pasquill, F. 1972. Q. J. Roy. Meteorol. Soc. 98:469-494.

Peet, M. M. and P. J. Kramer. 1980. Effects of decreasing source/sink ratio in soybean on photosynthesis, photorespiration and yield. Plant, Cell and Environment 3:201-206.

Perry, S. B. 1977. Measurement and theory of horizontal coherence at a two meter height. M.S. Thesis, Pennsylvania State University. 83 pp.

Phelps, G. T. and S. Pond. 1971. Spectra of the temperature and humidity fluctuations and of the fluxes of moisture and sensible heat in the marine boundary layer. J. Atmos. Sci. 28:918-928.

Plate, E. J. 1971. Aerodynamic Characteristics of Atmospheric Boundary Layers. U.S.A.E.C., 179 pp.

Potter, J. R. and P. J. Breen. 1980. Maintenance of high photosynthetic rates during the accumulation of high starch levels in sunflower and soybean. Plant Physiol. 66:528-531.

Prandtl, L. 1925. Bericht uber Untersuchungen zur ausgebildeten Turbulenz, Zs. angew. Math. Mech. 5:136-139.

Pruitt, W. O., D. L. Morgan, and F. J. Lourence. 1973. Momentum and mass transfer in the surface boundary layer. Q. J. Roy. Meteorol. Soc. 99:370-386.

Randall, D. L., T. E. Hanley and O. K. Larison. 1965. The NRL Lyman-alpha humidiometer in humidity and moisture. A Wexler (ed.), Vol. 1, Principles and Methods of Measuring Humidity in Gases, pp 444-454.

Raupach, M. R. 1978. Infrared fluctuation hygrometry in the atmospheric surface layer. Q. J. Roy. Meteorol. Soc. 104:309-322.

Rawson, H. M., N. C. Turner and J. E. Begg. 1978. Agronomic and physiological responses of soybean and sorghum crops to water deficits. IV Photosynthesis, transpiration and water use efficiency of leaves. Aust. J. Plant Physiol. 5:195-219.

Redford, T. G., S. B. Verma and N. J. Rosenberg. 1980. Humidity fluctuations over a vegetated surface measured with a Lyman-alpha hygrometer and a fine-wire thermocouple psychrometer. J. Appl. Meteorol. 19:860-867.

Redford, T. G., S. B. Verma and N. J. Rosenberg. 1981. Drag anemometer measurements of turbulence over a vegetated surface. J. Appl. Meteorol. 20:1222-1230.

Reynolds, O. 1883. An experimental investigation of the circumstances which determine whether the motion of water shall be direct or sinuous, and the law of resistance in parallel channels. Phil. Trans. Roy. Soc. London 174:935-982.

Reynolds, O. 1895. On the dynamical theory of incompressible viscous fluids and the determination of the criterion. Phil. Trans. Roy. Soc. London 186:123-161.

Rosenberg, N. J. and K. W. Brown. 1974. Self-checking psychrometer system for gradient and profile determinations near the ground. Agric. Meteorol. 13:215-226.

Rosenberg, N. J., B. L. Blad and S. B. Verma. 1983. Microclimate: The Biological Environment. John Wiley & Sons, NY. (in press).

Sakamoto, C. M. and R. H. Shaw. 1967. Apparent photosynthesis in field soybean communities. Agron. J. 59:73-75.

Salisbury, F. B. and C. W. Ross. 1978. Crop Physiology. Wadsworth Pub. Co., Belmont, CA. 422pp.

Shaw, R. H., R. H. Silversides and G. W. Thurtell. 1974. Some observations of turbulence and turbulent transport within and above plant canopies. Boundary-Layer Meteorol. 5:429-449.

Shaw, R. H. and A. R. Pereira. 1982. Aerodynamic roughness of a plant canopy: A numerical experiment. Boundary-Layer Meteorol. 26:51-65.

Silvius, J. E., R. R. Johnson and D. B. Peters. 1977. Effect of water stress on carbon assimilation and distribution in soybean plants at different stages of development. Crop Sci. 17:713-716.

Sinclair, T. R. 1980. Leaf CER from post-flowering to senescence of field-grown soybean cultivars. Crop Sci. 20:196-200.

Sitaraman, V. 1970. Spectra and cospectra of turbulence in the atmospheric surface layer. Q. J. Roy. Meteorol. Soc. 96:744-749.

Smith, S. D. and E. P. Jones. 1979. Dry-air boundary conditions for correction of eddy flux measurements. Boundary-Layer Meteorol. 17:375-379.

Swinbank, W. C. 1951. The measurement of vertical transfer of heat and water vapor by eddies in the lower atmosphere. J. Meteorol. 8:135-145.

Takeuchi, K., E. Ohtaki and T. Seo. 1980. Turbulent transfer of water vapor over paddy fields. Berichte des Ohere Instituts fur landwirtschaftliche Biologie Okayama Universitat. 18:1-30.

Tanner, C. B. 1960. Energy balance approach to evapotranspiration from crops. Soil Sci. Soc. Amer. Proc. 24:1-9.

Tanner, C. B. and G. W. Thurtell. 1969. Anemoclinometer measurements of Reynolds stress and heat transport in the atmospheric surface layer. Rep. RI-R10, USAEC Army Electronics Command, Ft. Huachuca, AZ.

Taylor, G. I. 1915. Eddy motion in the atmosphere. Phil. Trans. Roy. Soc. A215:1-26.

Taylor, G. I. 1938. The spectrum of turbulence. Proc. Roy. Soc. A164:476-490.

Tennekes, H. 1973a. Similarity laws and scale relations in planetary boundary layers, pp 177-216, in Workshop on Micrometeorology D. Haugen (ed.) Amer. Meteorol. Soc. 329 pp.

Tennekes, H. 1973b. The logarithmic wind profile. J. Atmos. Sci. 30:234-238.

Tennekes, H. and J. L. Lumley. 1972. A First Course in Turbulence. M.I.T. Press, Cambridge, MA. 300 pp.

Thom, A. S. 1975. Momentum, mass and heat exchange of plant communities. Vegetation and the Atmosphere, J. L. Monteith, ed. Academic Press. 278 pp.

Thompson, N. 1979. Turbulence measurements above a pine forest. Boundary-Layer Meteorol. 16:293-310.

Thorne, J. H. and H. R. Koller. 1974. Influence of assimilate demand on photosynthesis, diffusive resistance, translocation, and carbohydrate levels of soybean leaves. Plant Physiol. 54:201-207.

Thorpe, M. R., E. G. Banke and S. D. Smith. 1973. Eddy correlation measurements of evaporation and sensible heat flux over Arctic Sea Ice. J. Geophy. Res. 78:3573-3584.

Thurtell, G. W., C. B. Tanner and M. L. Wesely. 1970. Three-dimensional pressure-sphere anemometer system. J. Appl. Meteorol. 9:379-385.

Tillman, J. E. 1965. Water vapor density measurements utilizing the absorption of vacuum ultraviolet and infrared radiation. Humidity and Moisture, Vol. I, A. Wexler (ed.), Reinhold, pp 428-443.

Turner, N. C. and L. D. Incoll. 1971. The vertical distribution of photosynthesis in crops of tobacco and sorghum. J. Appl. Ecol. 8:581-591.

Turner, N. C., J. E. Begg, H. M. Rawson, S. D. English and A. B. Hearn. 1978. Agronomic and physiological responses to soybean and sorghum crops to water deficit. III. Components of leaf water potential, leaf conductance, CO_2 photosynthesis and adaptation to water deficits. Aust. J. Plant Physiol. 5:169-177.

Vanderlip, R. L. and H. E. Reeves. 1972. Growth stages of sorghum. Agron. J. 64:13-16.

Verma, S. B. and N. J. Rosenberg. 1976. Carbon dioxide concentration and flux in a large agricultural region of the Great Plains of North America. J. Geophys. Res. 81:399-405.

Verma, S. B., R. P. Motha and N. J. Rosenberg. 1979. A comparison of temperature fluctuations measured by a microbead thermistor and a fine wire thermocouple over a crop surface. Agric. Meteorol. 20: 281-289.

Vignes, D. and C. Planchon. 1979. Structure, eclairement et exchanges gazeux d'une culture de Soja (Glycine max.). Photosynthetica 13:136-154.

von Kármán, T. 1930. Mechanisch Ahnlichkeit und Turbulenz Nochr. Ges. Weis. Gottingen. Math.-Phys. Ki:58-76.

Webb, E. K. 1970. Profile relationships: The log-linear range, and extension to strong stability. Q. J. Roy. Meteorol. Soc. 96: 67-80.

Webb, E. K. and G. I. Pearman. 1977. Correction of CO_2 transfer measurements for the effect of water vapour transfer. In R. W. Bilger (ed.), Second Australasian Conference on Heat and Mass Transfer. University of Sydney. pp.469-476.

Webb, E. K., G. I. Pearman and R. Leuning. 1980. Correction of flux measurements for density effects due to heat and water vapour transfer. Q. J. Roy. Meteorol. Soc. 106:85-100.

Wieringa, J. 1980. A revaluation of the Kansas mast influence on measurements of stress and cup anemometer overspeeding. Boundary-Layer Meteorol. 18:411-430.

Wyngaard, J. C. 1982. 'Comments on flow distortion by supporting structure.' Boundary-Layer Meteorol. 22:263-265.

Wyngaard, J.C. and O. R. Coté . 1971. The budgets of turbulent kinetic energy and temperature variance in the atmospheric surface layer. J. Atmos. Sci. 28:190-201.

Wyngaard, J. C. and O. R. Coté. 1972. Cospectral similarity in the atmospheric surface layer. Q. J. Roy. Meteorol. Soc. 98:590-603.

Zangvil, A. 1981. Some aspects of the interpretation of spectra in meteorology. Boundary-Layer Meteorol. 21:39-46.

Appendix 1

Symbol	Description
A	Cross sectional area of drag anemometer sensing element
$a_{o,1,2,3}$	Calibration constants
$a'_{o,1,2,3}$	Calibration constants
$b_{o,1,2}$	Calibration constants
c	Speed of sound
C_p	Specific heat of air at constant pressure
C_{ppm}	CO_2 concentration (parts per million)
C_u	Angular dependent correction factor for drag anemomter sensor response
C_{xy}	Cospectral density of variables x and y
CWFR	Carbon-water flux ratio, defined in Chapter 4
d	Displacement height, also spacing of sonic anemometer transducers
D_T	Diffusivity constant for temperature
D_V	Diffusivity constant for water vapor
D_C	Diffusivity constant for CO_2
e	Vapor pressure, also exponential function
E	Energy transfer function, also vapor flux
f	Non-dimensional (reduced)frequency
F	Time constant of numerical filter
f_{21}	Oxygen correction to Lyman-alpha hygrometer output
f_v	Logarithmic voltage response of Lyman-alpha hygrometer output

F_c	CO_2 flux
g	Acceleration due to gravity
G	System or amplifier gain
h	Measurement or crop height
H	Sensible heat flux
H_A	Advected sensible heat flux
H_{sa}	Sensible heat stored in air within canopy
H_{sc}	Sensible heat stored in crop
I	Intensity of Lyman-alpha radiation
k	von Karman constant, also extinction coefficient of Lyman-alpha radiation
K_c	Eddy diffusivity coefficient for CO_2 transport
K_H	Eddy diffusivity coefficient for sensible heat transport
K_m	Eddy diffusivity coefficient for momentum transport
K_w	Eddy diffusivity coefficient for water vapor transport
l	Length scale, eddy free path length
L	Monin-Obukhov length scale
L_T	Monin-Obukhov length scale including only temperature effects on air density
L_{ρ_v}	Monin-Obukhov length scale including only water vapor effects on air density
LE	Latent heat flux
LE_A	Advected latent heat flux
LE_{sc}	Latent heat stored in crop
LAI	Leaf area index

M	Energy from miscellaneous metabolic activity
m_c	Molecular weight of CO_2
n	Natural frequency
N_ζ	Dissipation rate of the variance of a quantity ζ
P	Atmospheric pressure, also energy consumed in photosynthesis
q	Specific humidity
R	Universal gas constant
R_e	Reynolds number
R_f	Flux Richardson number
R_i	Gradient Richardson number, radiative flux density in direction i
R_{ij}	Correlation tensor
R_n	Net radiative flux
R_{xy}	Spectral correlation coefficient of variables x and y
R_1	One-dimensional correlation tensor
r_{xy}	Integral correlation coefficient of variables x and y
$\vec{r}$	Distance vector
S	Soil heat flux, also spectral energy, also shape factor of drag anemometer sensing element
T	Temperature, subscript (1) indicates deviation from reference state (o)
T_v	Virtual temperature
T_*	Scaled temperature
t	time

U	Mean value of u wind component
u	longitudinal wind velocity
u_R	Raw wind velocity, u component, drag anemometer
u_*	Scaled wind velocity, friction velocity
V	Mean value of v wind component, also voltage output of a sensor
v	Latitudnal wind velocity
V_u	Voltage of u component drag anemometer
V_v	Voltage of v component drag anemometer
V_w	Voltage of w component drag anemometer
V_c	CO_2 sensor output voltage in response to CO_2
V_{H_2O}	CO_2 sensor output voltage in response to H_2O
V_p	Logarithm of Lyman-alpha voltage output with corrections
W	Mean vertical wind velocity
w	vertical wind velocity
W_i	Weighting function of numerical filter
x	Lyman-alpha hygrometer path length, also distance or displacement
z	Height above surface
z_o	Roughness length
α	Kolmogorov constant, also Lyman-alpha decay rate constant
Δ	Integrated decay rate constant of Lyman-alpha hygrometer
δ	Kronecker delta

ε	Dissipation rate, also 3-dimensional unity tensor
η	Unit vector parallel to the earth's axis of rotation
κ	Wave number
λ	Wave length
ν	Kinematic viscosity, also frequency
π	Constant, 3.1416
ρ	Air density
ρ_a	Dry air density
ρ_c	Absolute CO_2 concentration
ρ_{c*}	Scaled absolute CO_2 concentration
ρ_v	Absolute humidity
ρ_{v_*}	Scaled absolute humidity
σ_x	Standard deviation of quantity x
τ	Reynolds (surface) stress
ϕ	Stability adjustment parameter (subscripts m, h, w, c for momentum, heat, water vapor and CO_2, respectively)
Ω	Coriolis acceleration
$(\bar{\ })$	Overbar quantity, indicates averaging
$(\ ')$	Prime quantity, indicates fluctuation from the mean